Heat Transfer Reduction Across the Walls of Refrigerated Van Trailers by the Application of Phase Change Material

By

Mashud Ahmed

Submitted to the graduate degree program in the Department of Mechanical Engineering and the Graduate Faculty of the University of Kansas in partial fulfillment of the requirements for the degree of Master of Science in Mechanical Engineering

_____
Mario A. Medina, Ph.D., P.E., Chairperson

_____
Ronald L. Dougherty, Ph.D., P.E., Committee Member

_____
Bedru Yimer, Ph.D., Committee Member

Date Defended: _____

The Thesis Committee for Mashud Ahmed certifies
that this is the approved Version of the following thesis:

Heat Transfer Reduction across the Walls of Refrigerated Van Trailers by the Application of Phase Change Material

Committee:

_____
Mario A. Medina, Ph.D., P.E., Chairperson*

_____
Ronald L. Dougherty, Ph.D., P.E., Committee Member

_____
Bedru Yimer, Ph.D., Committee Member

Date approved:_____

Abstract

The purpose of this thesis is to present the results obtained by incorporating phase change materials (PCMs) into the conventional insulated walls of commercial refrigerated van trailers (herein referred to as “refrigerated trucks”). The idea was to apply a building insulation technology (inclusion of PCMs) that was developed previously, at the University of Kansas, in the walls of refrigerated trucks. Although the technology had been applied to buildings, the concept is a novel one within the automotive industry. Although transportation experiences more dynamic challenges compared to its building counterpart, this analysis can open an interesting window for an innovative solution to an area of energy used in the transportation sector. In this research endeavor, two similar van trailer simulators were constructed and used to test the proposed technology under stationary environmental conditions. Both simulators were outfitted with the same number of measurement devices in the exact same locations. The technology was tested in similar days in terms of temperature and solar insolation. The relevant variables that were monitored were the heat flux across the walls of the simulators and temperatures, including surface and indoor air temperatures. Other relevant data, such as weather parameters (e.g., insolation) were also measured and recorded. The primary observation was how the peak heat flux and the total heat flow responded for the two simulators. The results obtained suggested that the van trailer simulator outfitted with PCMs had lower peak heat transfer rates by approximately 42.4% and total heat flow over a period of time one day by as much

as 27.7%. Month-long results suggested that the reductions produced by the proposed technology were 43.8% for peak heat transfer rate and 26.3% for total heat transfer.

The refrigeration units that cool the insides of refrigerated trucks do so by burning fossil fuel, usually diesel. Any decrease in the refrigeration load requirements would eventually result in lower fuel consumption. The reduction in heat transfer rate (i.e., peak load) would assist in reducing the size of the cooling equipment, which could also result in cost savings.

Acknowledgements

I would like to take this opportunity to greatly thank all who supported this academic aspiration. I am indebted to Dr. Mario Medina, my thesis advisor, who supported me all the way in my Master's degree. I have been enormously benefited not only by his academic supervision but also the research assistantship that he provided me to explore a great research experience. The professional ethics and academic teachings that I've learned from him will be an asset all through my life. I would like to express gratitude to Dr. Bedru Yimer for supporting me with various issues during my graduate studies and being a graduate thesis committee member. I am also grateful to Dr. Ronald Dougherty for his willingness to be a committee member of my graduate thesis.

I am very thankful to Oliver Meade, who has been a proficient coworker and a great friend. I have learned a lot from him. I would also like to thank Yuan Fang and Angie Evers for their assistance with the research. I really appreciate the assistance that I have received from Jim Weaver, Laboratory Manager of the CEAE department.

It is always a pleasure to remember my family, who has supported and encouraged me all through my life. My ardent respect goes to my parents who have been the motivation for all my achievements.

Last but not least, I would like to thank all my relatives and friends who are near and far from me but encouraged me every time.

Table of Contents

List of Figures

List of Tables

List of Symbols

Q = Total Heat Flow (W or Btu/hr)

q"= Heat Transfer Rate per Unit Area or Heat Flux (W/m^2 or Btu/hr ft^2)

A = Surface Area Perpendicular to the Heat Flow (m^2 or ft^2)

ΔT (T_{out} - T_{in}) = Temperature Difference (°C or °F), (T_{in} = Inside Wall Temperature;

T_{out}= Outside Wall Temperature)

U= Overall Heat Transfer Coefficient (W/m^2K or Btu/hr ft^2 ^oR)

k = Thermal Conductivity (W/mK or Btu/hr ft ^oR)

R_{TOTAL} = Total Thermal Resistance (K/W or hr ^oR/Btu)

$R_{ALUMINUM\ SHEET}$ = Thermal Resistance of Aluminum Sheet (K/W or hr ^oR/Btu)

$R_{FOAM\ INSULATION}$ = Thermal Resistance of Foam Insulation (K/W or hr ^oR/Btu)

$R_{FIBERGLASS\ BOARD}$ = Thermal Resistance of Fiberglass Board (K/W or hr ^oR/Btu)

x = Length (m or ft)

Cp= Specific Heat Capacity (J/kg K or Btu/lb_m ^oR)

Chapter I: Introduction and Motivation of the Research

1. Refrigerated Food Transportation: A Brief History

Refrigerated food transport is almost as old as refrigerated storage [1]. Although the idea of ice and cold storage date back to some ancient Egyptian times, it is in the late nineteenth century when this industry began to emerge and experience the advancement like other industries as a result of rapid technological innovation. According to historians, the early 1890s was the turning point for the adoption of mechanical refrigeration devices in the U.S. The widespread adoption of mechanical refrigeration at that time was not a revolutionary technical change, but rather largely the convergence of several evolutionary processes, including improvements in the machine-tool industry, finer tolerances in parts, high-pressure seals, and the addition of the electric motor. Eventually this development resulted in broad adoption of the technology in the perishable commodities market. Meat and dairy products were the main goods being shipped at that time. In 1869, George H. Hammond, a Detroit meatpacker, shipped dressed (slaughtered) beef to the east coast of the U.S. using primitive refrigerator cars. In the winter of 1874 Nelson Morris shipped dressed beef from Chicago, and another Chicago packer, Gustavus Swift, imitated Morris the following year [1]. However, the refrigeration used by Swift and Morris was supplied by cold winter air blowing through the cars. The Swift–Chase car, which used natural ice and salt supplied from overhead in vented containers placed in each corner of the

car, was very instrumental in the dressed beef transportation. This industry grew rapidly thereafter. This drew merchants' attention, which resulted in the popularity of refrigerated transportation for perishable goods. Ultimately, the integration of refrigerated transport into the perishable commodities market was the result of the improvement of mechanical refrigeration [1].

Increase in agricultural output and the need of rapid transportation also contributed to the expansion of the refrigerated truck industry. Railroads, which were the dominant and preferable mode of transportation, started facing competition from road transportation after WWII. Trucks were becoming the primary mode of transport for agricultural products. It was a direct effect of three post-war developments, which were, 1) the transportation revolution required better roads, 2) it required better trucks and engines, and 3) it required refrigerated trucks. Wessels Living History Farm chronicled this development from a Nebraska farms point of view [2].

A recent study estimates that in the U.S. 80% of communities across the country receive their goods exclusively by trucks [3]. Refrigerated trucks, which are climate-controlled, transport perishable goods, pharmaceutical items and many other temperature-sensitive commodities. Keeping the inside of a truck at a nearly constant temperature and relative humidity requires exact amounts of heat and/or moisture management throughout the shipment period, which is regulated via small fuel-burning refrigeration units, placed outside the truck.

2. Refrigerated Transportation: Today's Challenge

Petroleum consumption by the transportation sector increased significantly in the second half of the twentieth century, from 3.36 (1950) to 13.94 (2005) million barrels per day [4]. With the increased requirements of shipping various commodities, the trucking industry as a whole experienced a rapid growth. The fuel consumption by the trucking industry, both light and heavy, tripled from 1970 to 2005, resulting in approximately 6 million barrels per day in 2005 [4]. It is pertinent to mention that, 'Trucks' as indicated here are a general classification in the transportation sector. The present research focuses on refrigerated trucks, a classification based on body-type, within the truck industry. From the 2002 Economic Census, it appears that approximately 8.5% of trucks are considered to be refrigerated trucks, which make up about 11.9% of trucking miles in the U.S. [5]. With growing population and demand, this trend is expected to have a continuous growth in coming years. Recent publications show that the trucking industry, the leading transportation mode, will experience a heavy expansion in the U.S., in terms of volume, cost, and energy consumption [4, 6, 7]. In spite of the lowering energy intensity over the past years, energy use still remains high. In the U.S. trucks alone consumed about 65% of the total energy consumption by freight transportation in 2005 [7]. According to the U.S. Department of Energy [7], trucks will consume approximately 11.5 million barrels of petroleum per day by 2030, which will constitute half of the total consumption by all of the transportation modes.

Refrigerated trucks, often known as refrigerated van trailers, represent one classification of these trucks. Like other truck categories, refrigerated trucks can be of various sizes and types. The two basic types are single-unit and truck-tractor. Figures 1 and 2 show the two kinds of trucks.

Figure 1. Single-unit refrigerated truck (Photo courtesy: T Co Max)

Figure 2. Truck-tractor refrigerated unit (Photo courtesy: XTRA)

3. Passive Cooling Technology

It is essential to understand the effort made in finding alternative solutions to the existing problem of conventional energy usage by the trucking industry in general. There are not many encouraging solutions in this sector. Even though, alternative fuels are becoming more commonplace and making their way in the transportation sector. Although different cars and other light road vehicles have started to use alternative fuels, this is not the case for large trucks. This includes all trucks with or without the refrigeration option [4]. According to the Department of Transportation [6, 7] and Department of Energy [4], medium and heavy trucks used 4,577 trillion Btu's of energy, out of which 89.6% came from diesel, and the rest of the energy was from gasoline and liquefied petroleum gas (less than 1%). In spite of a drop in energy intensity of approximately 18% over the last 35 years (1970 to 2005), the growing demand in the trucking industry requires more efficient energy usage through various sustainable changes. With reference to transportation, energy intensity is defined as the ratio of energy inputs to a process to the useful outputs from that process; for example, gallons of fuel per passenger-mile or Btu per vehicle-mile traveled. All through these years, the core research has been done on the improvement of diesel engines. Improving performance and efficiency of diesel engines led to noteworthy outcomes in the trucking industry. Refrigerated trucks, which have added equipment, i.e., the refrigeration unit, require more energy to operate.

Passive cooling is largely used in buildings. Cavelius *et al.* [8] illustrated the principles and usage of several of those techniques used in the building industry. The most common example is air or coolant flow in any space to achieve the desired temperature without further use of cooling or heating equipment. The first and foremost principle of passive cooling is to achieve the desired temperature without extra power consumption. Extensive work has been done on building models to implement passive cooling technologies. Basically, it uses all available resources around the building environment and then utilizes those resources with mechanical hardware like bafflers, barriers and piping networks [8]. The use of a eutectic solution in transportation resembles closely to passive cooling technology. The eutectic solution also needs to be charged periodically in order to operate. Therefore, the incorporation of phase change material into the truck body, which is supposed to lower the heat transfer across the insulated wall without consuming any power, can be considered as a passive cooling technology. The hypothesis is based on PCMs thermal energy storage capacity that works in a natural phase change cycle and directed by PCMs thermal properties.

4. Similarity between Buildings and Transportation Energy Usage

One of the insulation methods used in buildings, namely, foam core used in structural insulated panels (SIPs) and the insulation that is most used in trucks are similar. That is, polyurethane foam, a widely used insulation, is most of the times sandwiched between two other surfaces. Buildings generally use plywood sheathing, oriented strand board (OSB), gypsum board, and other wood products. In refrigerated trucks, the same insulation is sandwiched between aluminum, stainless steel, glass board, or fiberglass composite.

Furthermore, the heat transfer processes across the walls of a building and the walls of insulated refrigerated van trailer trucks have many common features. Some of these include, but are not limited to, modes of heat transfer (i.e., conduction, convection, and radiation), solar loads on outer surfaces, and the nature of constant internal air temperature. In spite of their similarity, the fundamental difference between the heat transfer in buildings and transportation is the state of motion. Buildings in general, as stationary structures, do not experience the dynamic conditions that trucks experience. Trucks not only see a change in air motion and varying solar intensity, but they experience several types of environmental conditions as the trucks travel long distances and cross latitudes and longitudes. The current analysis is based on the situation of the truck that is commonly known as ‘engine idling’ for automotive. Commercial trucks experience a considerable amount of engine idling while making long distant trips.

5. Comparison of Various PCMs and Their Applications

PCMs are chemical compounds that solidify, liquefy or gasify in specific temperature ranges. Most of the chemical compounds can be described as phase change material for the clarification purposes, whenever PCMs are mentioned in engineering use this means a specifically designed chemical compound which can serve the purpose of heat storage under specified climatic conditions. Zhang [9] described a wide range of PCMs together with their physical properties. In addition, PCMs have several application areas, some of which are quite established within the engineering field. According to Salyer [10], these application areas are broad and expanding with a growing demand, which is in part the result of their usefulness.

The use of PCMs as a thermal storage medium has become one of their primary usefulness. Zalba *et al.* [11] listed and described extensively the use of PCM as a potential thermal storage. Results in the thermal storage application of PCMs in heating, ventilation and air conditioning (HVAC) are encouraging. Various space cooling and heating situations such as, peak space cooling or heating load management, reduction in space cooling or heating energy consumption, and lower building wall temperature swings are some of the scenarios where the use of thermal storage becomes helpful. In fact PCMs have made their way through as a thermal energy storage for several applications ranging from HVAC, solar heating systems, building heating systems, and commercial cooling systems.

Chapter II: Literature Review

1. PCM Research

The research conducted by Medina *et al.* [12] represents a record of PCM research on building insulation applications. The research team has investigated various combinations of PCMs and their integration within standard building walls. Their results are documented in [9, 13, 14]. Their core work focused on peak heat flux reduction in building walls as well as the total heat flow reduction over a period of time. Medina *et al*. [12] demonstrated the potential of heat transfer rate reductions in structural insulated panels (SIPs) outfitted with PCMs (PCM-SIPs) [12]. Their research showed peak heat flux reductions of 37% and 62% on south-facing walls when the concentrations of PCMs were 10% and 20%, respectively. The concentration percentages were in relation to the weight of the interior sheathing. More constant wall temperatures was another finding that was encouraging from the comfort and space cooling and heating equipment life points of view. Zhu [13] expanded the experiment further by introducing different PCM-core-PCM encapsulation combinations. Zhu used a dynamic wall simulator.

Zhang *et al.* [14] implemented the integration of phase change materials in building walls via macro encapsulation. The encapsulation was accomplished via copper pipes. Their results showed an 11 to 20% peak heat flux reduction with a

PCM concentration of 10%. In this case, the concentration of PCM was in terms of PCM added vs. the weight of the interior siding of the wall. Ismail and Castro [15] integrated PCM in buildings as a thermal barrier and demonstrated the effectiveness of such inclusion. Zafer [16] gave a brief idea about the possible use of PCMs in transportation applications but no results were provided to verify the hypothesis. The use of PCMs in transportation cooling systems (referred to as passive cooling system) has therefore attracted far less attention than its building counterpart.

In summary, PCMs have been the focus of research for over two decades and have been used successfully in several applications. In buildings, PCMs have been used for latent heat storage. Zalba *et al.* [11] extensively researched solid-liquid phase change, the materials used for such purpose, and their various scientific and industrial usage. PCMs have found similar applications in the food, medical, and pharmaceutical industries. Previous research has demonstrated the effectiveness of PCMs in lowering the heat transfer across the building walls [10, 12, 17].

2. Research in Transport Refrigeration

The refrigeration units of refrigerated trucks run on the vapor compression refrigeration cycle. Based on the way the refrigerating unit is run, vehicles can be classified into two types. The first one is self contained, where an independent motor runs the compressor, and the second one is the non self-contained, which depends on the vehicle motor [18]. Refrigerating units of both types use significant amounts of energy to keep the inside of the van trailers at a required temperature. The current research presented in this thesis was inspired by the possibilities that lie in this particular transportation sector, which is to evaluate the integration of PCMs within the walls of the refrigerated insulated van trailer.

Similar requirements and benefits to those found in buildings also exist in the case of refrigerated trucks; except that the desired temperature ranges are wider, ranging from -18 to +13°C (-0.4 to 55.4°F) (foods only) [18]. Also, in the case of refrigerated trucks, to achieve a constant temperature throughout the inside of the van trailer container represents a bigger challenge than in buildings. As an integral part of the cold chain, these requirements are very crucial. Several new approaches in refrigeration units have been tested in recent years [19, 20]. For example, James *et al.* [21] showed various results, including modeling, in refrigerated food transportation systems. Their review encompassed many experiments conducted in understanding food temperature, microbial growth and other parameters better in food transportation. Tso *et al.* [22] conducted experiments on the heat and mass transfer

characteristics of refrigerated trucks, which elaborated on the benefits of using air curtains over the use of plastic strip curtains. The study concluded that there was a reduction of 11% infiltration heat load. Also, energy saving of up to 40% was achieved using the air curtain. Chatzidakis [23, 24] studied the behavior of the van trailer in an isothermal chamber prescribed by the Perishable Transport Agreement (PTA). According to the PTA, the insulation used in the walls of refrigerated van trailers should have certain k-values for the insulating material, which should be in the range from 0.40 to 0.70 W/m^2K (0.07 to 0.12 Btu/hr $ft^2°F$) [25].

As large amounts of refrigerated food products move across continents, this has led to more unified standard codes for the transportation media involved in this industry. All of this literature reveals the variety of work that has been done to increase the efficiency of refrigerated trucks and carriers alike. Therefore, to the best of the author's knowledge, the experiment conducted and results presented in this thesis are unprecedented.

Polyurethane foams have been widely used as insulators in many applications, and the trucking company is no exception. The main challenge with polyurethane foam is its degrading k-value over time, which is caused by moisture and air entrainment. Chatzidakis [26] presented the effects of such decaying of the insulating materials on the environment. This study revealed that an increasing k-value would definitely require more energy to keep the interior at the same temperature. This situation would lead to an overall lower efficiency coolant unit, which would burn more fuel and emit more CO_2 into the environment. Over a period of 9 years, this

emission could increase up to 55%. The present work retrofits the regular insulation of refrigerated van trailer walls with PCMs. The primary focus is given to peak heat flux and total heat flow reduction.

A stationary truck model, which closely resembles the engine idling condition of commercial refrigerated trucks, is the focus of this analysis. As discussed above, different research pertaining to the improvement of energy use in trucks has been explained by many researchers. This particular analysis represents a new addition to the ongoing effort. Although exact data for engine idling condition as compared to regular on-the-road operation are not available, it is safe to assume that energy savings during idling time will increase the entire trip energy efficiency of any refrigerated truck. Many commercial trailers used by both rail and sea transport use insulated refrigerated containers [18]. This is a promising piece of information in conjunction with that of refrigerated trucks. Further investigation involving these sectors might attract a broader audience and thus is capable of wider impact.

Chapter III: Experimental Setup

1. Setup

Two insulated refrigerated van trailer simulators with dimension of 1.22 m. × 1.22 m. × 1.22 m (4 ft × 4 ft × 4 ft) were built. These simulators were outfitted with wall panels of identical construction to those used in refrigerated trucks. One test simulator used standard van trailer walls, while the other simulator used standard van trailer walls outfitted with PCMs. That is, the walls started out as the standard walls in which PCMs were integrated via encapsulation pipes. One of these small-scale trailer simulators is shown in Figure 3. One of the simulators was referred to as the 'control simulator', and the PCM outfitted simulator was referred to as the 'PCM-enhanced simulator.'

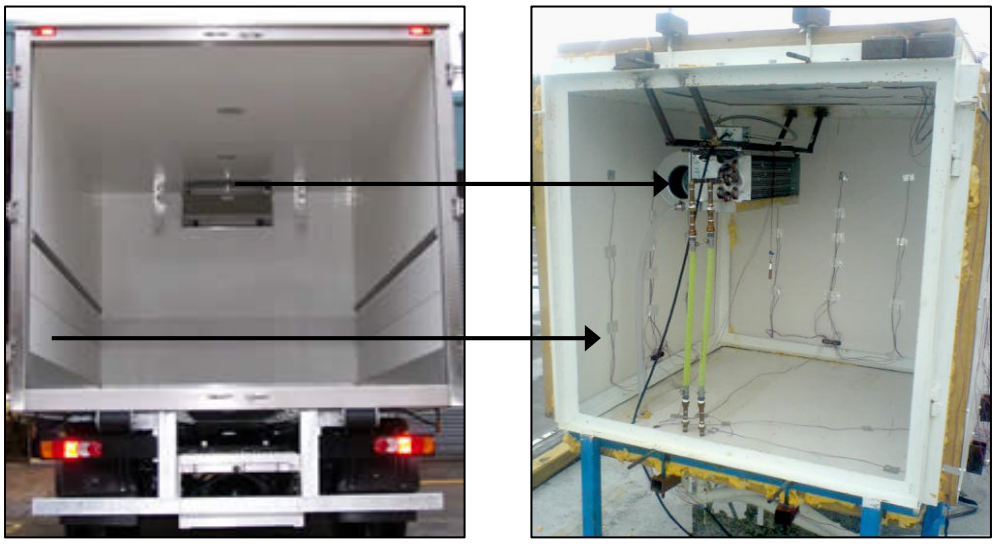

Figure 3. Van trailer simulator and the similarity between commercial [26] and test setup

A collage of pictures is shown in Figure 4, which is intended to show the progression in the development of the test setup.

Figure 4. Collage of pictures depicting the progression in the development of the test setup. The collage includes a) the frame of the simulators (left), a wall panel before installation (right top), and the completed set up (right bottom)

Once the walls were installed, foam sealant was used to airtight the simulators. It was essential to make the panels air-tight, as air infiltration would have increased the refrigeration load. Having air-tight simulators also helped to achieve a more stable inside temperature for the simulators. Three holes through the bottom panel were drilled to accommodate the chilled water supply, chilled water return,

electrical and sensor cables. These holes were then caulked to seal around the pipes and cables.

The simulators were placed side by side. The simulators were held down using heavy cement blocks. An equipment shed was built at the test site to house and protect the refrigeration units, data logger, and laptop computer used to collect the data. All of the refrigeration equipment, data acquisition system, thermostat, and other controls were housed in the shed, which gave the required protection from inclement weather and the hot sun. Figure 5 shows the entire setup on the rooftop of Learned Hall at the University of Kansas.

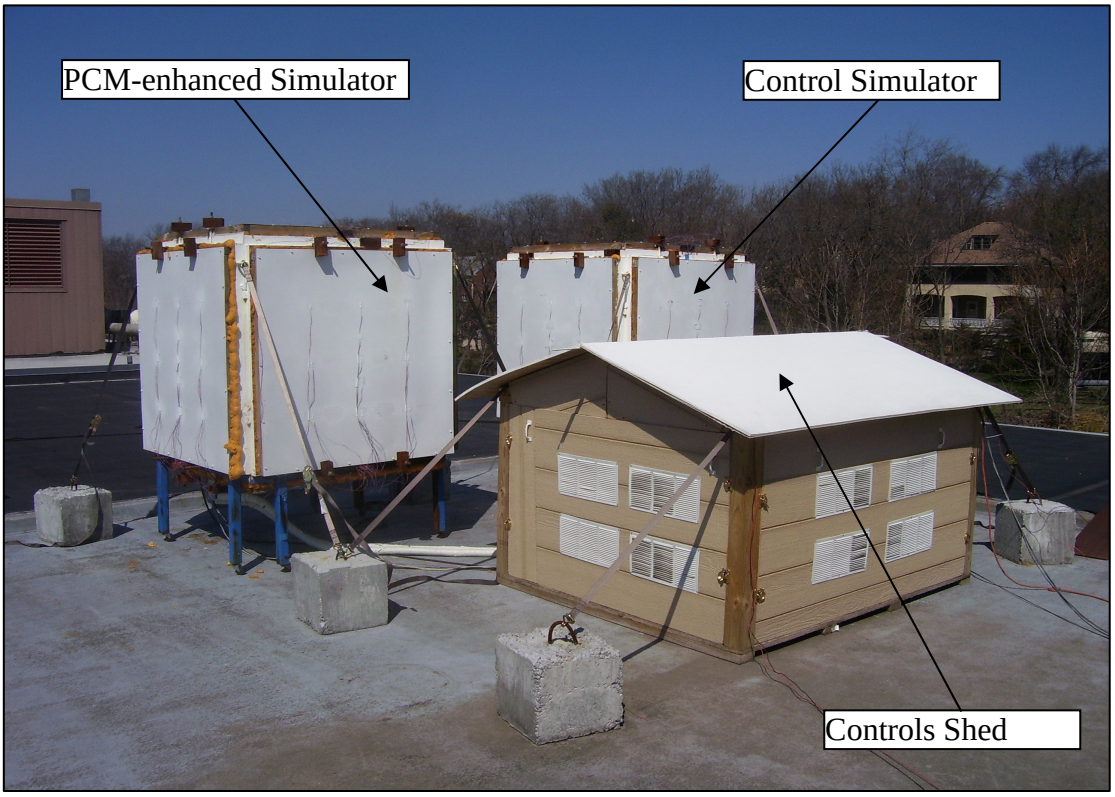

Figure 5. Experimental setup showing the two refrigerated trailer simulators and control shed

2. Wall Panel Construction

Wall panels were constructed using widely used guideline by the trucking industry [18]. The use of polyurethane foam insulation sandwiched between aluminum and fiberglass boards is the most common practice used to build the walls of van trailers. The same standard materials were used in this research. Table 1 shows the specifications of the wall panel construction. The difference between the walls of the two van trailer simulators was that, one was of standard construction and the other one was of standard construction, but fitted with 0.0127 m. (½") thin-walled copper pipes, which contained the PCM. Thus a PCM-enhanced wall would look identical to the standard wall except that it would contain the PCM encapsulating pipes internally. PCM was contained in eight copper pipes totaling 25% of the total polyurethane foam's weight. The polyurethane foam's weight was calculated based on published density data of the foam after expansion. Figure 6 gives a cut-away view of a PCM-enhanced panel showing all of the components of the wall. It shows equidistant copper pipes are placed horizontally, which were attached to the wood frame. The inside was sandwiched between the aluminum sheet and fiberglass board.

There existed the possibility of air intrusion during panel construction; however, extra care was taken to minimize this occurrence. In addition, maximum care was exercised so that no empty space would remain between the aluminum and the fiberglass board.

Table 1. Wall panel construction details

Material	Thickness	Area
Aluminum	0.102 cm (0.04 in.)	119.4 cm × 119.4 cm (47 in. × 47 in.)
Polyurethane Foam	8.89 cm (3.50 in.)	-
Fiberglass Board	0.229 cm (0.09 in.)	119.4 cm × 119.4 cm (47in. × 47 in.)
Wood Frame	-	5.08 cm. × 10.2 cm. (2in. × 4in.)
Copper Pipe	0.159 cm (0.0625 in.)	1.27 cm. × 111.76 cm. (0.5in. × 44in.)

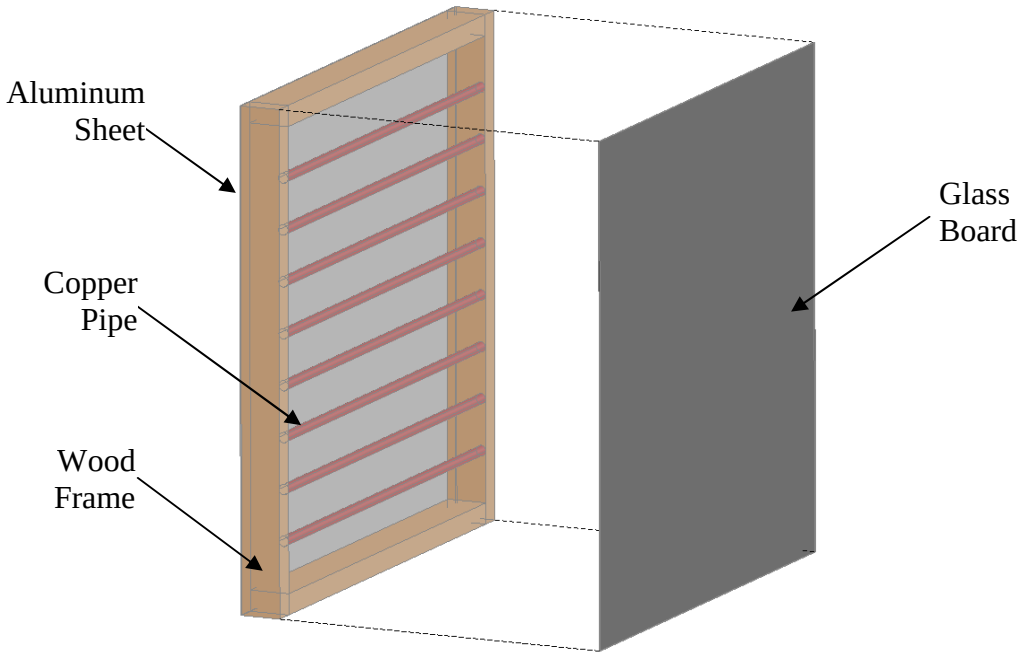

Figure 6. Cut-away schematic view of the PCM-enhanced simulator wall

Figure 7 shows a step in the construction of a PCM panel. The PCM pipes were laid down at equal distances. The ends of the pipes were sealed with copper pipe caps. Copper pipe clamps were used to glue the pipes to the fiberglass board. Although no definitive conclusion was drawn by the previous research within the group, it was assumed that placing the PCM encapsulating pipes closer to the inside wall would yield a better thermal performance by the PCM-enhanced wall panels. That was the motivation in placing the pipes closer to the indoor skin. This seemed to be the better location because the PCM would need to solidify after the melting process. Hence, placing the PCM closer to the indoor would seem to provide better chances for the PCM to solidify.

Figure 7. In the process of constructing a PCM wall panel

Figures 8 and 9 show the final steps in the wall construction, which includes the expansion of the polyurethane foam. Commercial polyurethane foams were used which expanded nine times their initial volume once they were prepared and poured in. Mechanical mixing of the component chemicals resulted in the required volume in the contained space between the aluminum and fiberglass board. Clamps were used while pouring the foam (Figure 8).

Figure 8. View of the wall panels during construction

Figure 9. Inside look at the wall while the polyurethane foam was expanding within the contained space of the wall

3. Refrigeration Loop

Obtaining the desired stable indoor temperature was an important requirement of the experiments as well as a technical challenge. A refrigeration loop was built on site to provide the required refrigeration load for the van trailer simulators. A closed loop system involving a chiller, a tank, and two heat exchangers was used. The inlet and outlet of the chiller were connected to heat exchangers which were inside the tank. Under this arrangement, the coolant (a chilled water glycol mixture) would flow through the chiller and then to the heat exchangers and back to the chillers. The heat exchangers were fabricated onsite and made from copper pipes. A 50-gallon tank was used and the heat exchangers were immersed inside it. From the tank, separate chilled water lines were directed to fan coil units, placed inside each simulator, through flexible copper piping. Figure 10 gives a complete schematic of the refrigeration system. Centrifugal pumps with a capacity of 373 kW (½ hp) moved the chilled water around the loop.

Figures 11 to 14 give details of various refrigeration components that were used. The chiller had a cooling capacity of 200 W (682 Btu/hr) at 0°C (32^{o}F). It was a reciprocating chiller with a possible low set point of -10°C (14°F). The chiller was set to -5°C (23°F) to achieve the required refrigeration load for the van trailer simulators. The entire piping network, including the tank, was insulated to prevent heat losses. Four axial fans, with a capacity of 6.51 m^3/s (230 CFM) were added to the controls shed to prevent overheating.

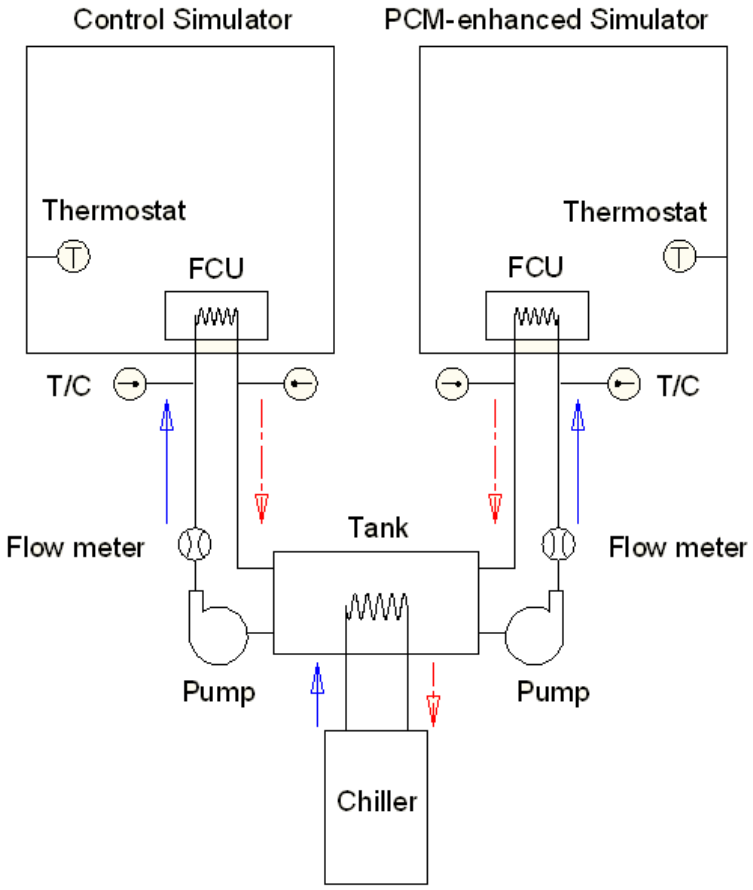

Figure 10. Schematic of the refrigeration system (solid arrows indicate chilled water, dashed arrow indicate chilled water return)

Therefore, the refrigeration system was divided into primary and secondary refrigeration loops. The primary refrigeration loop involved the chiller and the heat exchangers. The secondary refrigeration loop represented the actual refrigeration load required by the simulators. This included the heat exchangers, coolant storage tank, pump, and the fan coil unit. A glycol-based anti freeze was used to avoid freezing problems within the refrigeration system.

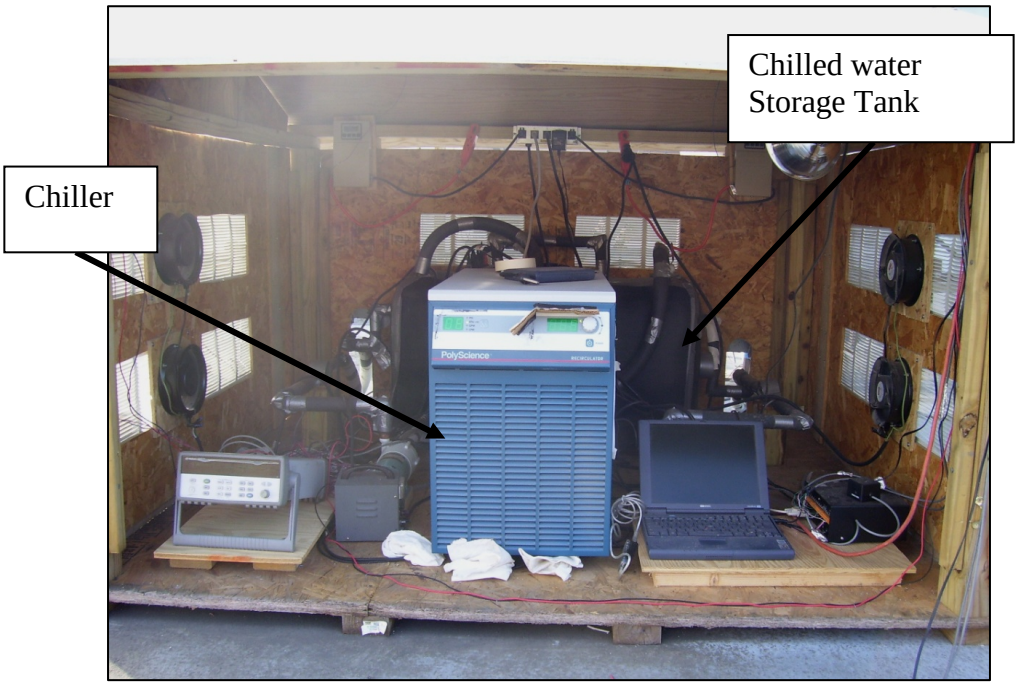

Figure 11. Controls shed showing the chiller (front), the chilled water tank (rear), the data logger (left), and the laptop (right)

Figure 12. Tank insulated with foam insulation

Figure 13. Heat exchanger

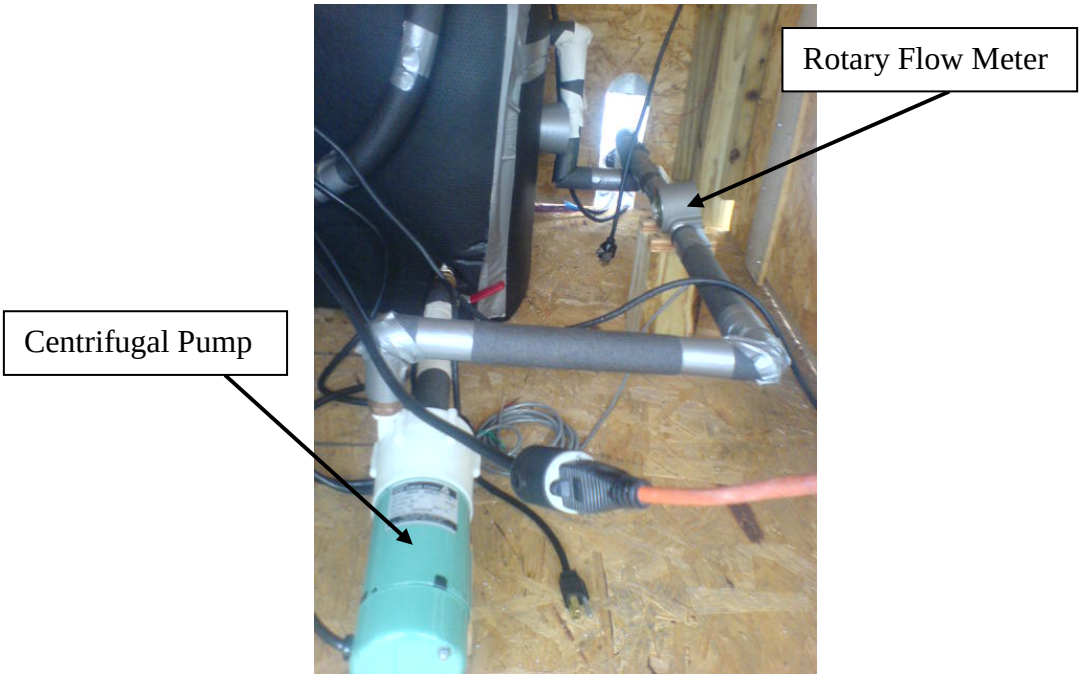

Figure 14. Centrifugal pump and rotary flow meter

The fan coil units (Figure 15) were the main refrigerating devices inside the simulators. Each fan coil unit was a 8.50 m^3/min. (300 CFM) capacity unit at 0.5 m^3/min (1.8 GPM) of coolant flow, and total refrigeration capacity was 2,638 kW (9.0 MBtu/hr). A remote temperature controller was connected to each fan coil unit. Therefore, remote control of the temperature with a wide range of temperature options was available. Also, rotary type flow meters measured the flow into the simulators. Appendix B shows the on-off cycle curve for the flow meters.

A propylene glycol-water mixture of 50-50 by volume was used as coolant for the refrigeration circuit. A differential scanning calorimeter (DSC) was used to estimate the properties of the coolant. The DSC analysis results are located in Appendix A. A specific heat capacity of 2.85 J/g°C (0.68 Btu/lb°F) at 0^oC (32°F) was used for the further calculations.

Figure 15. Fan coil unit

4. Indoor and Outdoor Conditions

Refrigerated trucks carry a variety of commodities with wide temperature range requirements. For this research a 4°C (39.2°F) inside temperature was selected. A significant number of produce items are transported at this temperature. For example, oranges, other citrus fruits, and potatoes are some of the produce items that require a 4^{o}C (39.2°F) temperature during transport. Usually, transportation of these items is done within a temperature range, which accounts for different indoor and outdoor conditions, such as, temperature, relative humidity, and wind speed [18].

The setup was located in the University of Kansas campus at Lawrence, Kansas. Lawrence is situated at 38°57′36″N, 95°15′12″W. It has a wide range of temperatures in different seasons. Temperatures range from an average low of almost −7 °C (20 °F) in January to an average high above 32 °C (90 °F) in July. Typically, the first fall freeze occurs between mid-October and the second week of November, and the last spring freeze occurs between the last week of March and the third week of April. During a typical year, the total amount of precipitation may be anywhere from 27 to 1,400 mm (1.06 in. to 54 in.). Winter snowfall averages almost 457 mm (18.0 in), but the median is less than 250 mm (10 in.).

5. Measurements

Temperatures and heat fluxes at different locations were measured. Figure 16 shows the grid network used for temperature and heat flux measurements. Type 'T' thermocouples (T/C) were used to measure temperature. Grids were designed in such a way to give a representative surface temperature for each panel. Indoor air temperatures were also measured. In addition, thermocouples were installed to measure chilled water temperature into and out of the fan coil units in each of the simulators. The heat flux sensors were 5.08 cm × 5.08 cm (2 in × 2 in). These were placed to give an accurate representation of the heat transfer rate across the panels. The heat flux sensors were placed in all panels, except the bottom one. A data logger and laptop computer were used for on-site data collection and storage.

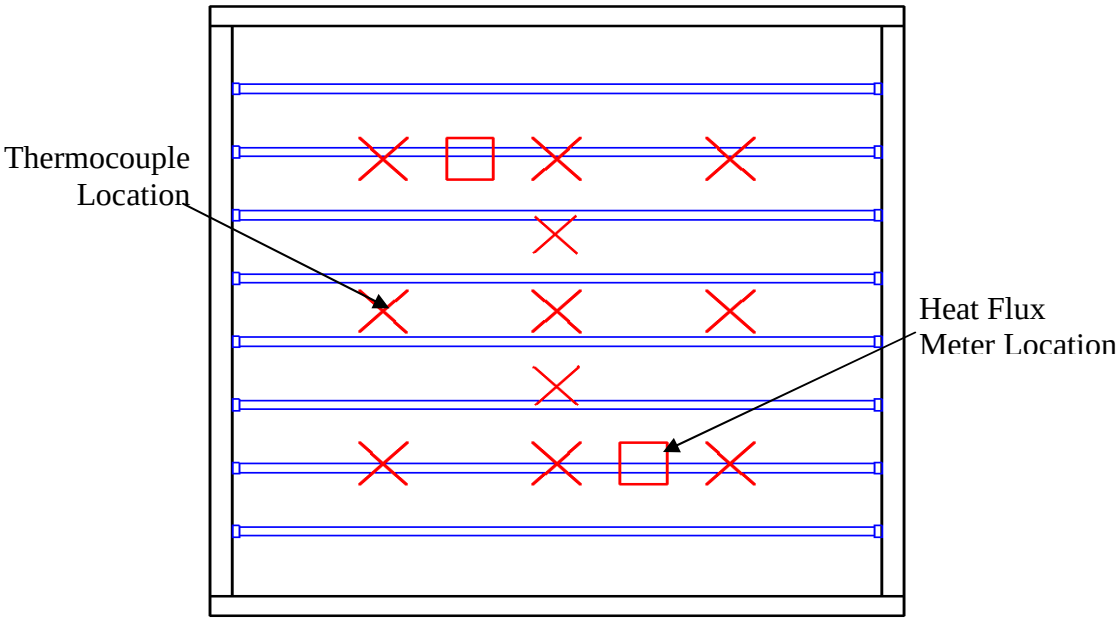

Figure 16. Thermocouple and heat flux meter locations

Figures 17 and 18 show the thermocouple grid on the inside and outside and on inside of the simulators respectively. Aluminum tape was used to attach the T/C to the walls.

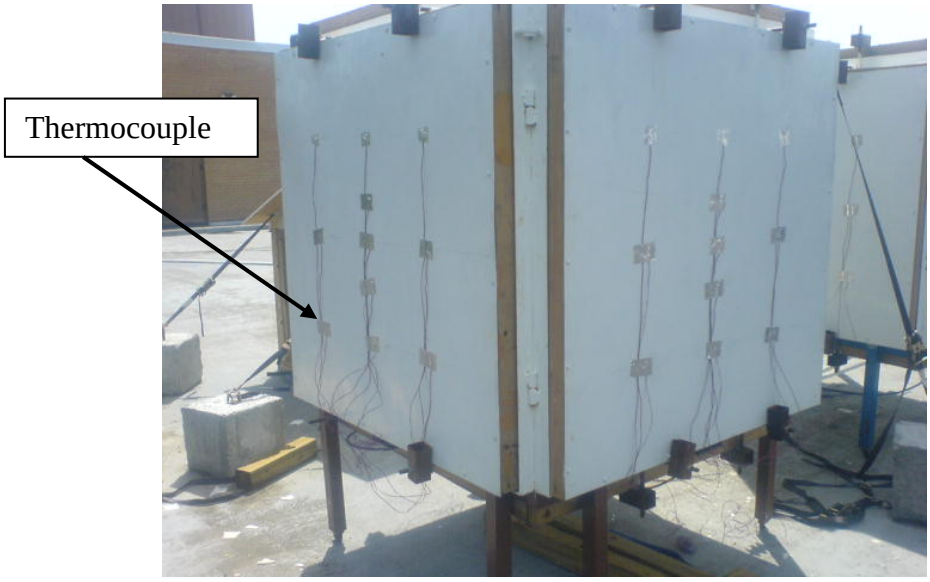

Figure 17. Thermocouple grid on the outside surfaces of the simulator wall

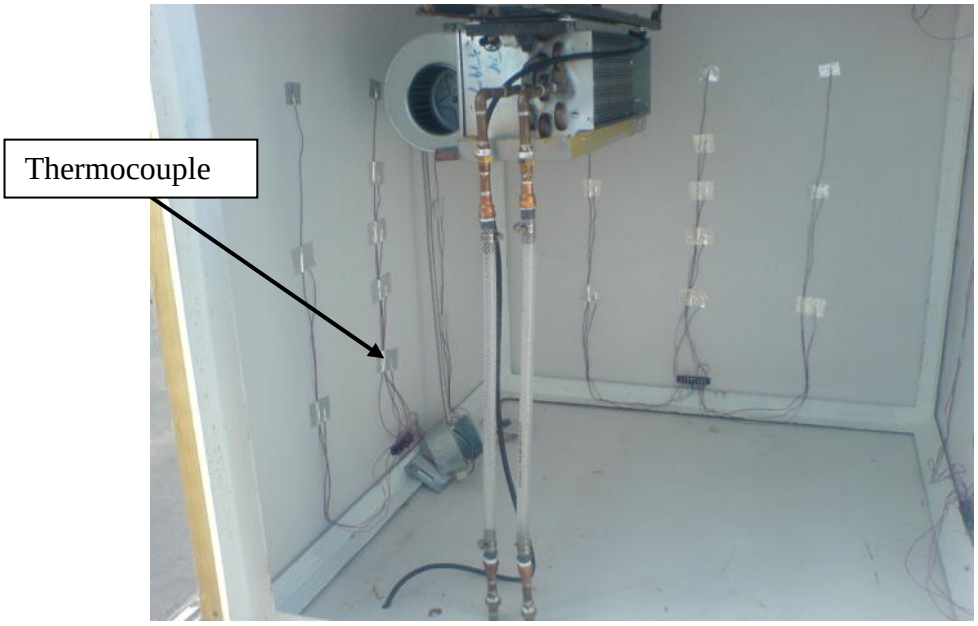

Figure 18. Thermocouple grid on the inside surface of the simulator wall

Measurement of the various parameters was one of the most crucial parts of the project. Table 2 shows their range, accuracy and sensitivity. Figures 19 and 20 show the remote thermostat and its controller respectively. It was set to 4°C (39.2 °F) and the deadband was 0.5 °C (0.9 °F), which was the lowest possible deadband temperature.

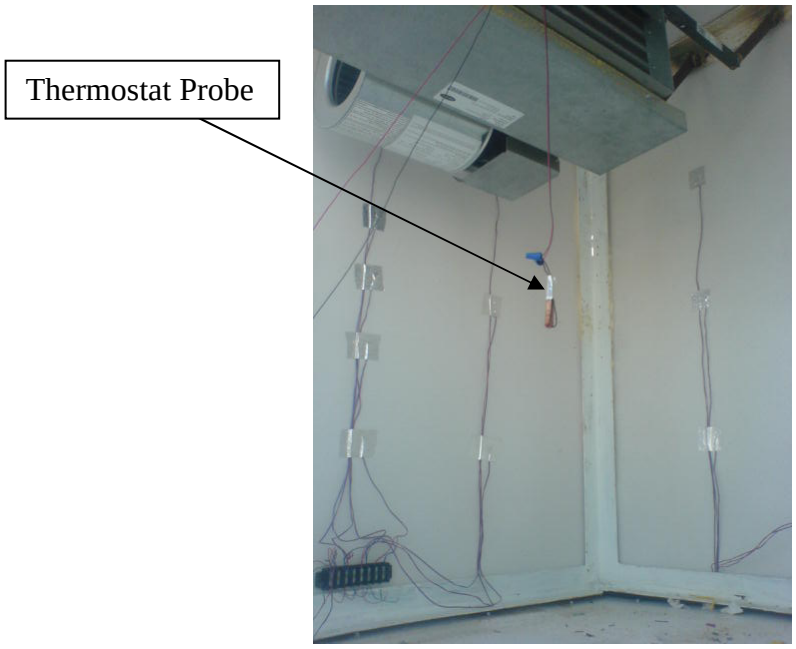

Figure 19. Thermostat probe inside the simulator

Figure 21 shows the heat flux meters. Two heat flux meters were installed on each of the south, east and top walls. One heat flux meter was installed in the north and west walls. Also, a weather station was set up near the simulators on the roof of Learned Hall (the building where the School of Engineering is located). The weather station was modular. As a standard unit, the weather station had temperature, relative humidity, wind speed, wind direction, and pressure measurement sensors. The sensors of the weather station were connected to a computer for data collection and storage.

An incident spectral pyranometer was placed on-site, which measured the total solar spectral radiation. Figure 22 shows the weather station. Figure 23 shows the pyranometer.

Figure 20. Remote thermostat controller inside the controls shed

Figure 21. Heat flux meters

Table 2. Sensors used and their range, accuracy and sensitivity

Sensor	Range	Accuracy	Sensitivity
Heat Flux Meter	0 to 3.1×10^{5} W/m^2	2%	-
	(0 to 9.83×10^{4} Btu/hr ft^2)		
Thermocouple T Type	-18 to +93°C	0.6°C	-
	(-0.4 to 199.4°F)	(1.08°F)	
Pyranometer	-20 to 40°C	±1%	8.82×10^{-6}
	(-4 to 104°F)		volt/W.m^{-2}
Water Flow Meter	1.89 to 56.78 l/min	±2%	4-20 mA
	(0.5 to 15 gpm)		
Thermostat	-4.44 to +104.44°C	±0.56°C	4.8 ohms/°F
	(24 to 220°F)	(1.008°F)	
Atmospheric Pressure*	717.4 to 780.5 mm Hg	1.27 mm. Hg	-
	(0.943 to 1.027 Atm. Pr.)	(0.05 in. Hg)	
Rain Fall Sensor*	Unlimited	±4%	-
Relative Humidity*	0 to 100%	±3%	-
Wind Speed*	0 to 55.9 m/s	±0.45 m/s	-
	(0 to 183.40 ft/s)	(1.48 ft/s)	
Wind Direction*	0 to 360°	±3%	-
Outdoor Temperature*	-4.44 to +60°C	±0.6°C	-
	(24 to 140°F)	(1.08°F)	

* Components of the Weather Station.

Figure 22. Weather station with anemometer, rain fall measurement device, and relative humidity measurement device

Figure 23. Solar spectral pyranometer

6. Data Acquisition System

All of the measurement devices were connected to a data acquisition system. The unit is shown in Figure 24. The data logger was an Agilent 34970A data logger. Three 20-channel multiplexers were used for all of the connections. One RS 232 connection was used between the data logger and the computer which was controlled by proprietary software. Similar connections were made between the weather station and the computer. Data from the computer was downloaded to other work stations for post processing analysis and archiving. The computer and the desktop unit used by the weather station are shown in Figure 25.

Figure 24. Agilent 34970A data logger

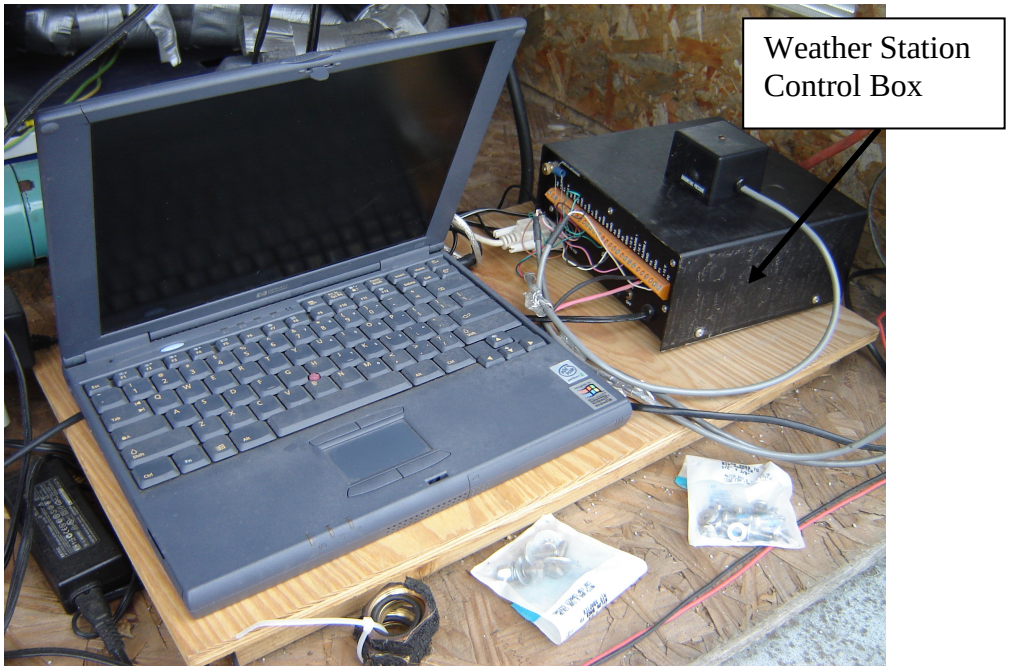

Figure 25. Laptop computer (left) and data acquisition unit for the weather station (right)

A complete list of channels used and descriptions of monitored points is given in Tables 3, 4 and 5. Three multiplexer cards were used for collecting the monitored variable measurements. Card number 1 was used for miscellaneous connections related to the simulators, tank and ambient temperature. The second card was used only for thermocouple connections, and card number 3 was used to connect all of the heat flux sensors. Some of the measurements in card 1 were duplicated considering the weather station being in place, like the ambient temperature. It was a good opportunity to observe the agreement between the thermocouple reading and the weather station data.

Table 3. Channel list: Card number 1* – Miscellaneous

Port Number	Abbreviation	Description
101	AAT	Ambient Air Temperature
102	SAT	Shed Air Temperature
103	TFT	Tank Coolant Temperature
104	PAT	PCM-enhanced Simulator Air Temperature
105	RAT	Control Simulator Air Temperature
106	PST	PCM-enhanced Simulator Supply Temperature
107	PRT	PCM-enhanced Simulator Return Temperature
108	RST	Control Simulator Supply Temperature
109	RRT	Control Simulator Return Temperature
112	PYR	Pyranometer (8.82×10^{-6} volt/W.m^{-2})
121	RFM	Control Simulator, Flow Meter $(0.90625\times mA - 3.125)^{\Pi}$
122	PFM	PCM-enhanced Simulator, Flow Meter $(0.90625\times mA - 3.125)^{\Pi}$

* Ports 110, 111, 113, 114, 115, 116, 117, 118, 119, and 120 were not used

$^{\Pi}$ Linear equation derived for the flow meter to obtain the flow rate in gallons per minute

The thermocouple grid network installed in each wall surface connected to one port. That is, the T/Cs were connected in parallel so that the one reading into the port was a representative temperature reading for the entire wall surface. The list of the heat flux sensors is given in Table 5. Each heat flux sensor had a specific color code to identify its exact location. Also, each sensor had different constant to convert from mV data to W/m^2 data. Walls in which one heat flux meter was installed, the top left location as shown in Figure 16 was selected.

Table 4. Channel list: Card number 2* – Temperature

Port Number	Abbreviation	Description
201	RNOT	Control Simulator, North Wall Outside Surface Temperature
202	REOT	Control Simulator, East Wall Outside Surface Temperature
203	RSOT	Control Simulator, South Wall Outside Surface Temperature
204	RWOT	Control Simulator, West Wall Outside Surface Temperature
205	RTOT	Control Simulator, Top Wall Outside Surface Temperature
206	RNIT	Control Simulator, North Wall Inside Surface Temperature
207	REIT	Control Simulator, East Wall Inside Surface Temperature
208	RSIT	Control Simulator, South Wall Inside Surface Temperature
209	RWIT	Control Simulator, West Wall Inside Surface Temperature
210	RTIT	Control Simulator, Top Wall Inside Surface Temperature
211	PNOT	PCM-enhanced Simulator, North Wall Outside Surface Temperature
212	PEOT	PCM-enhanced Simulator, East Wall Outside Surface Temperature
213	PSOT	PCM-enhanced Simulator, South Wall Outside Surface Temperature
214	PWOT	PCM-enhanced Simulator, West Wall Outside Surface Temperature
215	PTOT	PCM-enhanced Simulator, Top Wall Outside Surface Temperature
216	PNIT	PCM-enhanced Simulator, North Wall Inside Surface Temperature
217	PEIT	PCM-enhanced Simulator, East Wall Inside Surface Temperature
218	PSIT	PCM-enhanced Simulator, South Wall Inside Surface Temperature
219	PWIT	PCM-enhanced Simulator, West Wall Inside Surface Temperature
220	PTIT	PCM-enhanced Simulator, Top Wall Inside Surface Temperature

* Ports 221 and 222 were not used

Table 5. Channel list: Card number 3* – Heat Flux Meters

Port Number	Abbreviation	Description	Color	(W/m^2)/ mV
301	RNHF	Control Simulator, North Wall Heat Flux Meter	Orange	4.1
302	RWHF	Control Simulator, West Wall Heat Flux Meter	Blue	6.82
303	RSWHF	Control Simulator, South-West Wall Heat Flux Meter	Brown	4.66
304	RSEHF	Control Simulator, South-East Wall Heat Flux Meter	Green	4.55
305	RENHF	Control Simulator, East-North Wall Heat Flux Meter	Green	4.73
306	RESHF	Control Simulator, East-South Wall Heat Flux Meter	Blue	6.66
307	RTNHF	Control Simulator, Top-North Wall Heat Flux Meter	Orange	4.1
308	RTSHF	Control Simulator, Top-South Wall Heat Flux Meter	Brown	6.8
311	PSWHF	PCM-enhanced Simulator, South-West Wall Heat Flux Meter	Orange	4.33
312	PSEHF	PCM-enhanced Simulator, South-East Wall Heat Flux Meter	Blue	4.66
313	PWHF	PCM-enhanced Simulator, West Wall Heat Flux Meter	Green	6.5
314	PNHF	PCM-enhanced Simulator, North Wall Heat Flux Meter	Brown	4.54
315	PTNHF	PCM-enhanced Simulator, Top-North Wall Heat Flux Meter	Green	4.62
316	PTSHF	PCM-enhanced Simulator, Top-South Wall Heat Flux Meter	Brown	7.02
317	PESHF	PCM-enhanced Simulator, East-South Wall Heat Flux Meter	Blue	6.51
318	PENHF	PCM-enhanced Simulator, East-North Wall Heat Flux Meter	Orange	4.58

* Ports 309, 310, 319, 320, 321 and 332 were not used.

7. PCM Selection

PCMs are categorized based on whether they are organic or inorganic and also based on their melting point ranges and latent heats of fusion. Based on the inside temperature of the simulators, 4°C (39.2°F), and the average outdoor temperature of the experimental set up location, several PCMs were short listed. An in-house computer program that simulated PCMs in actual working condition was used to facilitate the selection process. Theoretically, a PCM with higher solidification temperature and lower melting temperature than the inside temperature would have been desirable. Since the computer program yielded better results for PCM RT-5, which has both solidification and melting temperatures higher than the inside temperature, it was selected for the experiment. RT-5, a paraffin-based PCM, is shown in Figure 26. Table 6 lists the properties of RT-5.

Figure 26. Sample of RT 5

Table 6. Properties of PCM RT-5 [27]

Property	Description
Melting Point (approx.)	7°C (44.6°F)
Congealing Point (PCM)	5°C (41°F)
Heat Storage Capacity (-5°C to 10°C) (23°F to 50°F)	156 kJ/kg (67.07 Btu/lb)
Density Solid (at -15°C) (5°F)	0.86 kg/l (53.69 lb/ft^3)
Density Liquid (at 15°C/70°C) (59°F/158°F)	0.77/0.73 kg/l (48.07/45.57 lb/ft^3)
Volume Expansion	10 %
Volume Expansion γ (w/o phase change)	0.001 1/K
Specific Heat Capacity	1.8/2.4 kJ/kgK (0.43/0.57 Btu/lb°F)
Heat Conductivity	0.2 W/mK (0.12 Btu/hrft°F)
Kinematic Viscosity (at 40°C) (104°F)	2.6 mm^2/s (27.98 ft^2/s)
Flash point (PCM)	122°C (251.60°F)
Corrosion	Chemically inert with respect to most materials
Water Hazard	Water hazard class (WGK) 1

8. Refrigeration Load Calculations

The refrigeration load required by the simulators was calculated using ASHRAE's [28, 29] prescribed load calculation method. The principles of cooling load calculation for a building envelope were used to get an idea about the load requirements for the van trailer simulators. Although more complex methods can be used for the estimation of refrigeration loads in commercial refrigeration involving van trailers, a simplified method prescribed by ASHRAE was used mainly because of the nature of the experiments performed in this research. The following basic cooling load equation was used.

Total Cooling Load (refrigeration load) = Heat Transmitted + Internal Load + Infiltration …… Equation (1)

Heat transmitted is the heat transfer across the walls, infiltration is the heat gain as the result of unwanted air entering from the outside, and internal load is the heat generation from lights, motors, fans in the fan coil units, etc. As mentioned earlier, the inside of the simulators were held at a constant 4°C (39.2°F). A design maximum ambient temperature of 35°C (95°F) was selected from the meteorological data of Lawrence, KS. An estimated heat gain of 5% of the internal load was considered as the infiltration heat load according to ASHRAE handbook [29]. The following heat gain formula was used to calculate the heat transfer rate across the insulated walls,

$$Q = U \times A \times \Delta T \quad \text{Equation (2)}$$

The temperature difference is between the interior and exterior surface temperatures of the walls.

The U-factor was the overall heat transfer coefficient of the wall. It is a function of thermal resistance and is expressed as,

$$UA=1/R \quad \text{Equation (3)}$$

Thermal resistance 'R' is an additive term, which implies for any direction of heat flow, all of the surface resistances in that direction would be added up to give the total thermal resistance. Equation (4) shows the total thermal resistance of the walls for the experiment.

$$R_{TOTAL}=R_{ALUMINUM\ SHEET}+R_{FOAM\ INSULATION}+R_{GLASSBOARD} \quad \text{Equation (4)}$$

The load calculation guides the whole process of selection of the equipment. In order to estimate the refrigeration load, the data for the hottest time of the year was used.

Chapter IV: Results and Discussion

1. Calibration

The two van trailer simulators were thermally calibrated before their use. This is depicted in Figure 27. Although the refrigeration units were off, it was evident that the PCM-enhanced simulator showed the characteristics observed in the performance of systems outfitted with PCM (e.g., the energy storage from 3 AM to 12 PM). The inside air temperature of both of the simulators followed the outside air temperature with slight time delay, which was reflected in the shift of the inside peak temperature by almost three hours for both simulators. Also, there was a rapid temperature drop as compared to the temperature rise inside the simulators at the later part of the day. This can be explained by the fact that the outside temperature was significantly lower than the inside temperature for that part of the day. As a result, the heat release accelerated, and the temperature fell at a faster rate. A similar explanation is applicable for the first part of the day. The insulation resisted the heat flow into the simulators; therefore, the temperature rise of the simulators occurred at a slower rate than the temperature rise of the surroundings. The closeness of the temperature between the two simulators was of great importance as the rest of the analysis was reinforced by this observation.

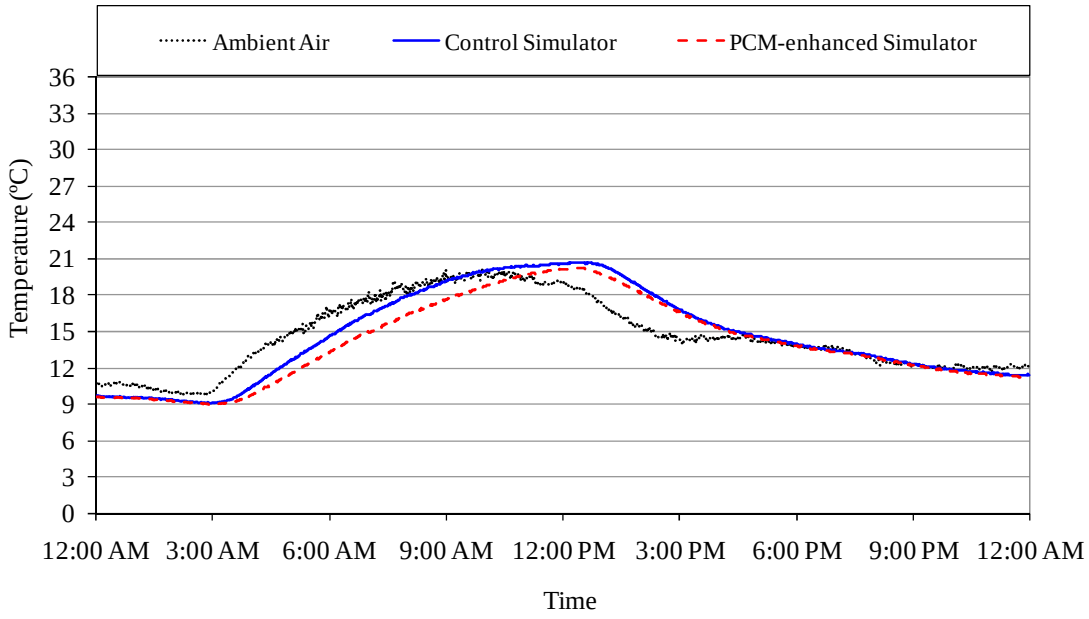

Figure 27. Inside air temperatures in the van trailer simulators during the calibration period

As has been mentioned earlier, the walls were fitted with thermocouples and heat flux meters. Figures 28 to 30 show the inside and outside temperatures of these surfaces. The graphs presented here show the surface temperatures in the absence of any refrigeration. These graphs are a clear indication of very close outside surface temperatures of the simulators. The magnitudes of the temperatures were in close agreement except for the north wall, where a lower PCM-enhanced outside wall temperature and a sudden drop in the control outside wall temperature was observed. This sudden change can be attributed to the measurement devices as no other environment or control parameters had changed. It is also worth noting that the inside wall temperatures of the PCM-enhanced simulator were lower than those of the control simulators' inside wall temperatures for most of the experiments.

In the latter part of the day, when the outside surface temperature of the wall dropped rapidly, the PCM once showed its effectiveness. Theoretically, the PCM-enhanced simulator should have had a higher inside wall temperature than that of the control simulator because it was supposed to release the heat absorbed in the earlier part of the day. Instead, the steady inside wall temperature decrease of the PCM-enhanced wall along with the control simulator wall, proved the PCM behavior of heat storage throughout that period. Although no clear evidence of the state of the PCM is known, it is safe to consider that, not all of the heat absorbed by the PCM was released into the simulator during the latter part of the day. Consequently, the performance of the PCM could be summarized by two observations. First, it slowed down the rise of the inside surface temperature for the earlier part of the day; and second, it kept the inside wall temperature of the PCM-enhanced wall the same as that of the control wall by not releasing heat adversely during the latter part of the day.

The data for the control and PCM-enhanced simulators prior to any refrigeration were of importance for setting the baseline for future comparison of the effect of the PCM in the performance of the PCM-enhanced walls. These analyses could be used to predict the behavior of PCM-enhanced van trailer walls that do not require refrigeration. It is worthwhile to mention for further clarification, that some of the trucks are only insulated and not refrigerated. Although exact data are not available for this category, it is believed that a significant number of trucks which transport goods have only insulated walls but do not require any refrigeration.

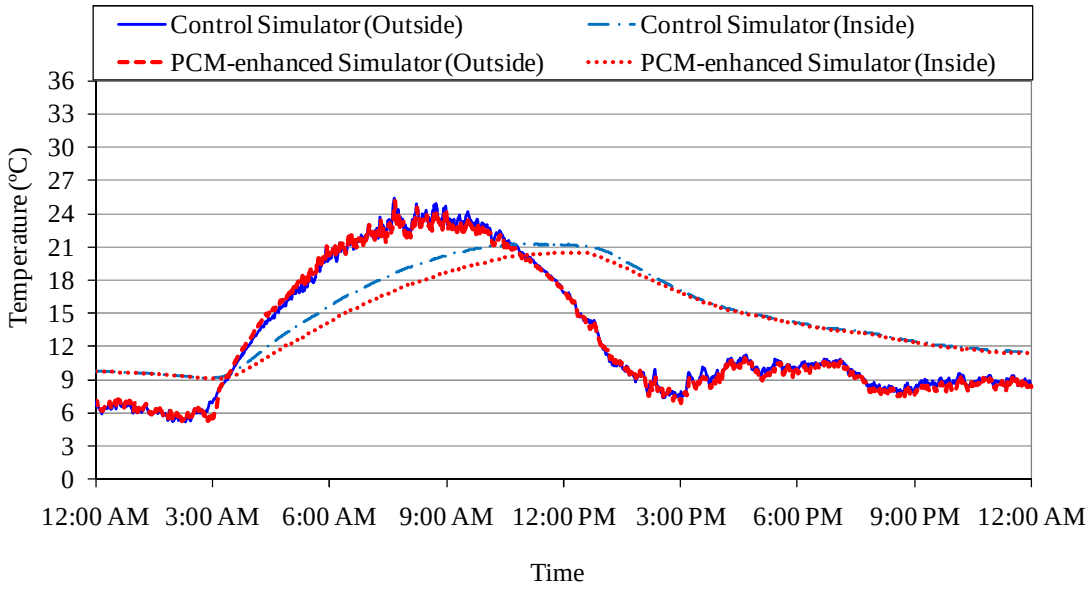

Figure 28. Outside and inside surface temperatures of the south wall

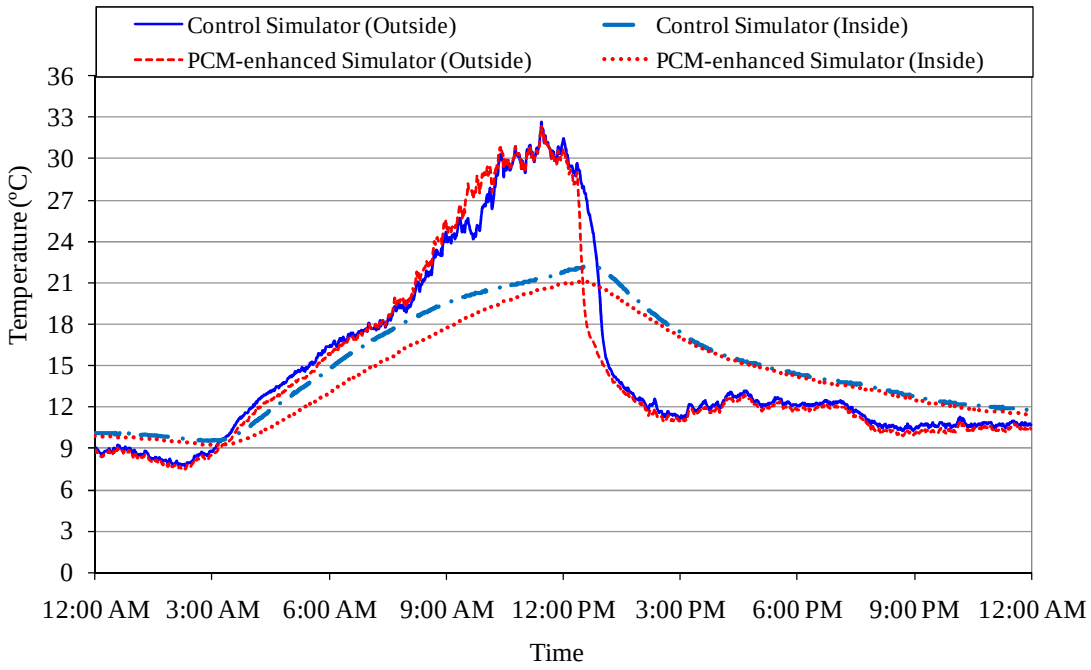

Figure 29. Outside and inside surface temperatures of the east wall

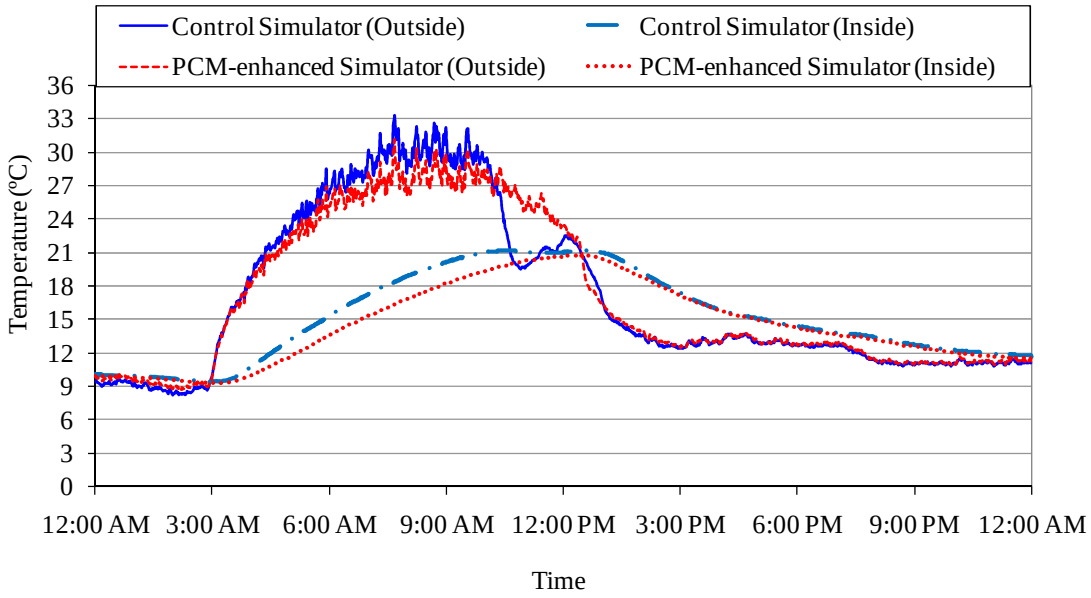

Figure 30. Outside and inside surface temperatures of the top wall

2. Single-Day Data Comparison

At the beginning of this research, the experiments were conducted on one refrigerated trailer simulator at a time. Therefore, either the PCM-enhanced simulator or the control simulator was used for an entire day, while the other simulator was idle. As the days may have been different during the testing of each simulator, it was necessary to compare only those days in which the ambient conditions were comparable. The solar spectral pyranometer and weather station data were used to select those days with similar weather data. Two comparable days, in terms of insolation and outdoor air temperature, were selected for the analysis. Figures 31 and 32 give an indication of the closeness of these two days.

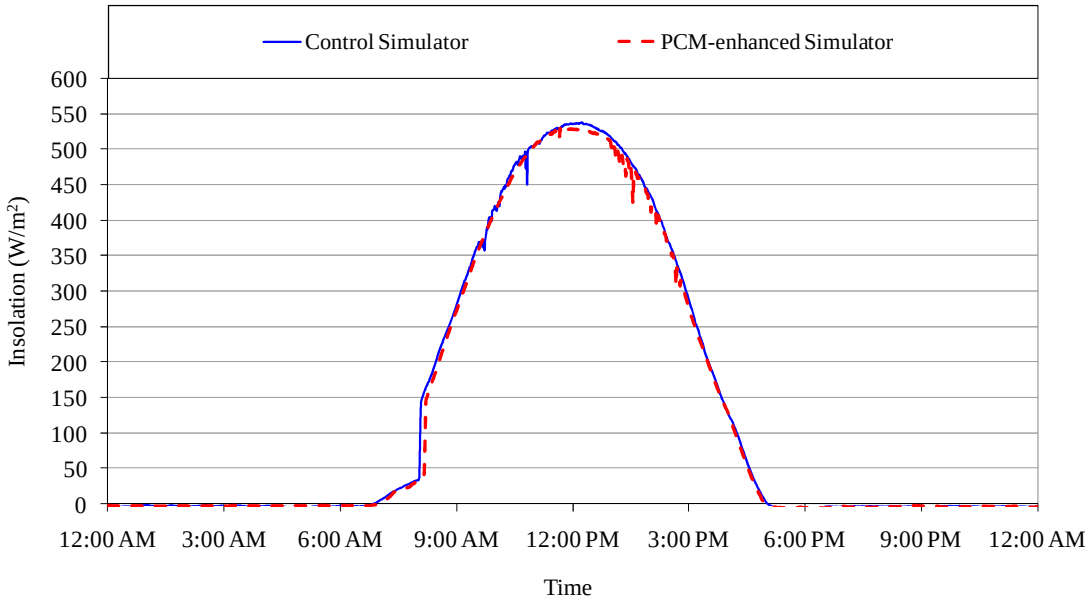

Figure 31. Spectral solar irradiation comparison for the days when the control and PCM-enhanced van trailer simulators were subjected to thermal testing

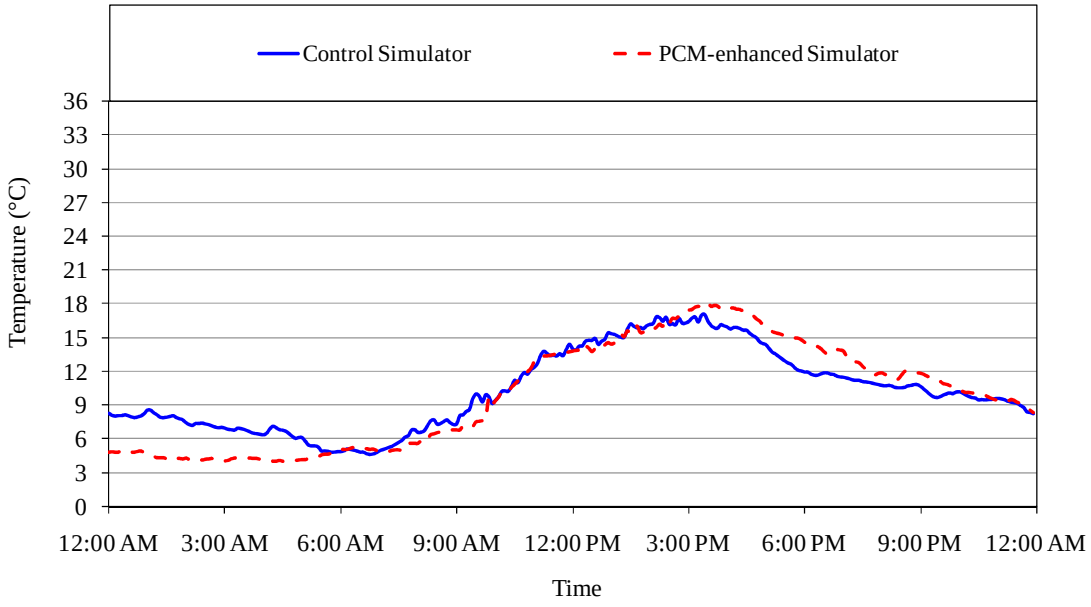

Figure 32. Ambient air temperature comparison for the day when the control and PCM-enhanced van trailer simulators were subjected to thermal testing

Inside air temperatures of both simulators are presented in Figure 33 and as mentioned earlier, the set point temperature for the experiments was 4°C (39.2°F). The figure difference illustrates the inside air temperature difference between the two simulators. Figure 33 also shows noticeable fluctuations in the graph that represent the on-off cycles of the fan coil unit. In the middle part of the day (from 9 AM to 3 PM), fluctuations occurred more frequently than for the rest of the day. A major solar heat gain occurred within that timeframe. Although the span of the fluctuations for both simulators was identical in terms of maximum magnitude and width of the span, the PCM-enhanced simulator displayed a slightly lower temperature than the control simulator. An average inside air temperature of 3.80°C (38.84°F) for the PCM-enhanced simulator and 4.01 (39.23°F) for control simulator were recorded. The

analysis compares the inside temperatures of the simulators with respect to the ambient air temperature of the PCM-enhanced simulator. Since, Figure 32 shows the agreement in ambient air temperatures of both days, the temperature when PCM-enhanced simulator was under experiment was taken as the reference for Figure 33.

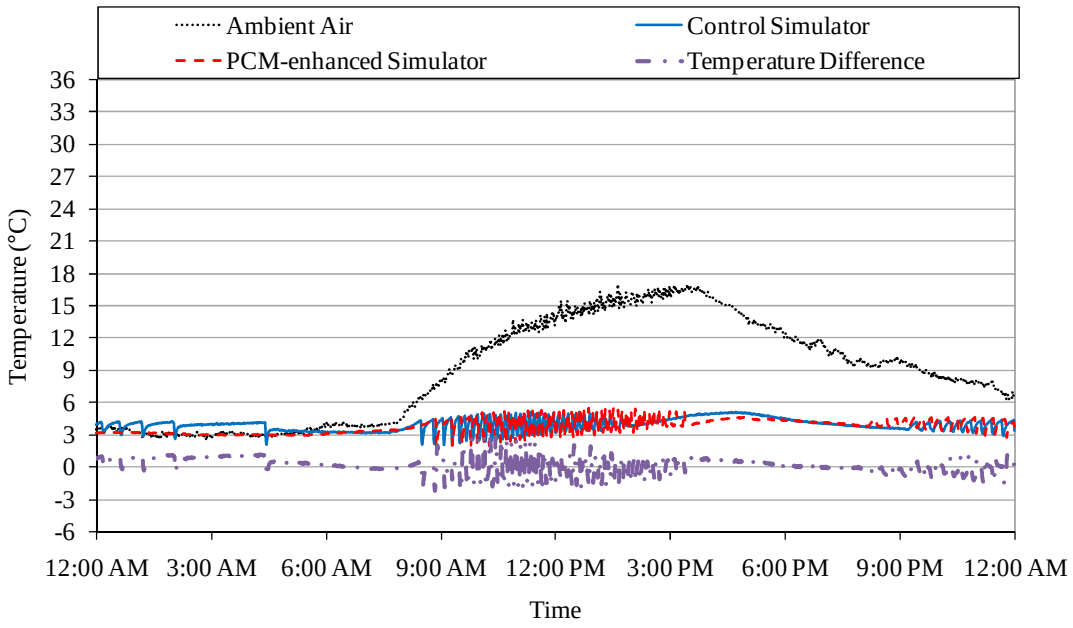

Figure 33. Inside air temperature of the simulators and ambient air temperature

Heat flux data for the south, east, north, west and top walls of the refrigerated van trailer simulators were collected. The graphs are presented in Figures 34 through 39. Figure 34 depicts the data for the south walls. The data lines in the graph depict the heat transfer rates per unit area across the south facing wall panels of the simulators. The heavy solid line represents the heat flux across the control simulator and the lighter dashed line represents the heat flux across the wall panel outfitted with PCM.

The graph clearly shows a reduction in peak heat transfer rate as well as a reduction in overall heat flow into the inside of the refrigerated trailer for the entire day. This is represented by the area under the curves.

Starting at approximately 9 AM, the PCM in the PCM-enhanced wall panel was in the process of melting. The shift in peak heat transfer rate, of a couple of hours, is also noticeable. That is, the heat flux across the wall in the control simulator peaked at about 1 PM while the heat transfer rate across the wall of PCM simulator peaked at a time closer to 3 PM. The peak heat flux reduction, as a result of using the PCM, was approximately 34.5%.

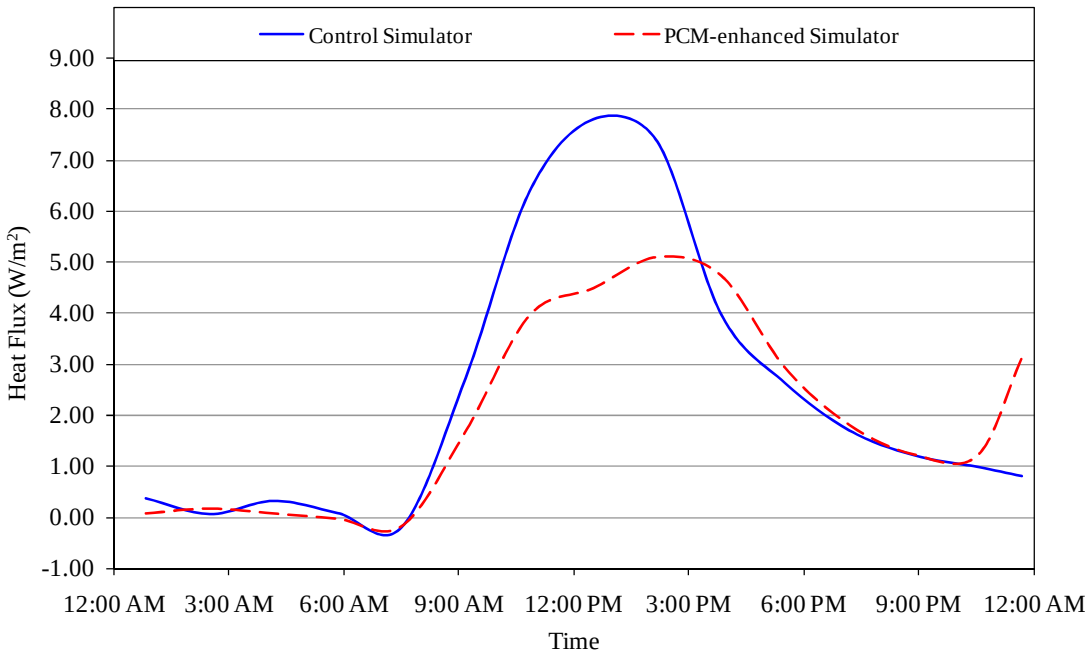

Figure 34. South wall heat fluxes

In Figure 35, which depicts the heat transfer rates for the east walls, also shows a significant reduction in both peak heat transfer rates and overall heat flow into the PCM-enhanced van trailer simulator of 42.5% and 27.7%, respectively. Also, the peak heat transfer rate for the control wall peaked at about 10:30 AM while the peak heat flux in the PCM-enhanced wall peaked at about 2:30 PM.

Figure 36 illustrates the comparison in thermal behavior of the north walls. The graph shows that in walls where the solar irradiation was substantially lower, the effects of using PCM were virtually non-existent. Although the data in Figure 30 came from days that were almost identical with respect to weather, the slightly higher outdoor air temperatures during the days when the PCM-outfitted simulator walls were tested, gave a slightly higher peak heat transfer rate in the PCM wall of 8.9% and 5.4% more total heat flow into the PCM-enhanced simulator.

Figure 37 depicts the heat transfer rates across the west walls. These data show a reduction in overall heat flow into the PCM-enhanced simulator of 12%. The peak heat transfer rate data, however, show an increase in the heat transfer rate of 6.2%. This is probably the result of having a slightly higher outdoor air temperature during the testing of the PCM-enhanced panels.

Figure 38, which is the representation of the heat transfer rate data for the top wall of the refrigerated simulators, shows a significant reduction in both peak heat transfer rate and overall heat flow into the PCM-enhanced simulator of 29.7% and 9.9%, respectively. A peak heat transfer shift of approximately 2-1/2 hours was observed.

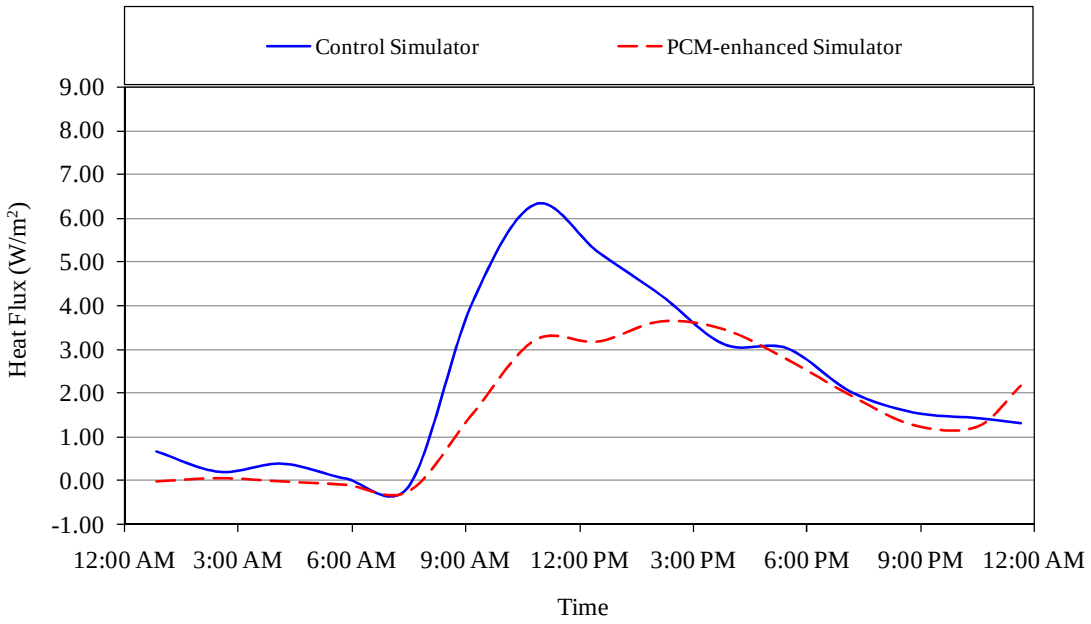

Figure 35. East wall heat fluxes

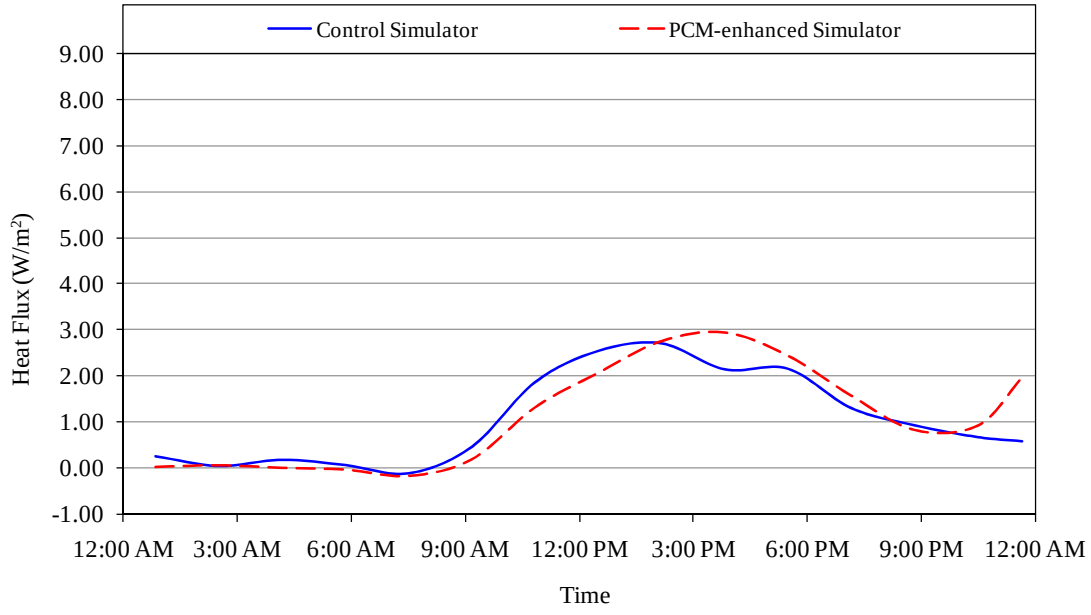

Figure 36. North wall heat fluxes

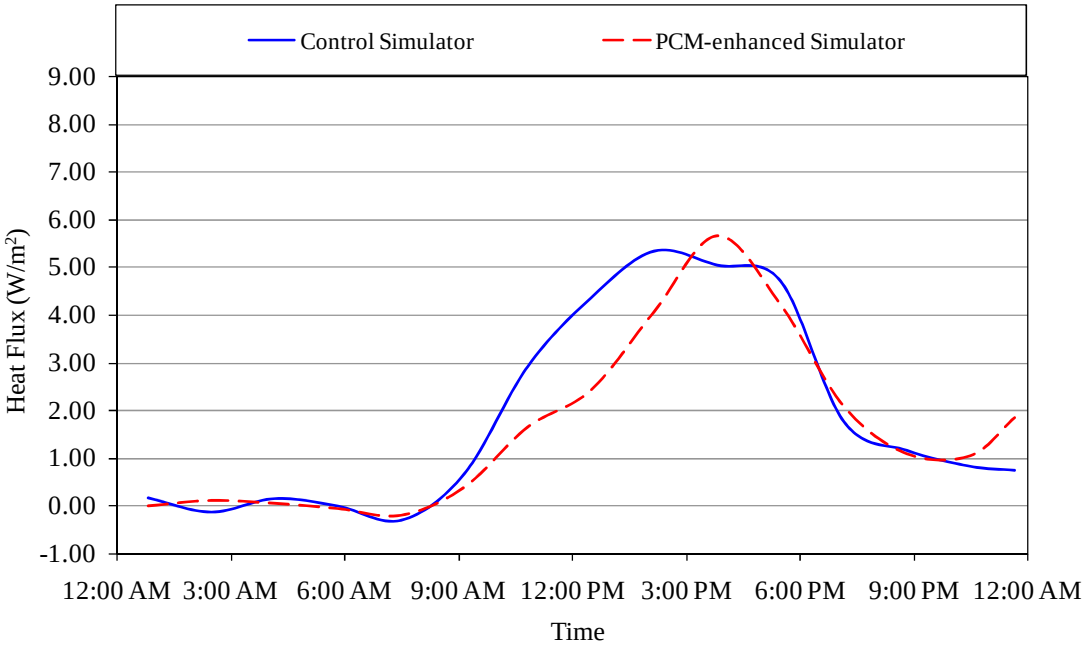

Figure 37. West wall heat fluxes

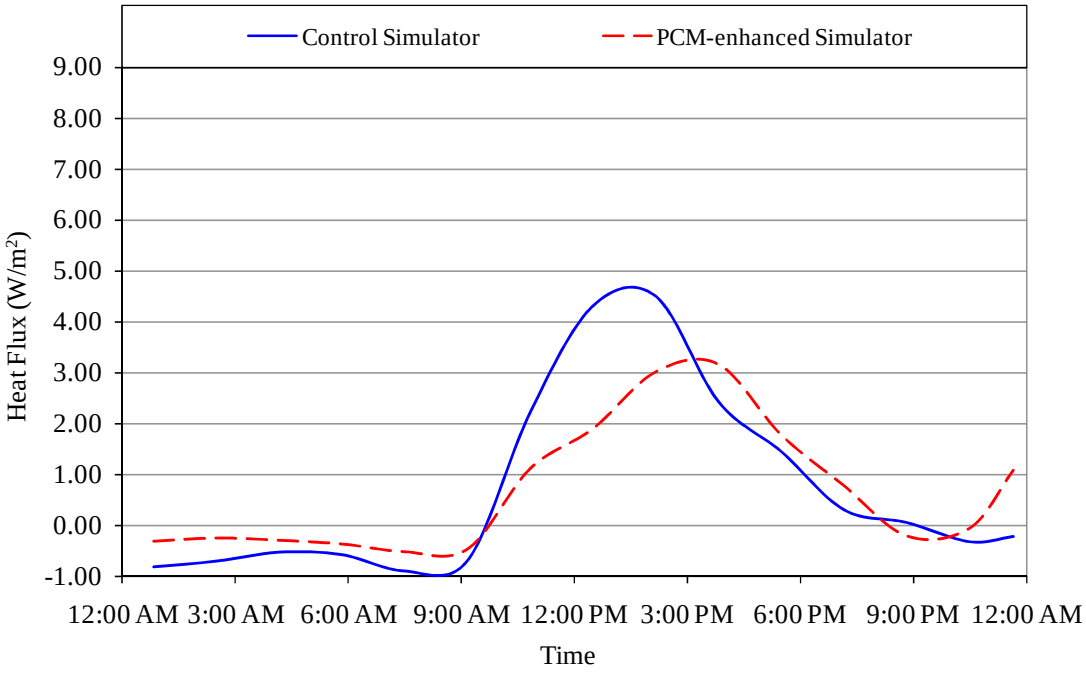

Figure 38. Top wall heat fluxes

The heat fluxes for all the surfaces are additive terms, thus a total wall heat flux can be calculated from all surfaces. Figure 39 shows the total wall heat flux, where the dependent axis, heat flux, has been scaled up three times from single wall heat flux graphs. Peak and total heat load reduction were observed for the PCM-enhanced simulator. A reduction of 18.3% in peak heat flux and 12.3% in total heat flow were achieved. Also, the heat flux data of the PCM-enhanced simulator dampened the fluctuation observed in the unfiltered data for the simulators. A decrease in heat flux fluctuation can be interpreted as fewer on and off times for the refrigeration unit.

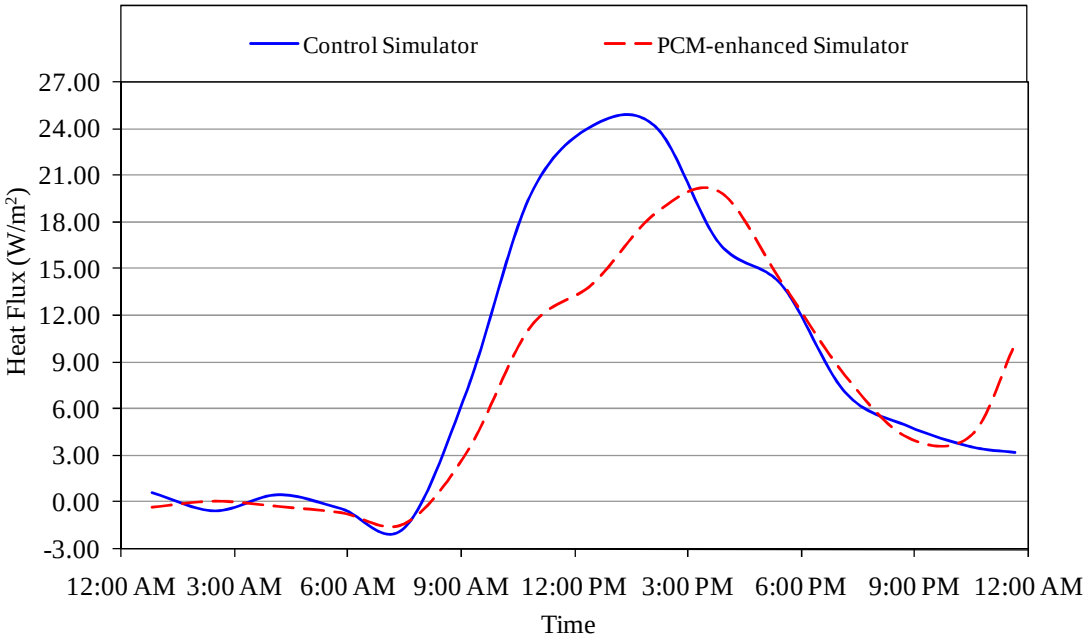

Figure 39. Total heat fluxes combining all five wall heat fluxes

Figures 40 and 41 summarize the peak heat transfer rate data and total heat flow reduction into the refrigerated space of the simulators. These results could have been higher had the outdoor air temperature during the testing of the PCM-enhanced simulator been identical to the outdoor air temperature during the testing of the control simulator. The outdoor air temperature during the PCM-enhanced simulator test was 1 to 2°C (1.8 to 3.6°F) higher than the outdoor air temperature of the control simulator test day. However, the results are still promising in which a reduction of 18.3% in peak heat fluxes and 12.3% in overall heat transfer can be achieved. This can potentially translate into smaller refrigeration units as well as lower fuel use to power the refrigeration units.

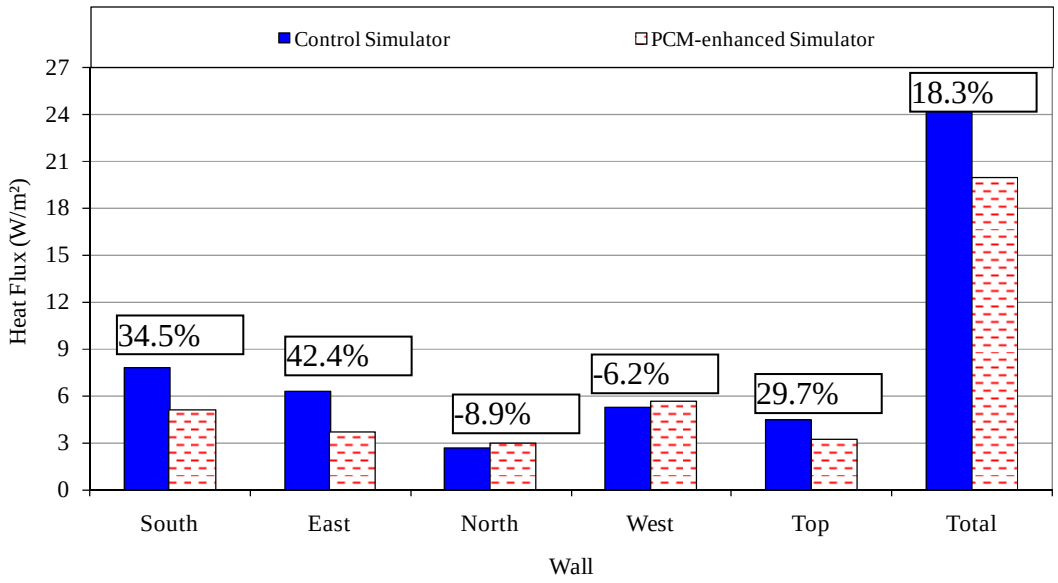

Figure 40. Peak heat flux and corresponding percent reductions

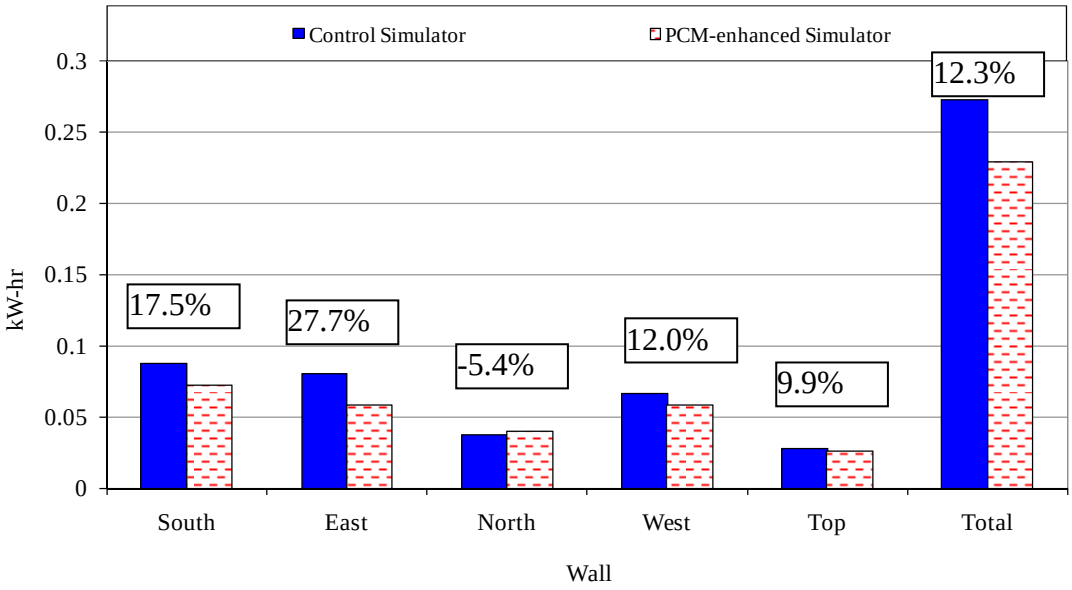

Figure 41. Daily heat energy flows and corresponding percent reductions

3. Wall Surface Temperatures

Another way to look into the effectiveness of the PCM-enhanced walls was to compare the inside and outside surface temperatures with the corresponding wall temperature of the control simulator. Figures 42 to 46 show the surface temperatures of the simulators. The inside and outside surface temperatures of the walls are presented alongside the ambient air temperatures. A uniform indoor surface temperature of the walls close to the desired set point temperature, $4^{o}C$ ($39.2^{o}F$), indicated the performance achieved by the refrigeration unit. Even with the differing outside air temperature, the inside surface temperature was maintained at the desired level. Combined with the fact that the inside air temperature was held to a reasonable set point temperature, it correlates well to a real-world scenario where the indoor temperature is kept constantly at the desired level. Achieving a constant inside wall temperature was vital to understand the scope of PCM usage. The following analysis presents relevant behavior of the PCM-enhanced simulator walls.

The temperature profiles of the outside surfaces of the walls of the control simulator were indicative of their relative position with respect to solar energy gain.

The south wall outside surface temperature of the control simulator, shown in Figure 42, increased rapidly immediately after the sunrise, implying that the solar heat gain occurred instantly on that surface. The aluminum sheet metal, which was used as the outer surface, is a very conductive material, which assisted the process too. The south wall gained the most heat during the middle part of the day, which

surface temperature indicated. The south wall received less solar radiation after 1 PM as the day progressed; and the thereafter, outer surface temperatures started to decrease at around 1 PM. The temperatures fell further and were lower than the ambient temperature after 3 PM. The increase in temperature of the PCM-enhanced simulator outside surface was not as rapid as the control simulator. The peak surface temperature of the PCM-enhanced simulator's south wall was 10°C lower than that of the control simulator. Also, the shift in peak temperature is clearly observable in Figure 42. Although no conclusion regarding the use of PCM affecting the outside surface's wall temperature could be drawn from the analysis, it's a possibility that PCM helped to lower the outside wall temperature.

Generally, when the temperature of the outside surface is much higher than the air temperature, it indicates the use of insulation underneath the outer wall. The outer surface (Al) is conducts heat more rapidly, which is resisted by the insulation material. Therefore, the temperature of the outside surface tends to go up. Since the PCM-enhanced simulator had PCM materials contained in a copper pipe, these pipes were a significant source of heat absorption. For the same amount of heat entering the control and PCM-enhanced simulators, more heat was be absorbed by the PCM-enhanced walls. The heat absorption capacity by the PCM could have been high enough to keep the outside surface temperature low for the earlier part of the day. This idea was further bolstered by the fact that, in the latter part of the day, 3 PM onward in Figure 42, when the PCM started releasing heat, the outward heat flow might have caused the temperature rise at the outside surface.

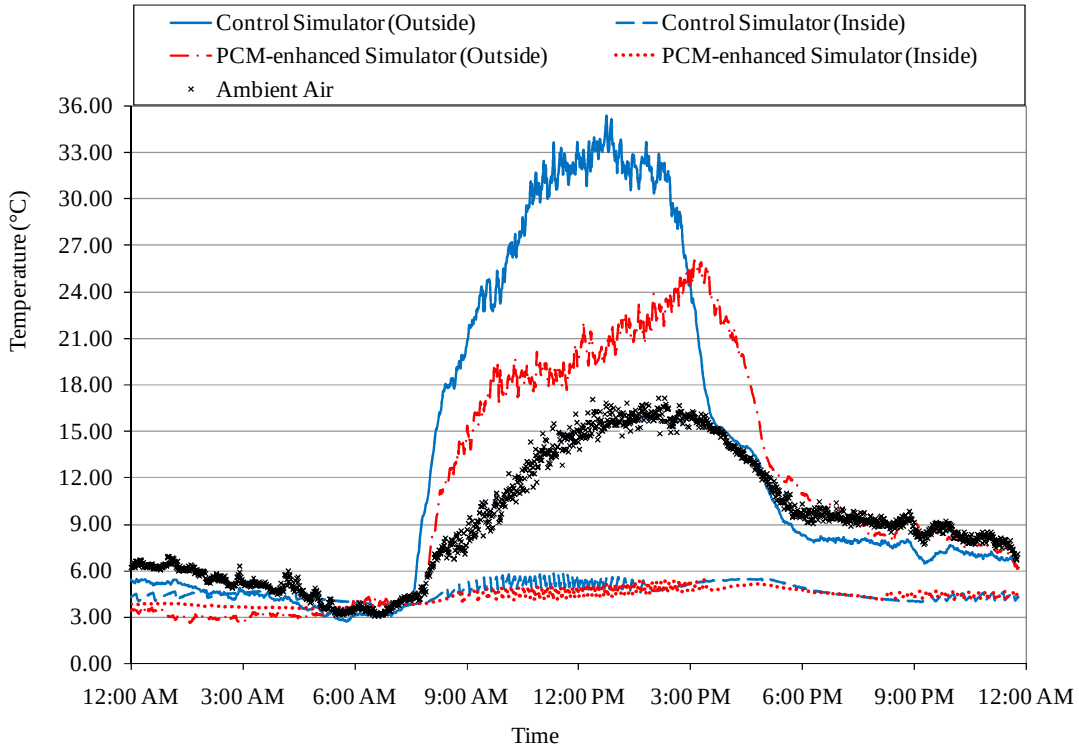

Figure 42. Exterior and interior surface temperatures of south wall

Figure 43 shows how the east walls outside surface temperature responded during the day. A sudden rise in the control simulator's outside surface wall temperature was apparent because of solar radiation hitting the east wall first. After the temperature hike, the temperature stayed at around the 20°C (68°F). There was a temperature drop and rise at around 12 PM. This can be attributed to the fact that, after the initial drop in temperature, which occurred because the sun moved away from the east, the temperature started to rise again because of the overall high ambient temperature. Therefore, the first part of the east wall outside temperature change is attributed exclusively to solar energy gain and the latter part occurred because of the high ambient air temperature.

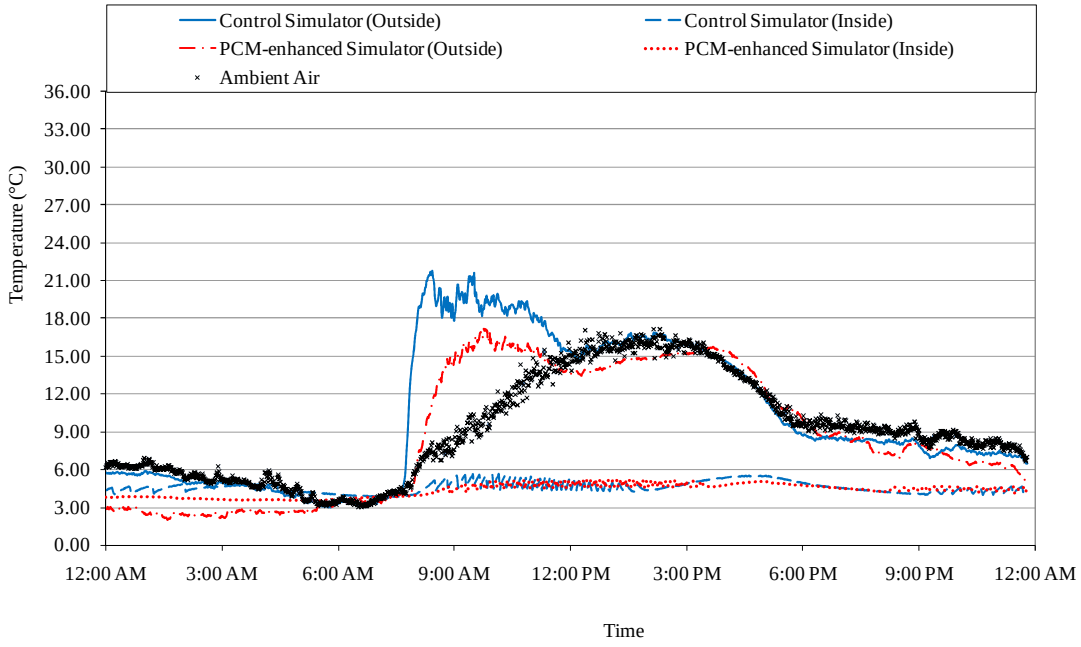

Figure 43. Exterior and interior surface temperatures of east wall

The north wall received the least amount of solar energy and thus was mostly affected by the ambient air temperature. Figure 44 shows the outside surface temperatures, which were the lowest among all the walls, for both simulators. The PCM-enhanced and control simulator outside surface temperatures closely followed the ambient air temperature. Coinciding peak temperatures were also observed between the simulators and ambient conditions. In the latter part of the day, when solar energy gain by the panels had dropped, the north wall exhibited a lower outside surface temperature than that of the surroundings.

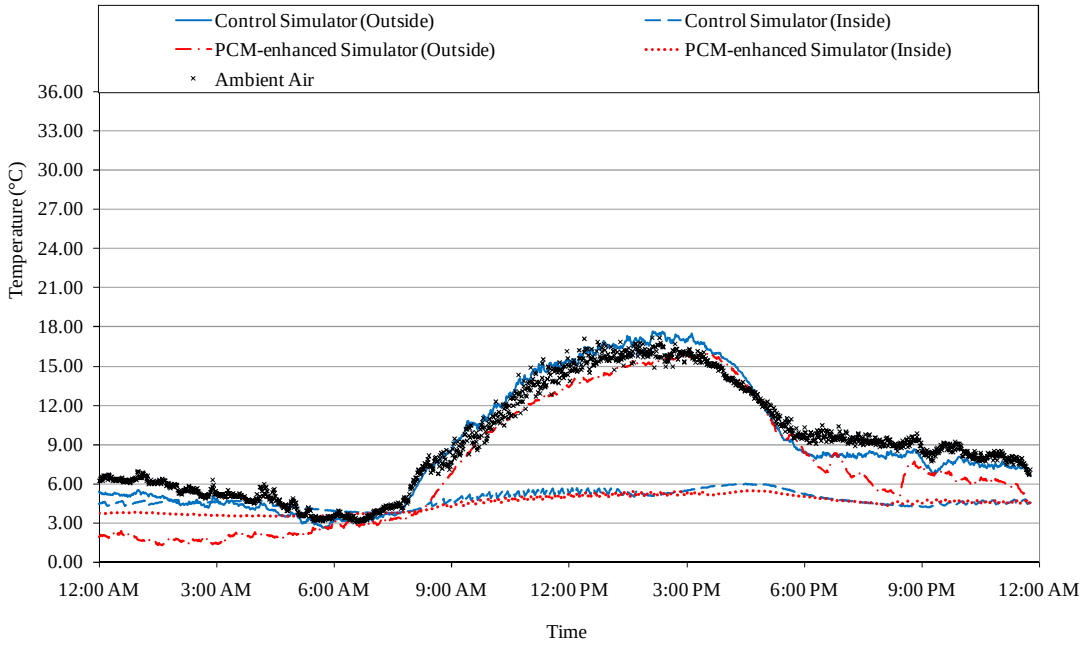

Figure 44. Exterior and interior surface temperatures of north wall

The direct effect of solar heat gain and ambient air temperature also became noticeable in Figure 45. This figure shows the outside surface temperature for both PCM-enhanced and control simulators along with the ambient air temperature. The outside surface temperatures followed the ambient air temperature until mid-day. After that, as the west walls of both simulators started coming under direct solar radiation, the temperatures started to rise. Thus, most solar energy gained by the west wall was evidenced in the temperature peak occurring around 3 PM. The PCM-enhanced and control simulators showed similar temperature patterns. Out of the ordinary situations only occurred when the control simulator's outside wall surface temperature experienced a sudden temperature drop and rise. This was more than the usual temperature fluctuations and was probably caused by control parameters.

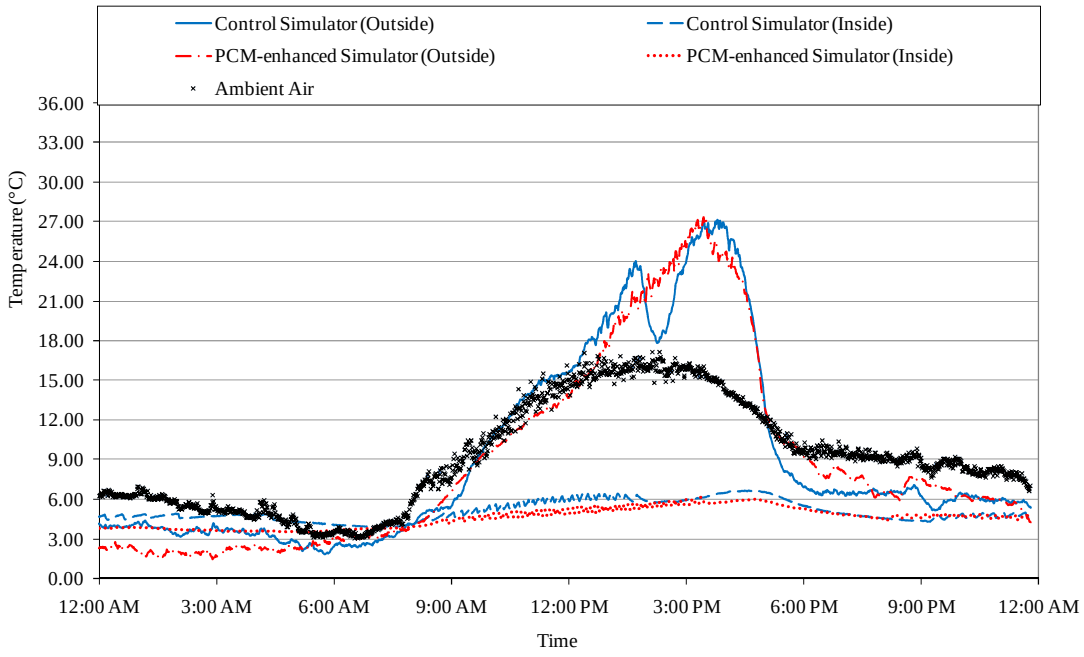

Figure 45. Exterior and interior surface temperatures of west wall

The top wall for both simulators displayed a very symmetrical temperature pattern throughout the day. This is observed in Figure 46. Having the peak temperature around 12 noon, the temperature rise and fall throughout the day was gradual. Unlike the east or west walls, where a peak outside wall temperature occurred fairly quickly, the top wall gained solar heat energy throughout the day and did not show such a rapid temperature rise. Also, the top wall temperature profile was independent of wind direction. This potentially would have carried some heat away from the outside surface of the top wall and eventually assisted in lowering the temperature of the surface.

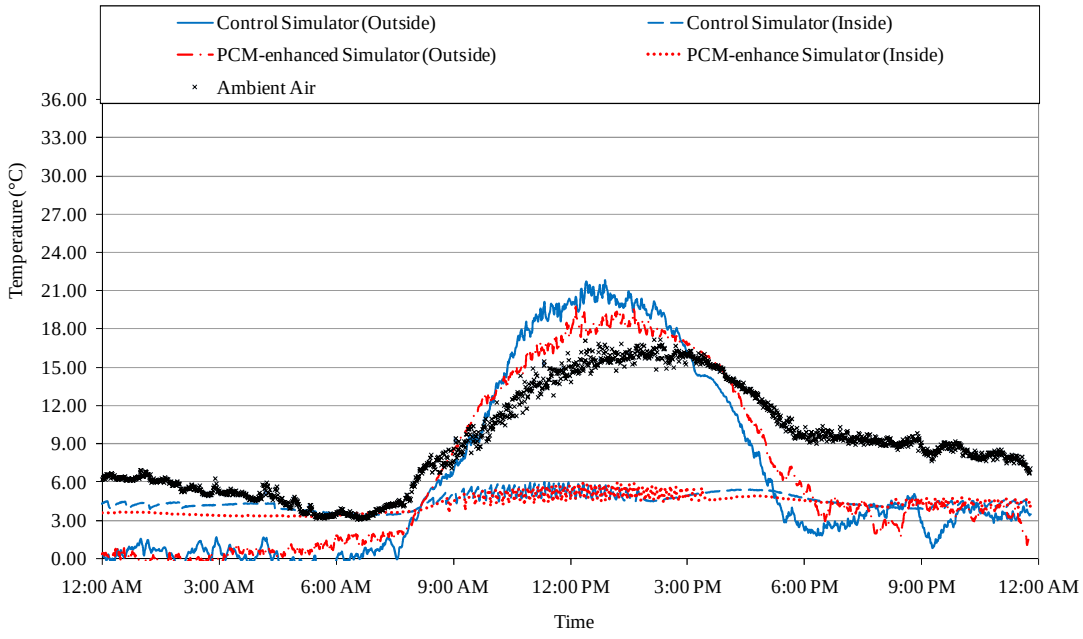

Figure 46. Exterior and interior surface temperatures of top wall

4. Temperature Differences vs. Heat Fluxes

An analysis of temperature difference vs. heat flux values for the various walls revealed further characteristics of the PCM-enhanced walls. As was shown in the previous section, the inside wall temperature remained almost constant, therefore, the higher temperature difference between the outside and inside surfaces would imply a higher outside wall temperature. Figures 47 to 56 show the heat flux behavior with respect to the temperature difference for both the control and PCM-enhanced simulators. The slopes of the trend lines can be viewed as the U-value for the respective wall. A higher U-value is indicative of higher heat transfer rates. The lower U-value of the PCM-enhanced simulator walls for all of the walls demonstrated the potential of the PCM to reduce the heat transfer across the walls.

A positive U-value was expected for all of the walls, whereas, top and north PCM simulator walls resulted in negative values. As most of the values for these two graphs are close to the zero line, it implies more negative temperature differences. Also, the fact should be taken under consideration that, the sensitivity and accuracy of the measuring devices were involved. Thus, sometimes a smaller negative value indicated a zero value or a very low positive value for that instance. It is necessary to comprehend that the idea of labeling different sides of the simulator as south, east, north, and west wall was is to portrait the engine idling case of the trucks. A moving truck would definitely not have such a permanent label throughout its trip. The following table (Table 7) summarizes the percentage reduction in the U-value for south, east and west walls.

Table 7: U-values and reductions produced by the PCMs

Wall	Control, W/m^2K (Btu/hr ft^2 °F)	PCM, W/m^2K (Btu/hr ft^2 °F)	% Reduction
South	0.3650 (0.0643)	0.2161 (0.0381)	40.8%
East	0.4521 (0.0797)	0.0053 (0.0009)	98.8%
West	0.3302 (0.0582)	0.1321 (0.0233)	60.0%
North	0.2634 (0.0464)	-0.1387* (0.0244)	47.3%
Top	0.2813 (0.0496)	-0.0071* (0.0013)	97.5%

(*) The negative sign in the equation presented in the figures corresponds to a negative ΔT

Figures 47 and 48 show the performance of the south wall in terms of temperature difference and heat flux. A wide range of temperature difference has been observed for both simulators. The control simulator had more positive temperature differences whereas the PCM-enhanced simulator experienced more negative temperature difference. A positive temperature difference indicates that the outside temperature was higher than the inside temperature and vice versa. Also, most of the negative heat flux values were close to zero, indicating negligible heat flux in any direction. At a higher temperature difference, indicating more solar energy gain, both simulators showed greater dispersed heat flux values. At negative temperature difference the PCM-enhanced simulator experienced positive heat flux value. This meant that heat was flowing toward the inside of the simulator. This phenomenon can be attributed to the PCM as it was releasing heat in both directions and some of which was moving towards the inside of the simulator. Finally, lower slope value for PCM-

enhanced wall indicate a lower heat transfer coefficient and eventually lower heat flow.

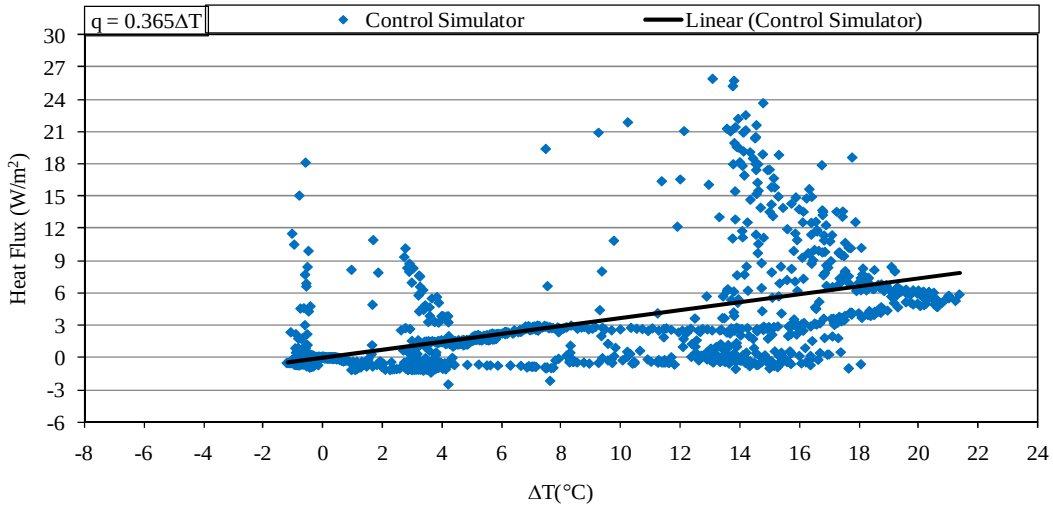

Figure 47. Temperature difference vs. heat flux behavior of control south wall

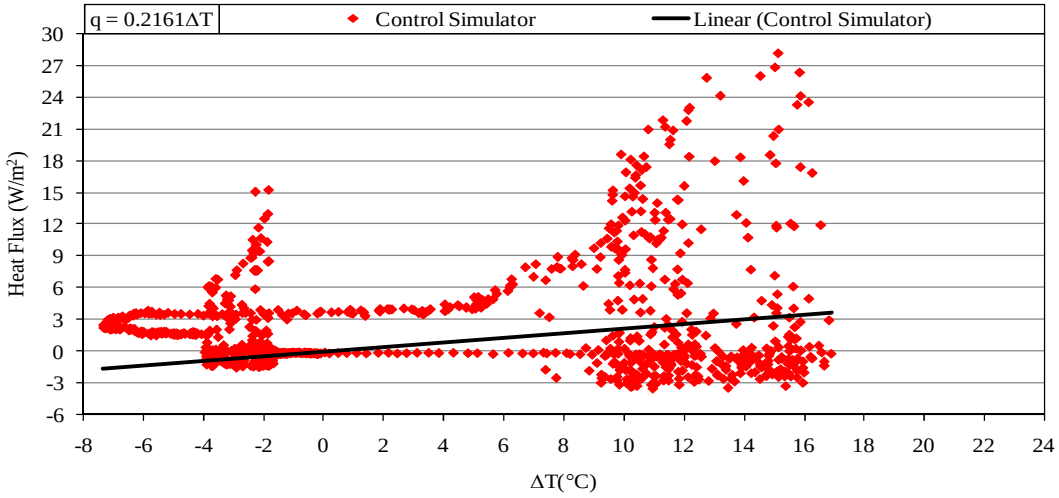

Figure 48. Temperature difference vs. heat flux behavior of PCM-enhanced south wall

The east wall shows similar behavior as the south wall. Figures 49 and 50 illustrate the heat flux response with temperature difference. The range of the temperature difference for the control simulator was -2 to 13°C, whereas it expanded from -8 to 15°C for the PCM-enhanced simulator. At higher temperature differences the control simulator displayed higher positive heat fluxes. This is not the case for the PCM-enhanced simulator. The explanation for Figure 50 would be a lareg thermal resistance of the medium that helped to keep the slope of the curve low. Particularly, in spite of the increase in potential (temperature difference), there was consistent low heat flux values.

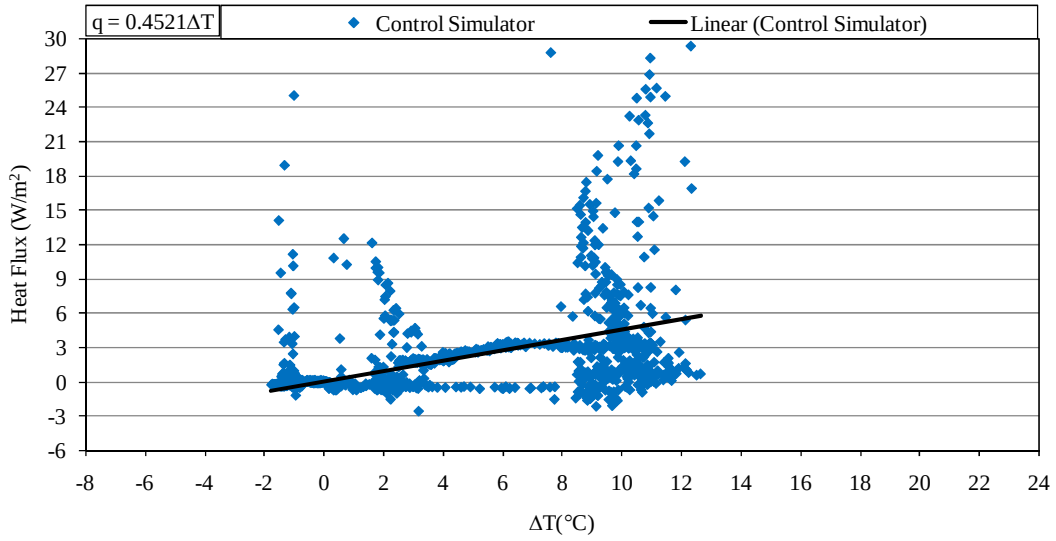

Figure 49. Temperature difference vs. heat flux behavior of control east wall

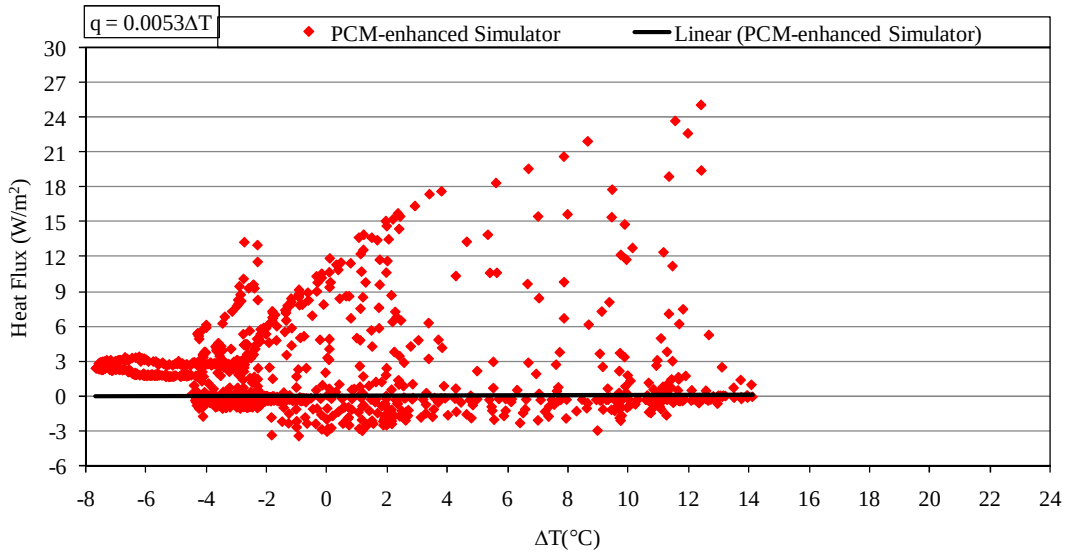

Figure 50. Temperature difference vs. heat flux behavior of PCM-enhanced east wall

Among all of the control simulator walls, the top wall displayed the most negative temperature differences implying lower outer surface temperatures than other walls. Figure 51 also displays the lower heat flux values experienced by the top wall as compared to the south and east walls. In Figure 5, the top wall of the PCM-enhanced simulator displays more localized temperature and heat flux values. A concentration of negative temperature and corresponding heat flux values were recorded for the top wall. Although the linear trend line that has been drawn for PCM-enhanced simulator represents a negative slope, it is physically not possible to have negative U-values; therefore, the negative slope is the result of negative temperature differences. Thus, instead of any meaningful heat gain or loss, these pipes constantly have created interfering heat flows. Therefore, a small disturbance heat flux component by the PCM might have furnished such results.

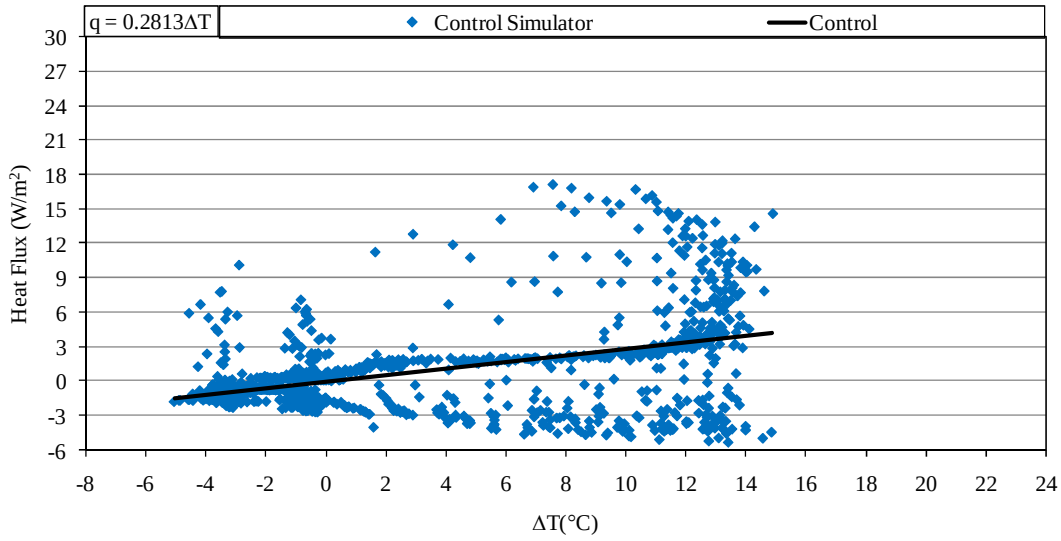

Figure 51. Temperature difference vs. heat flux behavior of control top wall

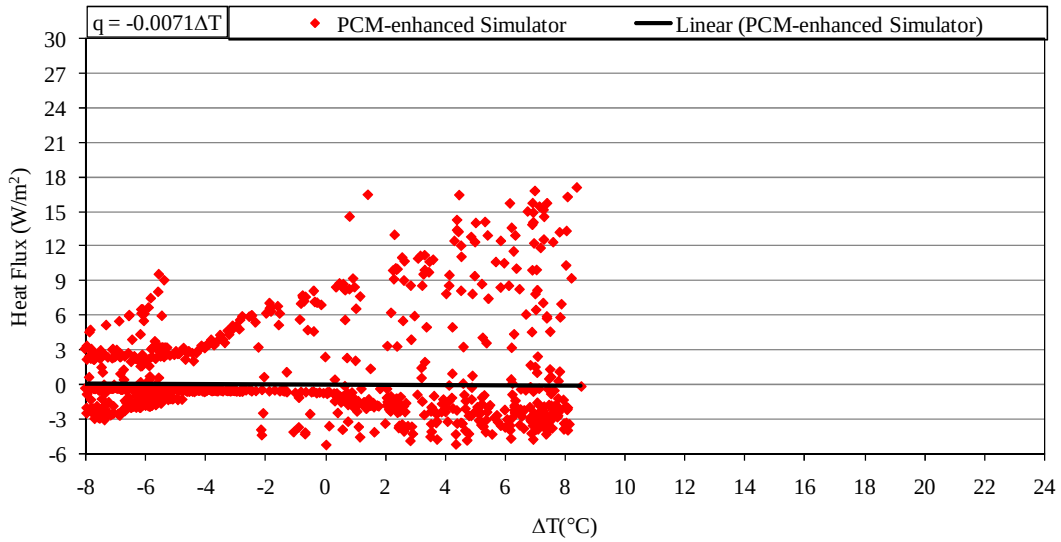

Figure 52. Temperature difference vs. heat flux behavior of PCM-enhanced top wall

Because of the lack of solar energy gain, the north wall for both simulators displayed the least amount of dispersion in heat flux and temperature difference values. This is shown in Figures 53 and 54. A negative slope for PCM-enhanced north wall was calculated and the same explanation as for Figure 52 applies.

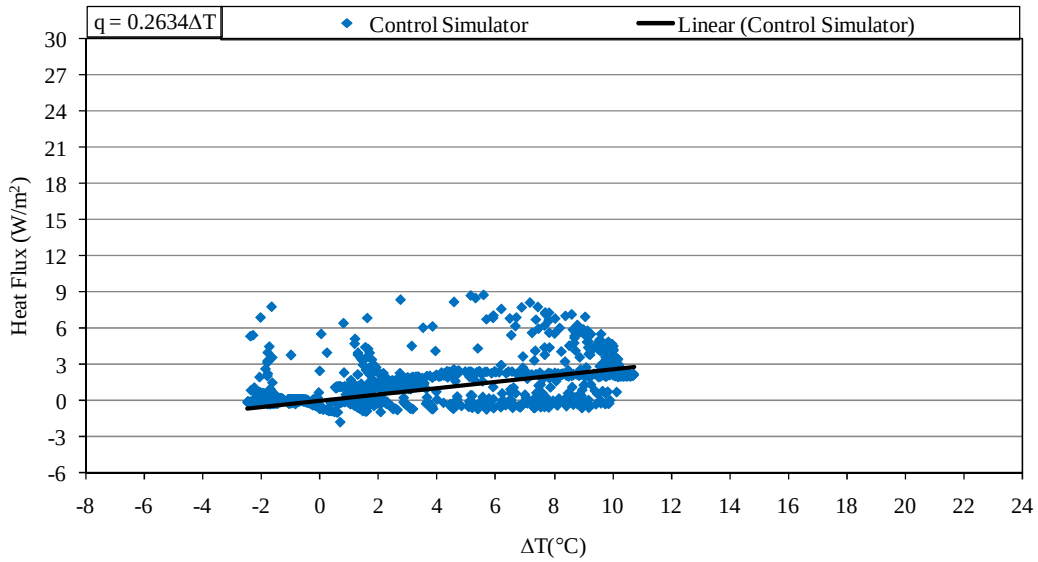

Figure 53. Temperature difference vs. heat flux behavior of control north wall

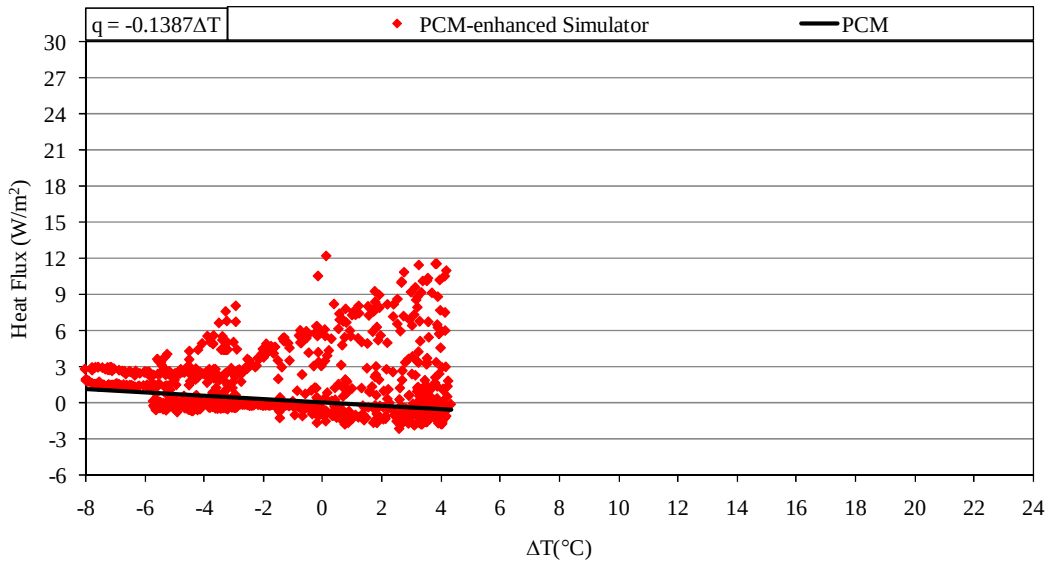

Figure 54. Temperature difference vs. heat flux behavior of PCM-enhanced north wall

The west wall temperature difference vs. heat flux behavior as seen in Figures 55 and 56 showed the greatest dispersion in the data collected. Although the west wall received solar energy throughout the entire day, it is the later part of the day when the west wall gained most of its solar heat. The maximum heat flux recorded with a given temperature difference was not as high as for the south or east walls.

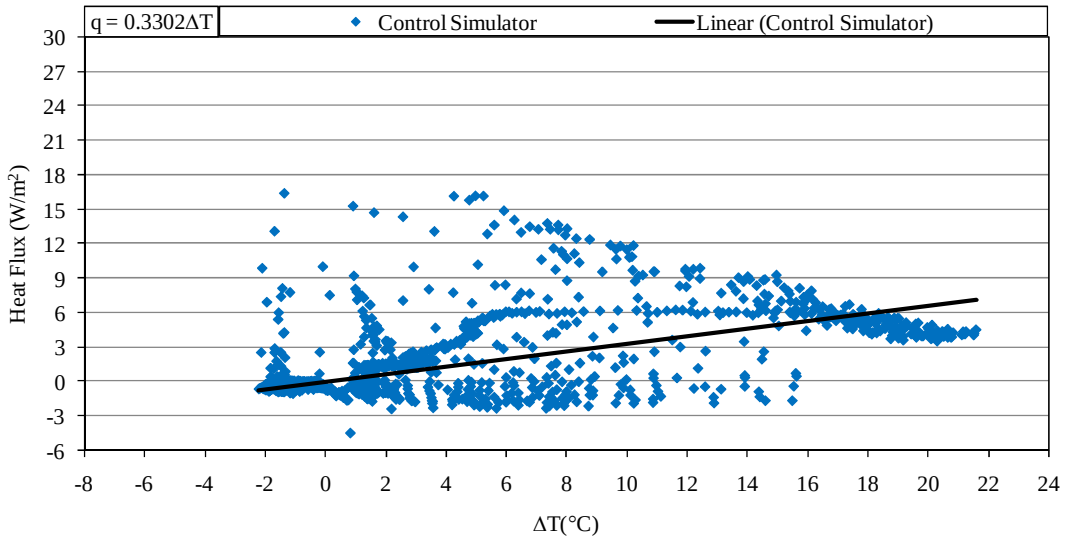

Figure 55. Temperature difference vs. heat flux behavior of control west wall

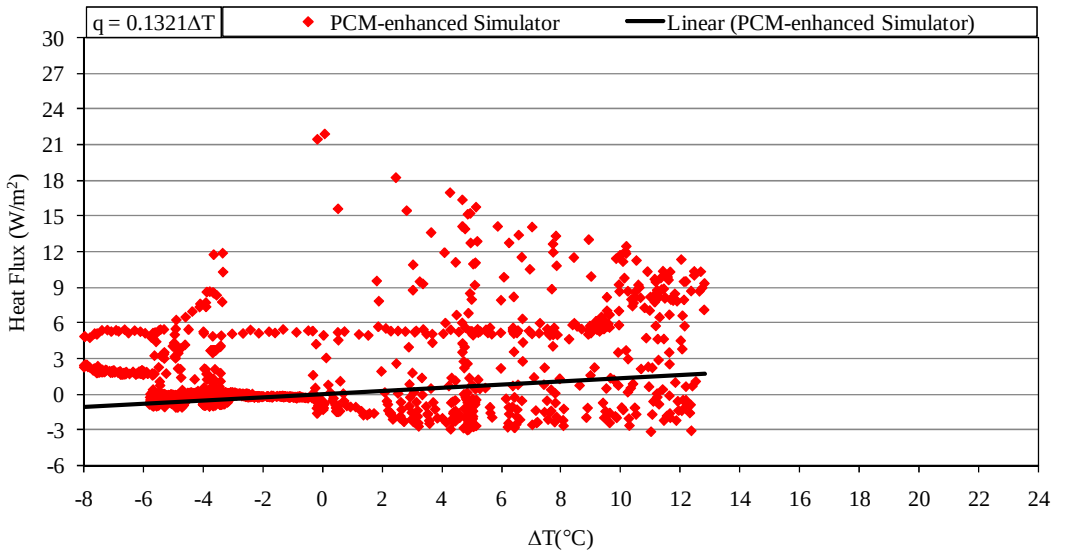

Figure 56. Temperature difference vs. heat flux behavior of PCM-enhanced west wall

5. Insolation and Heat Flux

The insolation is a measure of solar radiation energy received by a given surface in a given time. As described in Section 1, that solar insolation was important for identifying the similarity of the test days and was a parameter used to understand the heat gain by the simulators. Figures 57 and 58 give the solar insolation and corresponding total heat flux measured by the heat flux meters. A breakdown of heat gain by the various walls is also presented in the same figures. The PCM-enhanced simulator showed a time shift in peak load as well as a decrease in magnitude of the heat fluxes. The total heat gain by the two simulators is presented on an hourly basis in Figures 57 and 58. For the control simulator, the peak load occurred around 1:30 PM, whereas, for the PCM-enhanced simulator, it was around 3:30 PM.

The maximum total heat fluxes entering the simulators were 26 W/m^2 (8.24 Btu/hr ft^2) for the control simulator and 22 W/m^2 (6.97 Btu/hrft^2) for the PCM-enhanced simulator, which is plotted on the secondary axis. The walls that contributed the most to the total heat gain were the south and east walls. A direct influence of the solar radiation energy on the simulator was established by the analysis. The thermal energy storage capability of the PCM was also represented in this analysis. The PCM's change of phase resulted in lower energy gain by that simulator. Therefore, the figures presented here are considerable evidence of the PCM response with the solar heat gain.

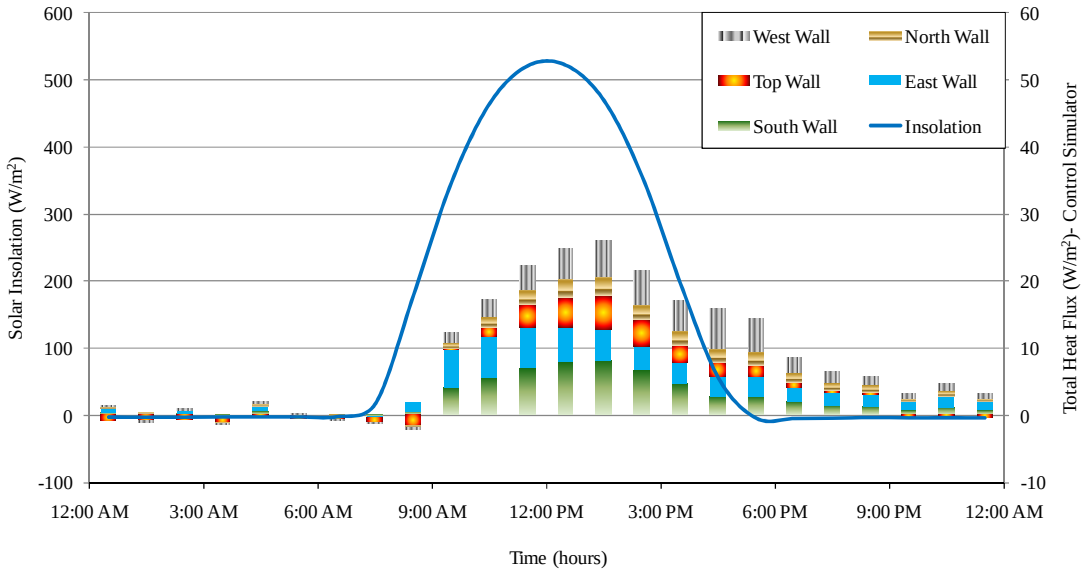

Figure 57. Solar insolation and corresponding heat fluxes for different walls of control simulator

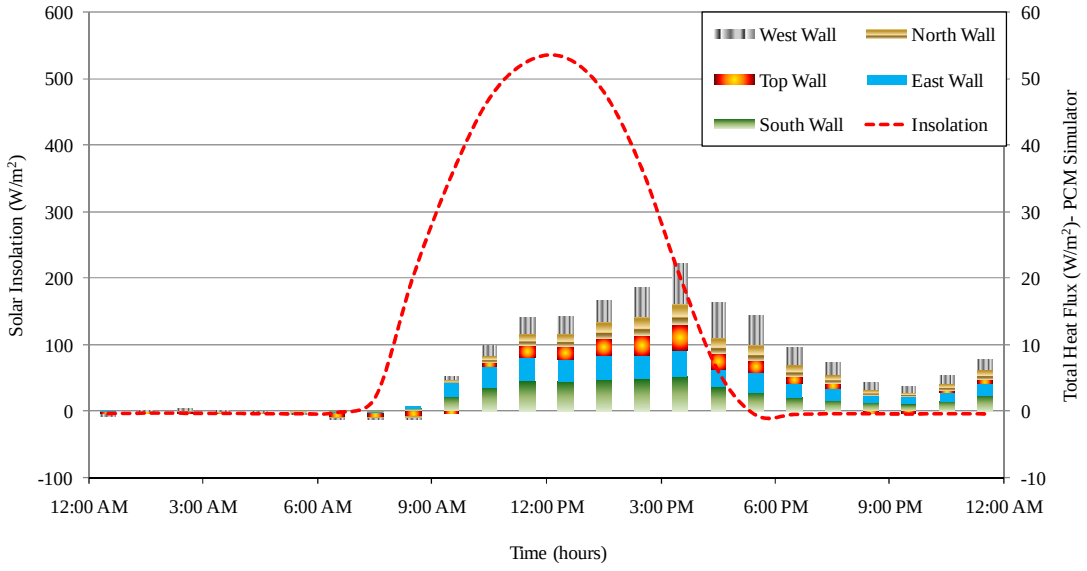

Figure 58. Solar insolation and corresponding heat fluxes for different walls of PCM-enhanced simulator

6. Month-Long Results

Monthly data were collected and averages were calculated. This gave a more representative view of the performance of the simulators. Figures 59 and 60 give a comparison between both sets of data in terms of insolation and temperature. The data were collected at one-minute intervals for all the days. From these figures one can conclude that the days for both testing periods were similar. Slightly hotter evenings were still observed in those days in which the PCM-enhanced simulator was tested.

For the entire month, results similar to that of a single day were observed for different walls. An approximated one and one-half hour average of heat flux data is presented in the following analysis.

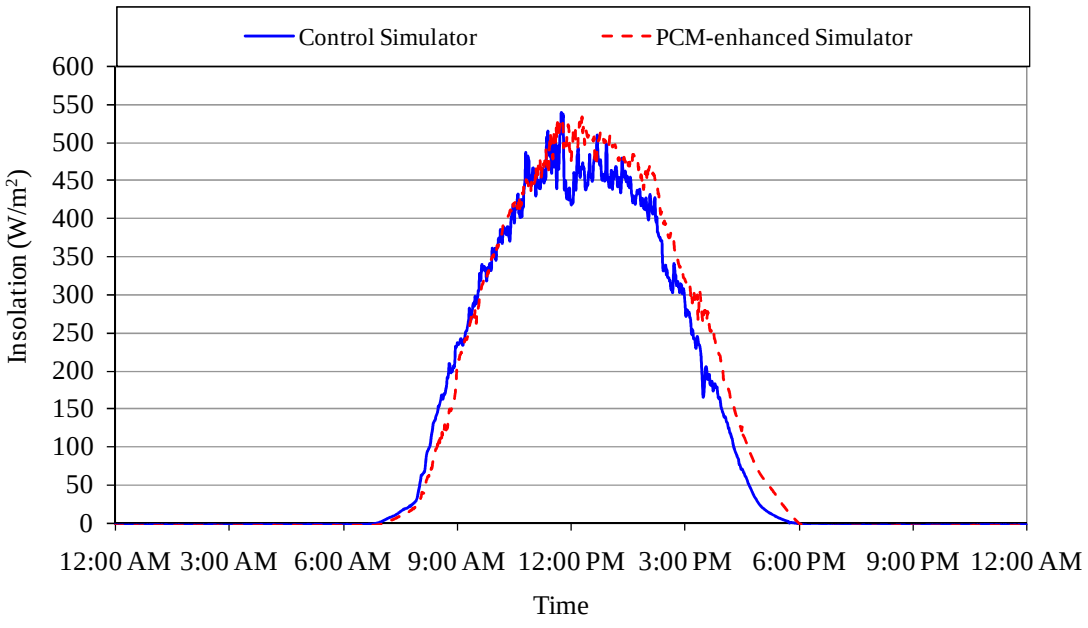

Figure 59. Average insolation for one month

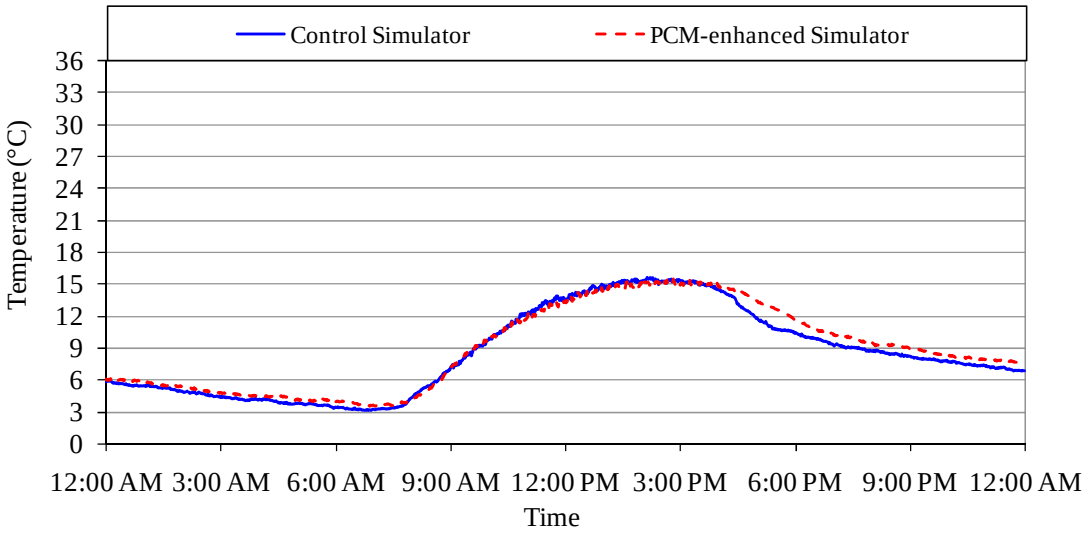

Figure 60. Average outdoor air temperature for one month

The results of the performance of the PCM-enhanced walls are shown in Figures 61 to 66. Results for the entire month for the various walls followed similar trends as for the daily results. Heat flux reduction by the south, east and top walls were significant. The north wall heat flux reduction was not as much as the other walls. The total heat flux for the entire PCM-enhanced simulator showed a heat flux reduction, produced by the PCM, over the control simulator for the entire month.

Figure 61 shows a representative view of the south wall heat flux values. The PCM-enhanced simulator clearly showed improved performance by lowering peak and total heat flux values. A higher heat flux value for the first part of the day was indicative of the solidification of the PCM. Thus the released energy would travel both ways, a portion of which would enter the simulator. It is not clear at this point,

the percentage of PCM material solidifying or melting during heat gain and heat rejection processes. The increase in heat flux by the PCM at the beginning of the day was less than 1 W/m^2. But still the peak and total heat load reduction was significant. The temperature swing control by the PCM was more discernable on a daily basis rather than for an entire month.

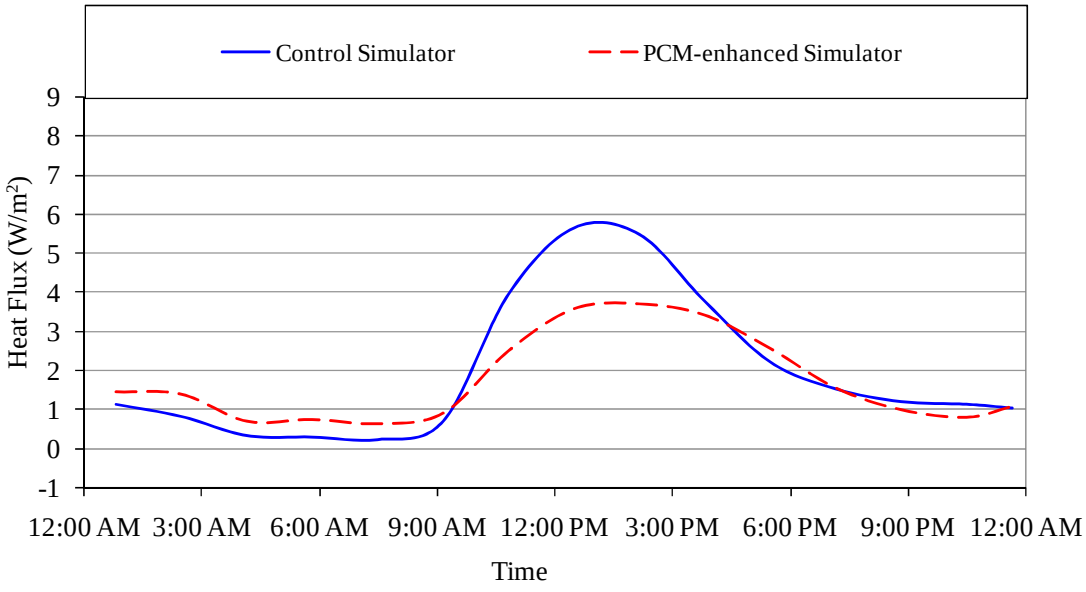

Figure 61. South wall average heat flux for one month

By getting the solar radiation exposure first in the day the east wall experienced the peak heat transfer occurring earlier than for the rest of the panels. Figure 62 demonstrates the fact that the peak load shifted four hours from the east to the south wall for the control simulator. The PCM-enhanced simulator experienced a peak heat flux around the same time as the control simulator, but a steadier heat flux was observed in this case.

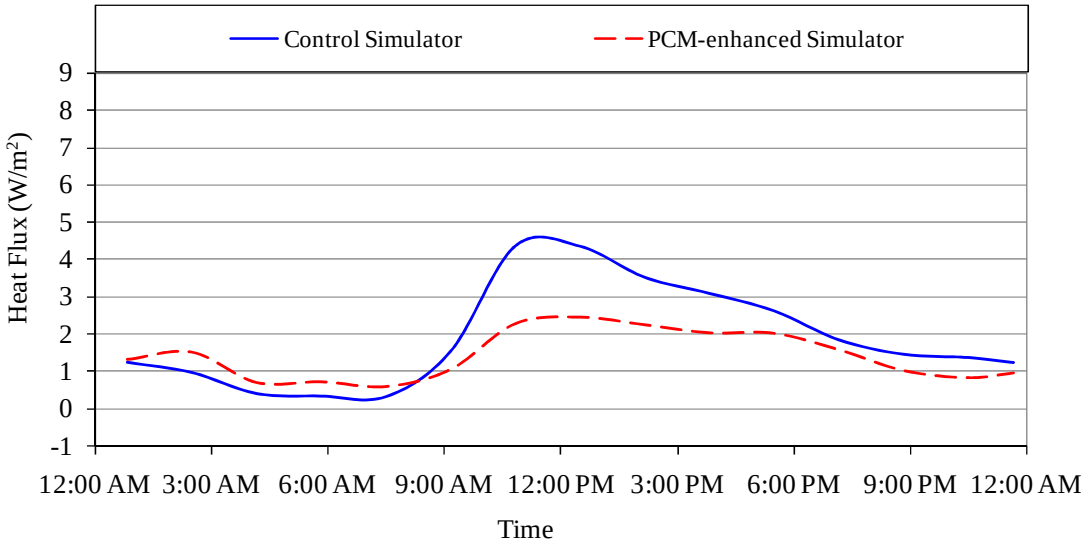

Figure 62. East wall average heat flux for one month

Throughout the experiment period the north wall received the least amount of solar energy. This is shown in Figure 63. The control simulator's peak heat flux for the north wall was 62% and 58% lower than the south and east walls, respectively. The heat flux reduction for the north wall by the PCM-enhanced simulator was compromised by the heat gain at the beginning of the day.

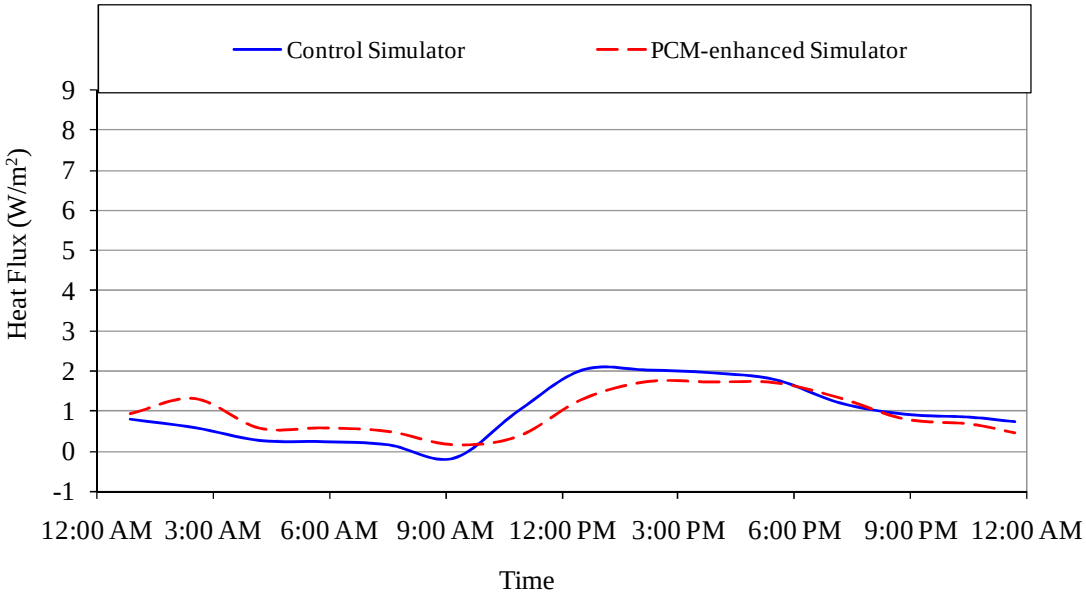

Figure 63. North wall average heat flux for one month

The west wall, as seen in Figure 64, had experienced the solar heat energy gain in the latter part of the day. The heat gain by the PCM-enhanced simulator was even slower than that of the control simulator heat gain. Although, the peak heat flux reduction by the PCM-enhanced wall was not significant enough as compared to the rest of the walls, the total heat flux reduction was substantial. Figure 65 illustrates the heat flux behavior of the top wall. The top wall experienced steady solar radiation throughout the day. The top wall was the only flat surface and the concept of solar angle can be applied. One such parameter is the 'solar altitude,' which is the vertical angle up from the horizon and changes with the time of the year. Therefore, a solar heat gain by the top wall in a different part of the year, preferably during the summer,

might demonstrate higher heat flux when compared to other walls' heat fluxes during that time.

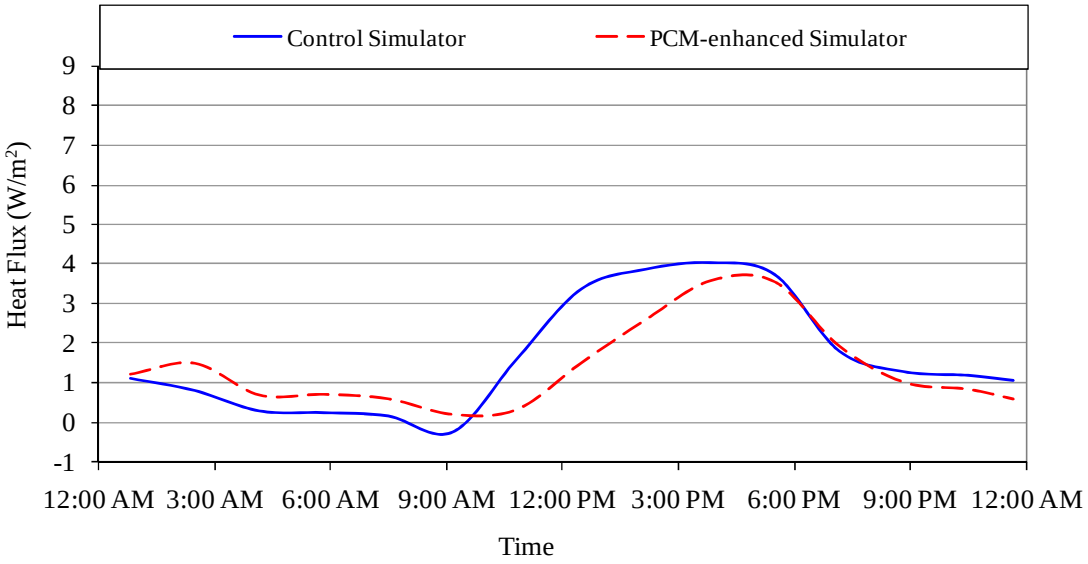

Figure 64. West wall average heat flux for one month

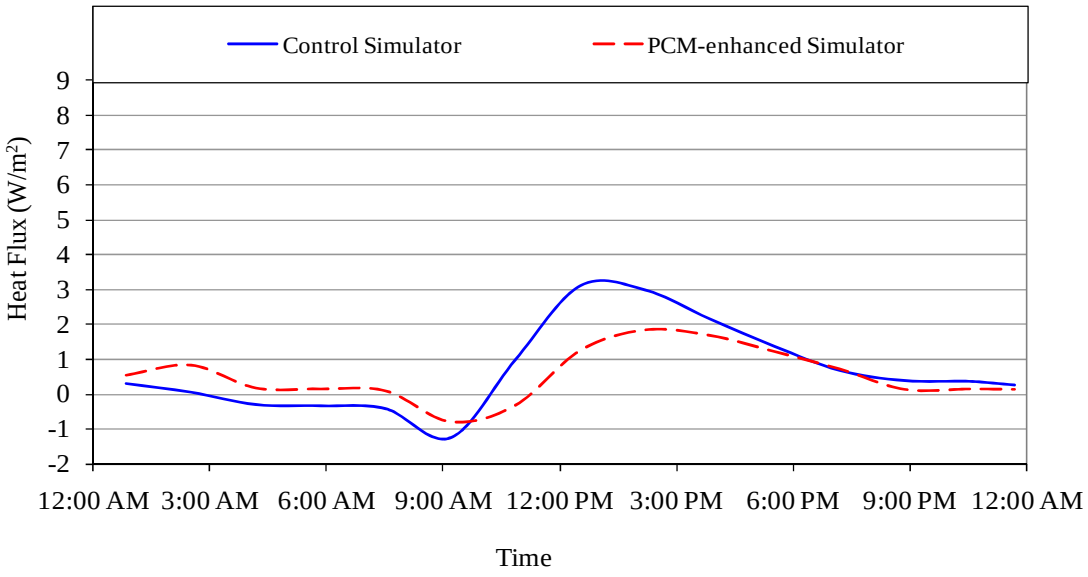

Figure 65. Top wall average heat flux for one month

The total wall average heat flux is depicted in Figure 66. This figure presents the cumulative effects of the solar heat energy gain of the two simulators. This figure is similar to Figure 39. Figure 66 is more representative of the simulators' overall heat gain behavior as a result of ambient exposure. The area of the heat fluxes were considered to calculate the final heat flow. The occurrence of peak heat flux in both Figure 39 and Figure 66 for the control simulator was observed at 1 PM. It was also observed that the PCM-enhanced simulator not only lowered the peak heat flux but also flattened it, showing a constant peak heat flux, for a longer period of time. The PCM-enhanced simulator exhibited the attributes of PCM at the beginning of the day, when the PCM released heat energy and showed higher heat flux values than the control simulator heat flux values. It is noteworthy to mention here that all of these graphs are part of a continuous cycle. Therefore, the heat energy released by the PCM into the simulator is something that had been collected from the previous day.

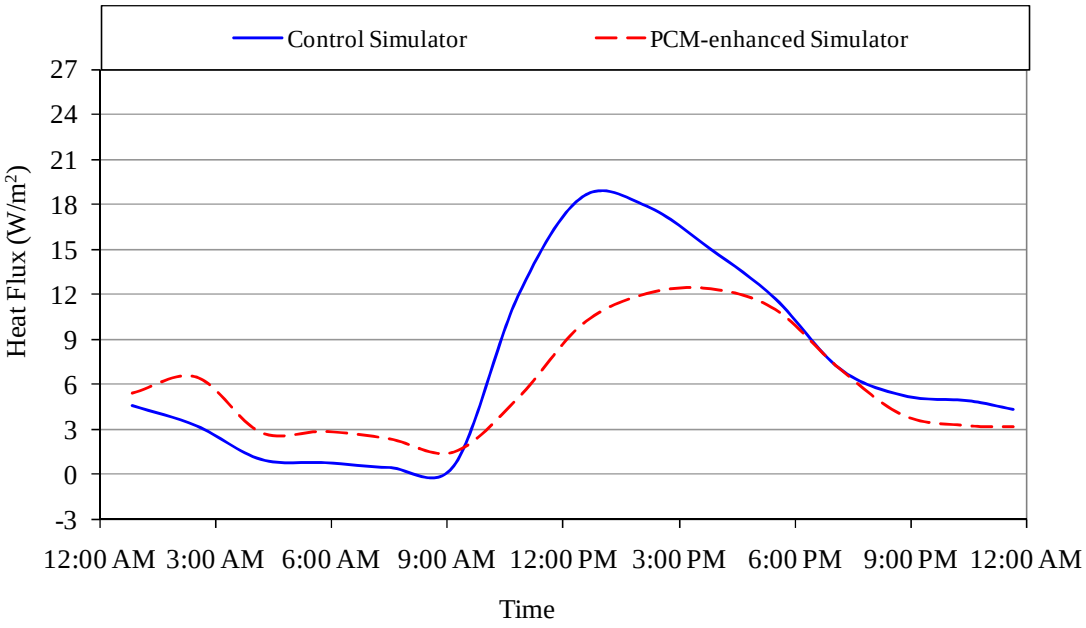

Figure 66. Total average heat flux for one month combining all five walls

The results are summarized in Figures 67 and 68. The reductions in peak heat transfer rates were significant with an average of 29.1%. In terms of overall heat flow into the refrigerated space of the PCM-enhanced simulator, the reductions averaged 16.3%. The total energy transfer was calculated based on the area of the simulators over the length of the day.

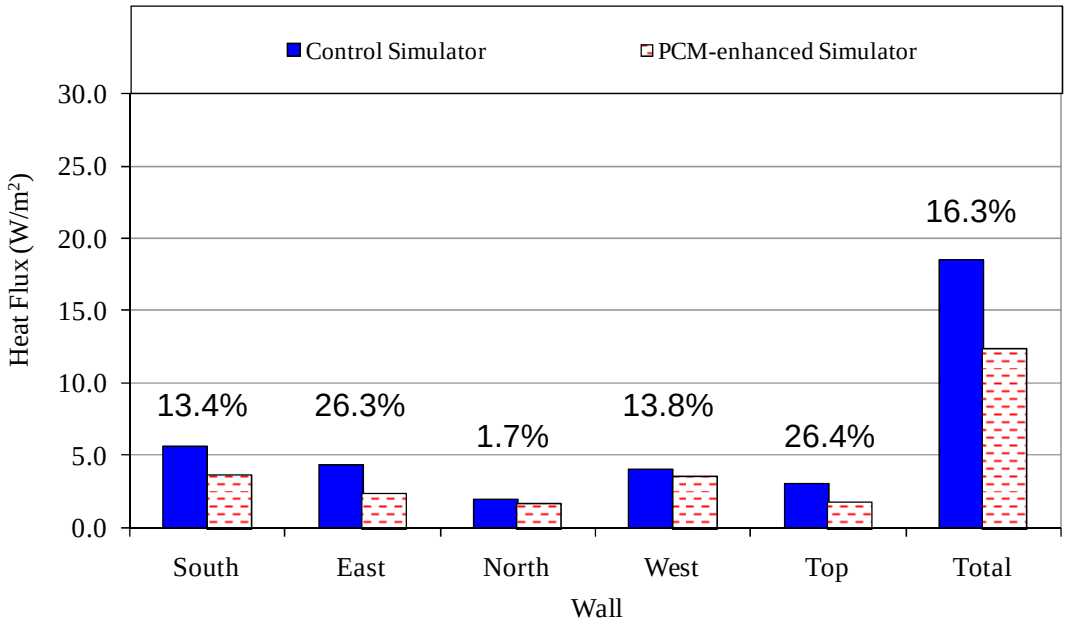

Figure 67. Average peak heat flux and corresponding percent reduction for one month

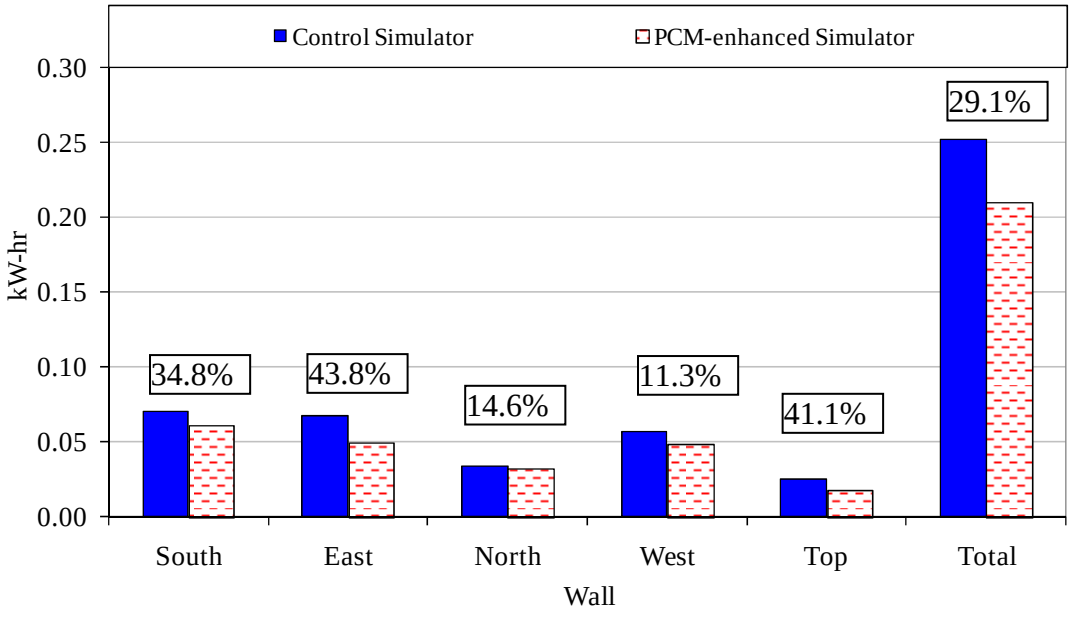

Figure 68. Average total heat flow and corresponding percent reduction for one month

7. Summer Results

The primary reason for the data collection in the month of November was the lower outside ambient air temperature, which would be suitable for the cooling system. It helped to establish the groundwork for future research and analysis. Very limited amount of data were collected during the summer time. The analysis is presented in this section. Similar analysis as in Sections 2 to 5 are performed for the data collected during the month of August.

Figures 69 through 73 show the heat flux behavior during one entire day for all the walls. The south wall heat fluxes for both the simulators are shown in Figure 69. A peak heat flux of 9.2 W/m^2 (2.9 Btu/hr ft^2) for the control simulator south wall was observed, whereas the peak heat flux for the PCM-enhanced simulator south wall was 8.2 W/m^2 (2.6 Btu/hr ft^2). Although peak heat flux reductions by the PCMs during the summer were not as high as early winter, similar heat flux patterns for the PCM-enhanced walls were observed in both summer and early winter. The peak heat flux during the summer time occurred at around 4 PM, whereas it was at around 3 PM during early winter. A steady rise in the heat flux values of the PCM-enhanced wall was observed compared to the control wall heat flux values during both times of the year. Slightly higher heat flux values for the PCM-enhanced walls during the later part of the day were also noticeable. Heat released by the PCM either in sensible or latent heat form created the extra component of heat flux that caused the heat fluxes to go up.

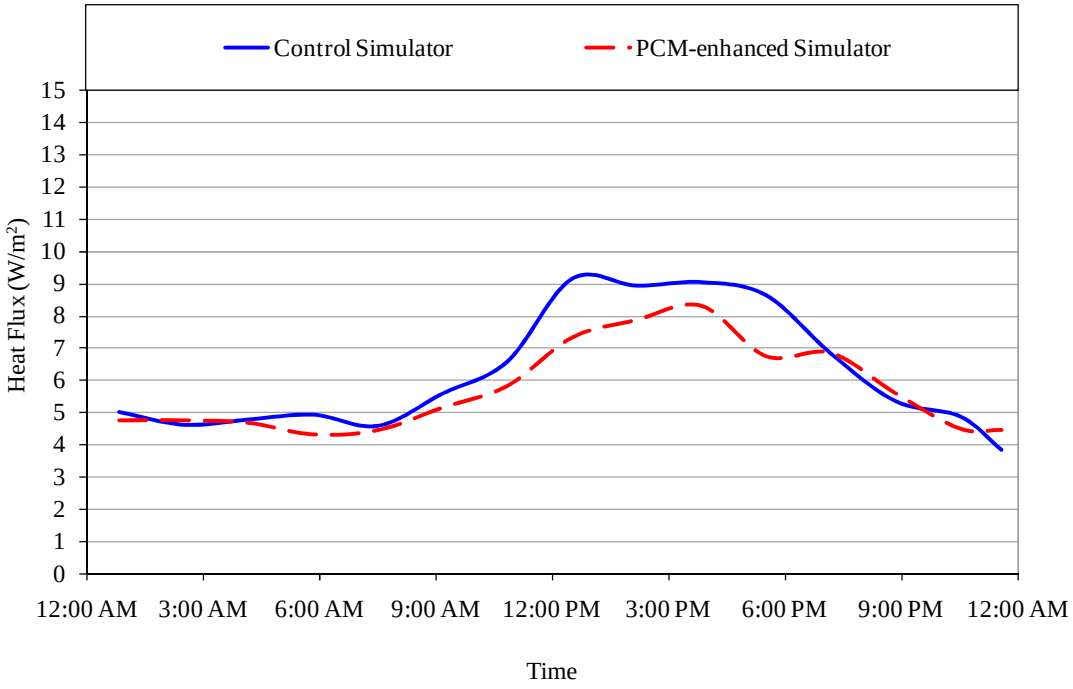

Figure 69. South wall heat fluxes for August

Control simulator east wall heat flux values show similar patterns during both times of the year. As shown in Figure 70, the control simulator east wall peak heat flux occurred early compared to other wall peak heat fluxes. The heat flux for the PCM-enhanced east wall was lower than the heat flux recorded for the control east wall for the entire day. Heat absorption by the PCM throughout the day caused the PCM-enhanced wall to transfer less heat into the simulator compared to the control counterpart.

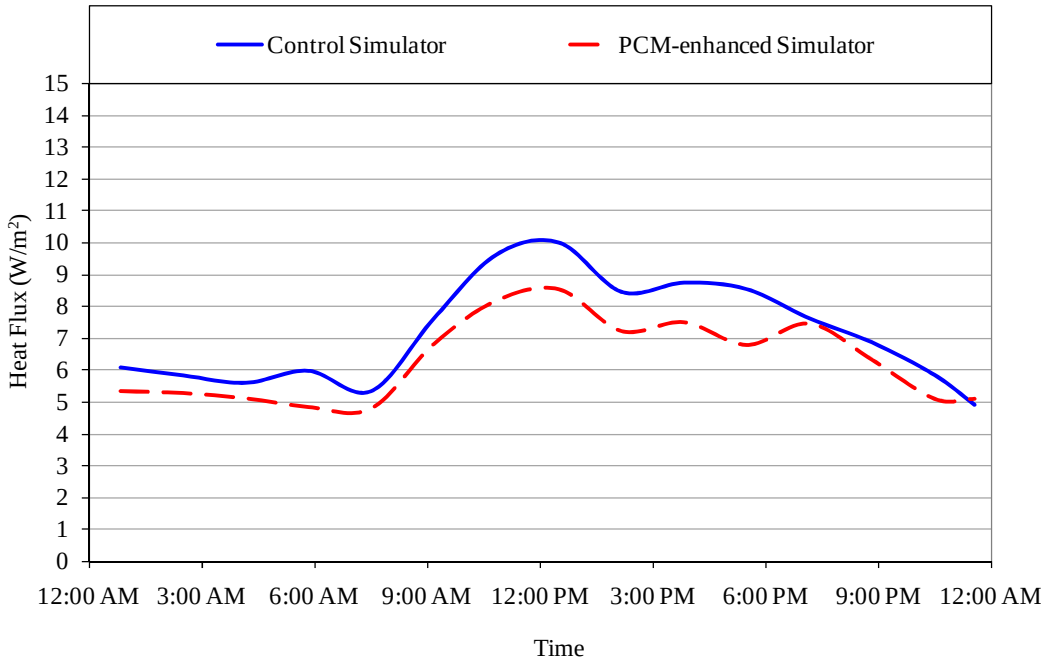

Figure 70. East wall heat fluxes for August

The top wall experienced consistent heat gain throughout the day. Figure 71 shows the heat gain by the PCM-enhanced and control top walls for one day. It was observed that the peak heat flux for all the walls stayed on for a short time; however the peak heat flux for the top wall retained an almost constant value from about 12 noon to 5 PM. The PCM-enhanced simulator experienced higher heat fluxes through the top wall during the first part of the day (12 midnight to 10 AM). A higher heat flux during the later part of the day was also observed for the PCM-enhanced simulator.

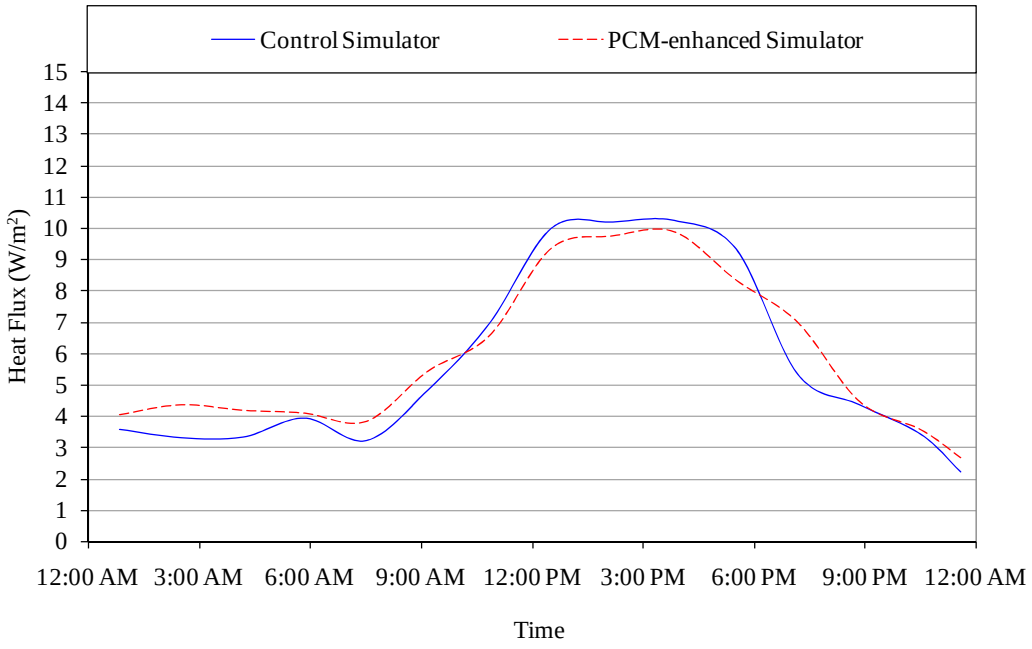

Figure 71. Top wall heat fluxes for August

Figure 72 shows reductions of heat flux by the PCM-enhanced west wall for most of the day, from 12 noon to 7 PM. Also, the peak heat fluxes obtained by the two simulators were the highest among all other walls. The increase of heat flux values at the later part of the day was because most solar heat was gained during afternoon. The peak occurred at around 6 PM for the control simulator west wall, whereas it occurred at 7 PM for the PCM-enhanced simulator west wall.

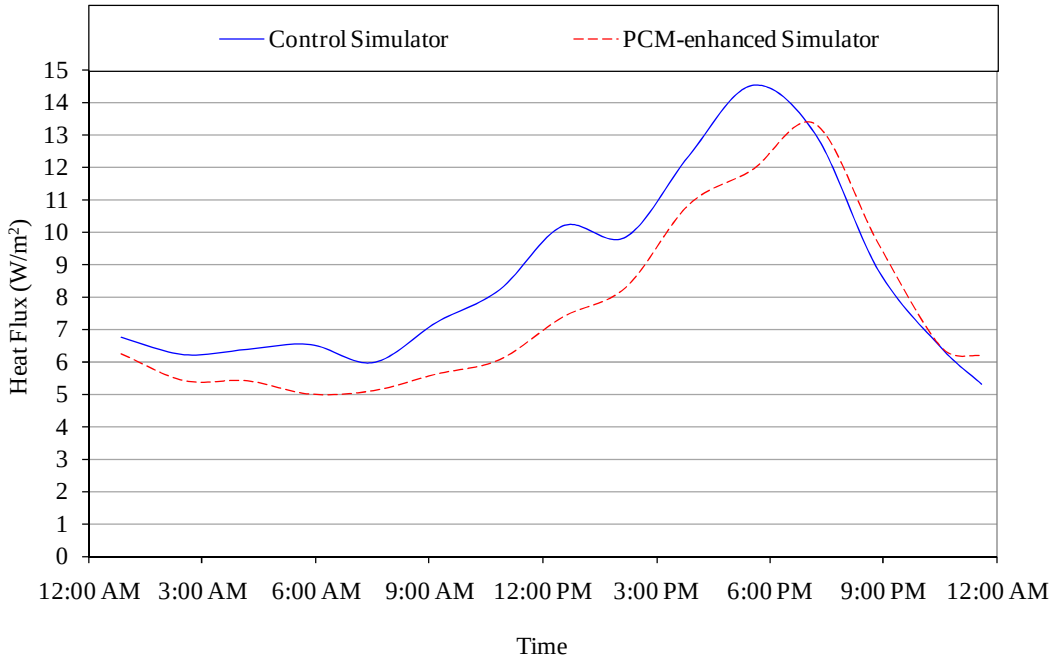

Figure 72. West wall heat fluxes for August

The results obtained for the north wall are presented in Figure 73. The PCM-enhanced north wall showed higher heat flux values compared to the control north wall throughout the entire day. This implied more heat flux entering through the north wall of PCM-enhanced simulator than the control simulator. The north walls of both simulators experienced the least amount of solar energy gain among all the walls. Similar results were obtained for the north wall for summer and early winter (Figure 73 and Figure 36).

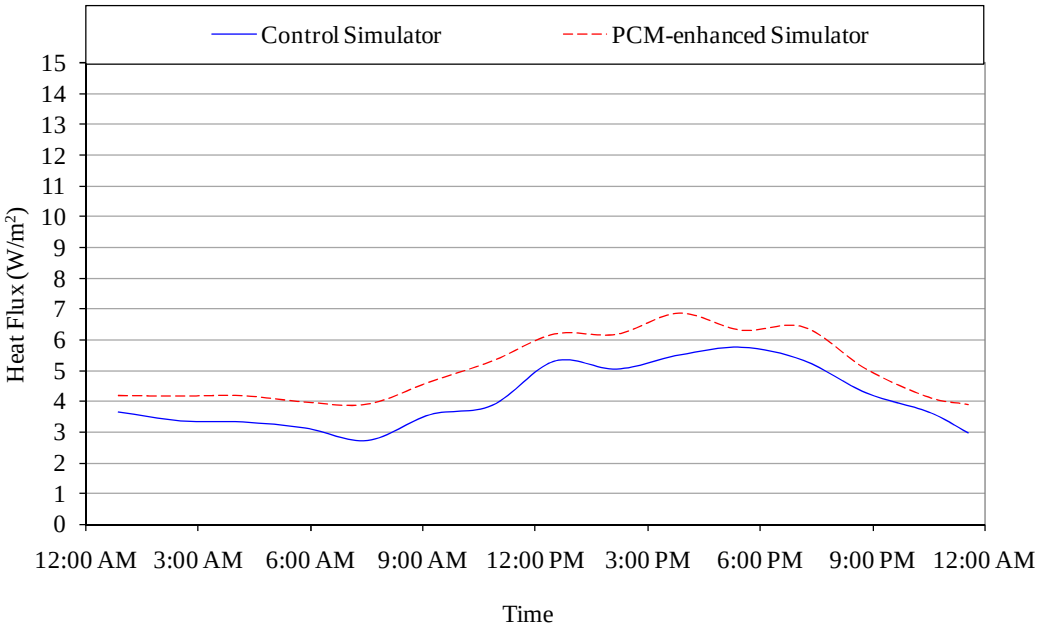

Figure 73. North wall heat fluxes for August

Total heat fluxes combining all five wall heat fluxes are presented in Figure 74. More fluctuation in heat flux was observed for the PCM-enhanced simulator during summer (Figure 74) than early winter (Figure 39). The heat fluxes observed during early winter showed relatively rapid increase and decrease in heat flux values compared to those of the summer. The peak heat flux value for the control simulator was 47 W/m^2 (14.9 Btu/hr ft^2) for summer, whereas it was 25 W/m^2 (7.9 Btu/hr ft^2) for early winter. The peak heat flux value for PCM-enhanced simulator was 43 W/m^2 (13.6 Btu/hr ft^2) for summer and 20 W/m^2 (6.3 Btu/hr ft^2) for early winter. Therefore, a significant rise in heat flux values was observed for both simulators. Theoretically, the heat flux graphs for the two simulators should be identical since these simulators were of the same construction and these were subjected to test during the same time. Therefore, any deviation in measurement across the simulator walls was the affect from the PCM. As the PCM absorbed heat, both in latent and sensible heat forms, the lower heat flux in the PCM-enhanced simulator was attributed to the PCM.

The PCM-enhanced simulator also experienced higher heat flux values than the control simulator during the early and later part of the day. The exact state or temperature of the PCM was not known at this point. Therefore, the heat released by the PCM in either latent heat or sensible heat form caused the extra heat flux gain by the simulator.

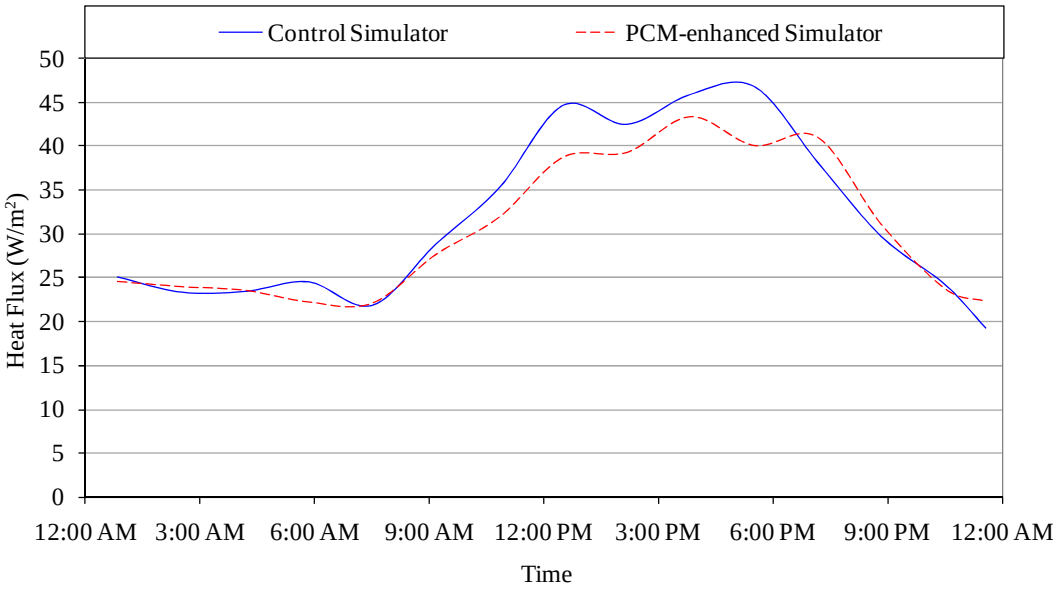

Figure 74. Total heat fluxes combining all five wall heat fluxes for August

The summary of peak heat flux and total energy flow into the simulators are summarized in Figures 75 and 76. A 17.5% peak heat flux reduction was achieved by the east wall. The peak heat flux reductions by south, top and west wall were respectively 10.1%, 3.8% and 8.8%. All the other walls show positive heat flux reduction except the north wall. The north wall experienced a rise of 16.2% in peak heat flux. The PCM-enhanced simulator proved its effectiveness by lowering the peak heat flux up to 7.9%.

Daily heat flow values also dropped for south, east and west wall. The percentage reduction in daily heat flow was respectively 9.5, 14.3 and 14.4% for south, east and west wall respectively. The top and north walls didn't show any

reduction in daily heat flows into the simulators. The total heat energy flow into the simulator for the PCM-enhance wall was lower than the control simulator.

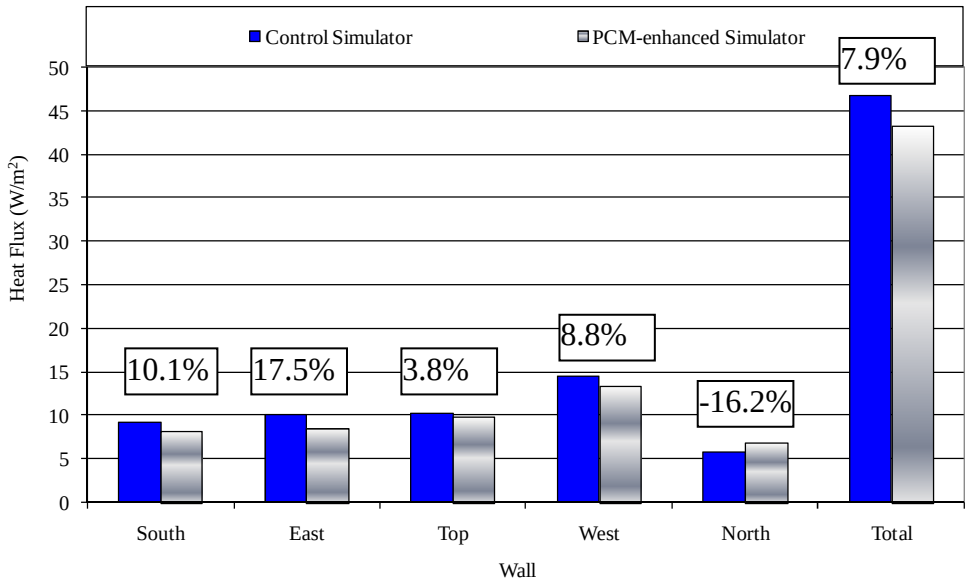

Figure 75. Peak heat flux and corresponding percent reductions for August

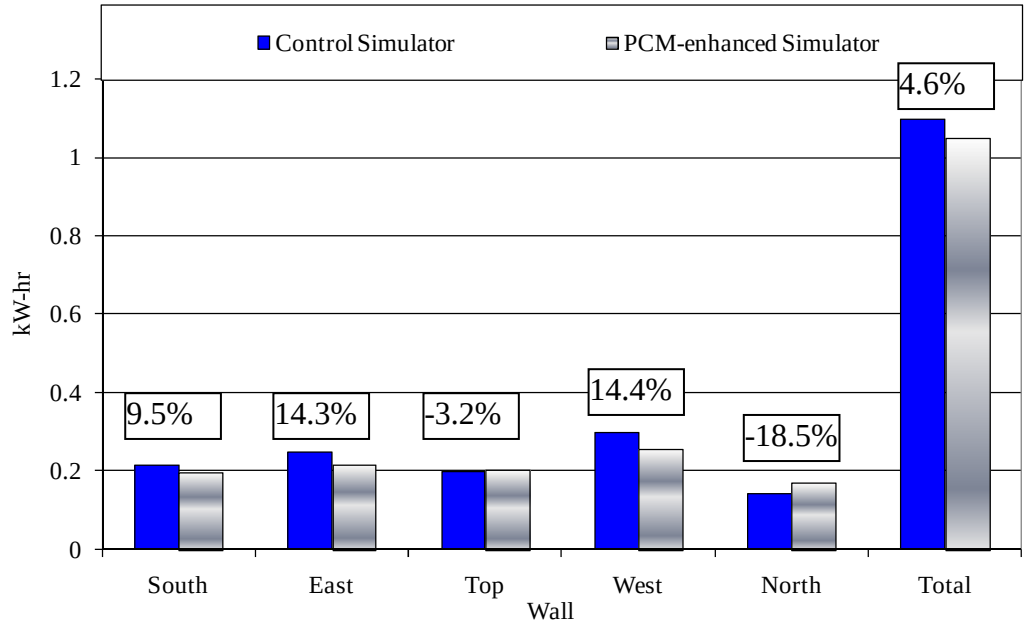

Figure 76. Daily heat energy flows and corresponding percent reductions for August

The interior and exterior surface temperatures for the PCM-enhanced and control simulators are presented in Figures 77 to 81. The south wall interior and exterior temperatures showed similar patterns. The interior surface temperature was about 6°C (42.8°F). During the period of 12 midnight to 8 AM the exterior surface temperatures of both simulators stayed almost at a constant 21°C (69.8°F). But as the day progressed and the simulators started gaining solar energy, the exterior surface temperature began to increase. Throughout the entire day, the PCM-enhanced simulator exterior surface temperature followed closely that of the control simulator. Only during the middle part of the day, from 11 to 5 PM, the PCM-enhanced simulator surface temperature was lower than the control simulator surface temperature. Therefore, the behavior observed by the south wall exterior and interior surface temperatures during the summer was different from the temperature behavior during the early winter (Figure 42).

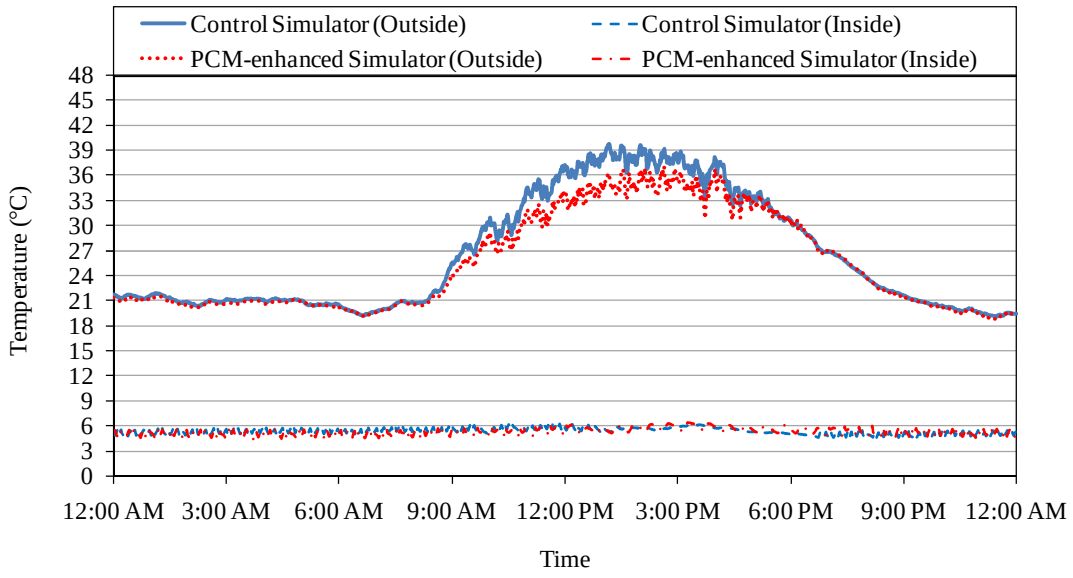

Figure 77. Exterior and interior surface temperatures of south wall in August

The east wall interior and exterior surface temperatures for both simulators displayed same pattern. The temperature differences between the PCM-enhanced wall and control wall were insignificant. Figure 78 shows the interior surface temperatures of both simulators as just below 6°C (42.8°F) for most of the day. Only from 11 to 7 PM the PCM-enhanced wall temperature was at 6°C (42.8°F). The temperature was slightly higher in the PCM-enhanced simulator. In Figure 78, similar patterns in exterior temperature were observed as in Figure 43. As the east wall received direct solar energy earlier than the other walls, the sudden rise in temperature during 8 to 10 AM was similar to the sudden temperature rise observed in Figure 43 for the early winter days.

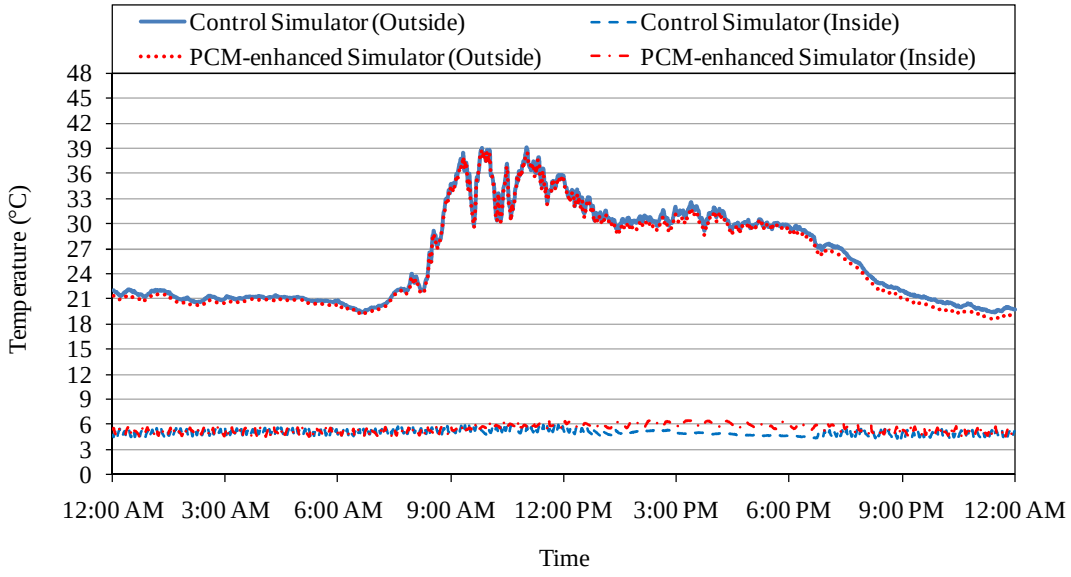

Figure 78. Exterior and interior surface temperatures of east wall in August

A close agreement between the two simulators top wall temperatures was observed. Figure 79 shows interior and exterior surface temperatures of the top walls of both simulators. The interior surface temperatures for both simulators were around 6°C (42.8°F). The exterior surface temperature reached 45°C (113°F) for both simulators.

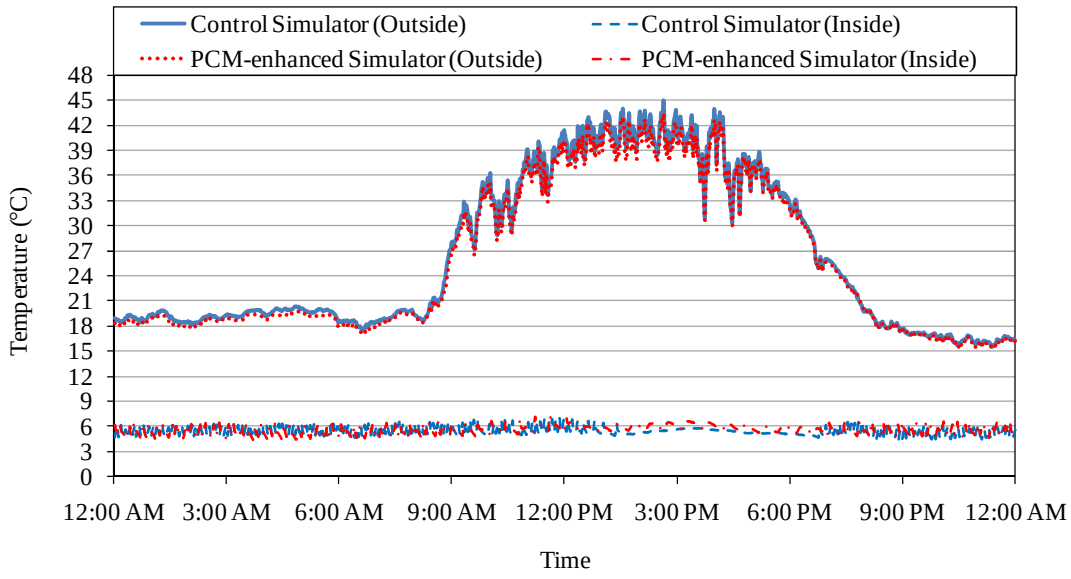

Figure 79. Exterior and interior surface temperatures of top wall in August

The west wall interior and exterior surface temperatures for both simulators are presented in Figure 80. Similar patterns in west wall temperatures were observed in Figure 45 and Figure 80. In both cases, the exterior surface temperatures peaked during the later part of the day. The exterior surface temperatures of the west wall were the maximum surface temperatures observed among all other wall surface temperatures during summer. The PCM-enhanced simulator and control simulator

surface temperatures remained almost at the same level and not much difference was observed.

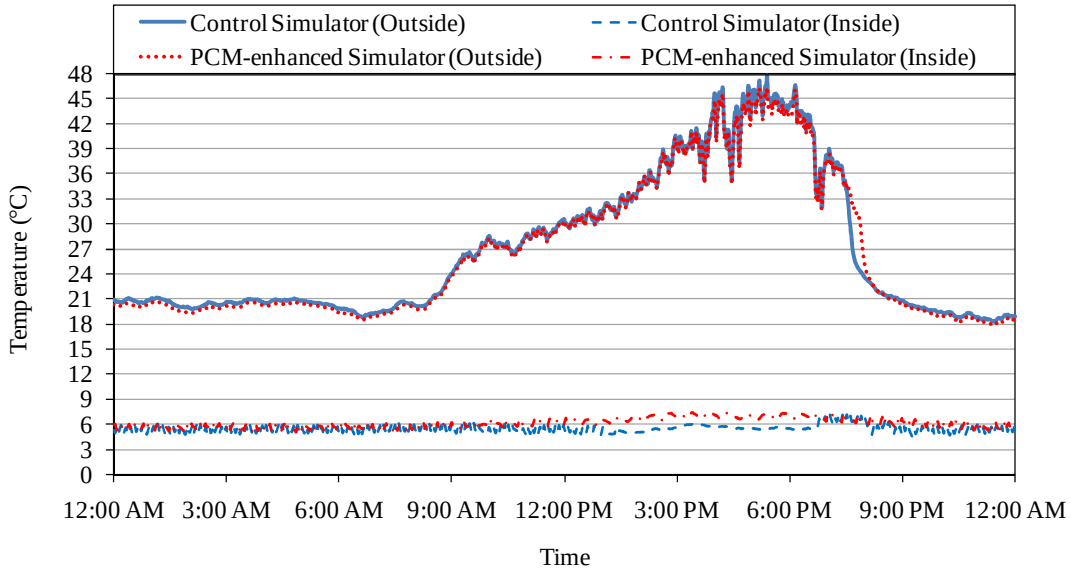

Figure 80. Exterior and interior surface temperatures of west wall in August

Figure 81 presents the exterior and interior temperatures of the north wall for both simulators. The PCM-enhanced simulator displayed almost same temperatures as the control simulator throughout the day for both interior and exterior surfaces.

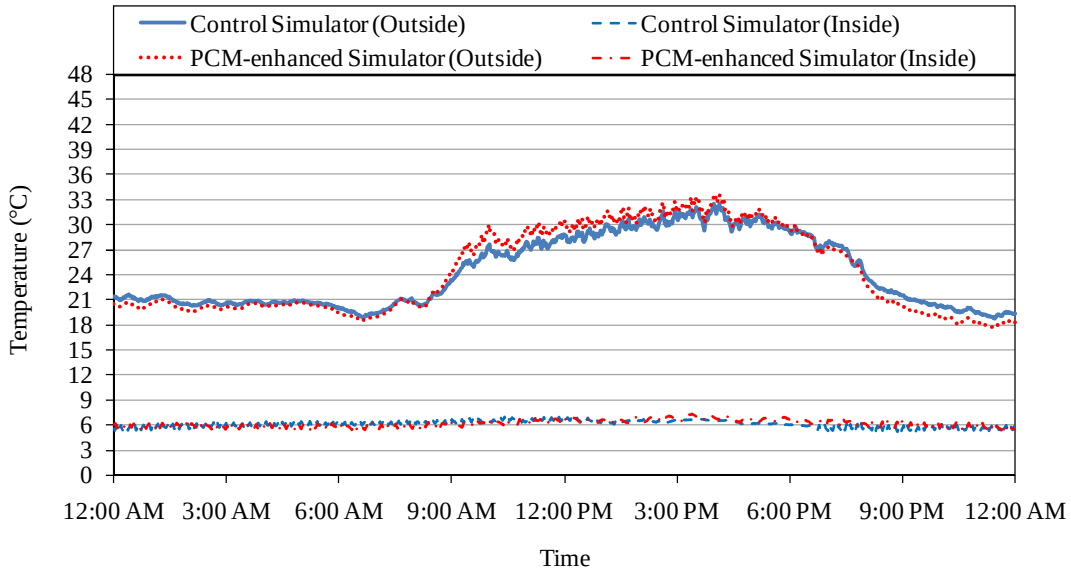

Figure 81. Exterior and interior surface temperatures of north wall in August

The relationship of the heat fluxes with the solar insolation is shown in Figure 92 and 93. Total hourly heat fluxes are presented for both simulators. There is no shift in peak heat flux observed during summer. During the early winter some negative total heat fluxes is observed, but all the heat fluxes are positive value during summer. Even when there is no solar insolation, positive heat fluxes are observed. This is because of the temperature difference between the interior and the exterior surface temperatures of the simulators.

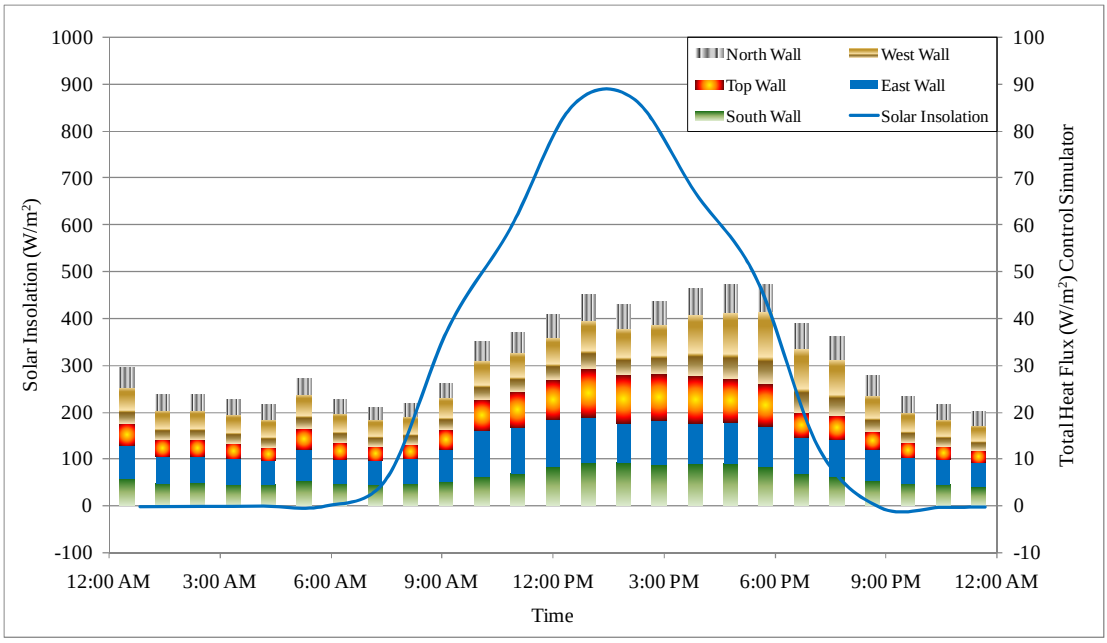

Figure 82. Solar insolation and corresponding heat fluxes for different walls of control simulator in August

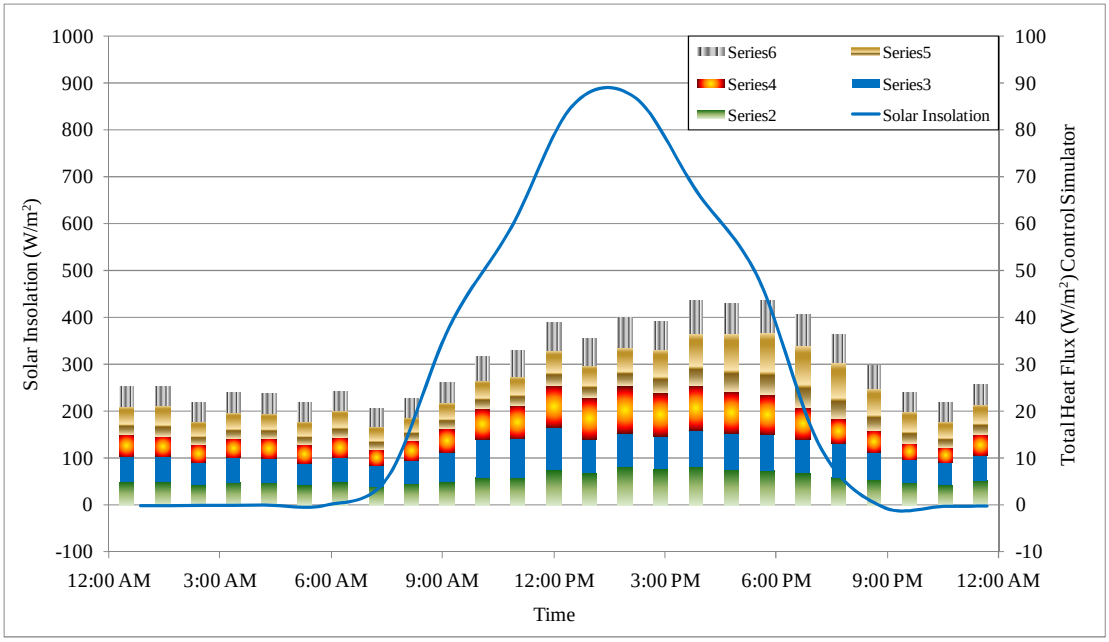

Figure 83. Solar insolation and corresponding heat fluxes for different walls of PCM-enhanced simulator in August

Chapter V: Conclusions and Recommendations

This research work presented a novel method of insulating the walls of refrigerated van trailers by using the latent heat of fusion and solidification of phase change materials (PCMs). The analysis of the data, based on the inclusion of paraffin-based PCMs in standard refrigerated van trailer walls, as a heat transfer reduction technology, provided encouraging results. It lowered peak heat transfer rates and total heat flow, thus potentially saving energy and reducing pollution from diesel-driven refrigeration equipment. PCMs are popularly considered as energy storage media, and their effects were evident in this case. The PCMs lowered the fluctuations in temperature within the refrigerated van trailer simulators. That is, the interior of the trailers would experience fewer temperature swings, which could lead to more stable operation and control, longer operating life for the refrigeration equipment, reduction in equipment size, energy conservation, and a decrease in pollution from diesel-driven refrigeration units.

During an entire month of experiments, an average reduction of 29.1% in peak heat transfer and an average reduction of 16.3% in total heat transfer were achieved by adding PCMs to the insulation foam of the trailer walls. If the panels were accounted for separately according to their performance in peak heat flux reduction, then the panels would be ranked as, top (26.4%), east (26.3%), west (13.8%), south (13.4%), and north (1.7%). For total heat flow reduction, the ranking would be east

(43.8%), top (41.1%), south (34.8%), north (14.6%) and west (11.3%). Therefore, it is interesting to note that the top, south and east walls showed some dominant effects in terms of heat flux reduction.

Summer data were collected and analyzed to investigate the further applicability of RT-5. A single day peak heat flux reduction of 7.9% was achieved using the PCM RT-5 during summer. A total heat flow reduction of 4.6% was achieved. The data collection during summer was limited and thus requires more investigation and analysis.

The literature review revealed that work had been done in areas of van trailer inside temperature homogeneity, which is very crucial for many products, especially perishable goods. The experiments presented in this thesis showed that PCMs were able to maintain an almost uniform temperature on the interior surfaces of all of the walls. In addition, the inside temperatures of the PCM-enhanced simulator was held steady. Thus, this represents an indication that the PCMs can contribute in the stabilization of the indoor temperature of refrigerated van trailers during operation.

The PCM-enhanced walls proved its usefulness by not taking more space than the control walls. Therefore, the use of PCM in the walls of any commercial trucks would not take more space than the current models.

The experiment presented in this thesis had a 25% PCM concentration based on total insulating material's weight (5.25% by volume). There are several types of refrigeration systems used in truck trailers, such as, diesel driven units, hydraulic drive units, and eutectic systems. Eutectic systems also use the thermal storage

concept for refrigeration purposes. However, one advantage of a PCM-enhanced system over the eutectic one is that the eutectic system needs to be charged periodically, which is not the case for PCM. Although the cost benefit analysis is beyond the scope of this research work, it is clear that PCM will definitely benefit the regular refrigeration units without further maintenance. Therefore, inclusion of PCM into the insulating walls might be preferable over some other existing options if the cost benefit analysis were taken into account.

In spite of every possible effort being made with limited resources, there are some guidelines which could be of considerable benefit for future work. One such recommendation relates to the size and shape of the simulators. The current simulators are of a square shape. A proportionately sized simulator would give more insight with respect to the length of the refrigerated van trailer. Also the air flow pattern outside the refrigerated van trailer could provide useful information.

A study of PCM-enhanced van trailer walls in a climate controlled chamber could be of benefit. Such a chamber would give more control over the experiments and eventually enable different combinations of climatic conditions. This could even involve wind tunnel test. Therefore, a complete test in a controlled environment could definitely open a future window for this research.

Orientation, number, or shape of PCM pipes could be of further interest. Various PCM with various ranges of melting and solidification temperatures could be incorporated to have a clearer picture of PCM behavior in the walls. The current PCM percentage of the total foam weight can be changed to observe different behavior for

different amounts of PCM. Cylindrical copper pipes, those used in this research, were found very efficient in containing the PCM and were convenient for installation. There are also different inclusion methods proposed by the previous researches, which can be implemented to investigate comparative benefits of all of these PCM inclusion techniques.

References

[1] Goodwin BK, Grennes TJ, Craig LA. Mechanical Refrigeration and the Integration of Perishable Commodity Markets. Explorations in Economic History 2002; 39: 154-82.

[2] Wessels Living History Farm. Farming in the 1940s: Revolution in Transportation. 2008 [cited; Available from: http://www.livinghistoryfarm.org/farminginthe40s/money_14.html.

[3] American Trucking Association. Fuel Facts. 2007 [cited; Available from: http://www.truckline.com/fuelpricecrisis/fuelfacts.

[4] Davis SC, Diegel SW, Oak Ridge National Laboratory. Transportation Energy Data Book: Edition 26. 2007, U.S. Department of Energy.

[5] U.S. Department of Commerce. Vehicle Inventory and Use Survey, 2002 Economic Census, In: Geographic Area Series. 2004, U.S. Census Bureau.

[6] Office of Freight Management and Operations. Freight Facts and Figures 2005. 2005, U.S. Department of Transportation, Federal Highway Administration.

[7] Office of Freight Management and Operations. Freight Facts and Figures 2007. 2007, U.S. Department of Transportation, Federal Highway Administration.

[8] Cavelius R, Isaksson C, Perendis E, Read GEF. Passive Cooling Technologies 2005 [cited; Available from: www.energyagency.at/publ/pdf/keepcool_passivecooling.pdf.

[9] Zhang M. Performance Evaluation of a Phase Change Frame Wall, In: Civil, Environmental and Architectural Engineering. 2004, University of Kansas: Lawrence.

[10] Salyer I, Sircar A. A review of phase change material research for thermal energy storage in heating and cooling applications at the University of Dayton from 1982 to 1996. International Journal of Global Energy Issues 1997; 9: 183–98.

[11] Zalba B, Marin MH, Cabiza FL. Review on Thermal Energy Storage with Phase Change: Materials, Heat Transfer Analysis and Applications. Applied Thermal Engineering 2003; 23(3): 251-83.

[12] Medina MA, King JB, Zhang M. On the heat transfer rate reduction of structural insulated panels (SIPs) outfitted with phase change materials (PCMs). Energy 2008; 33(4): 667-78.

[13] Zhu D. A Comparative Heat Transfer Examination of Structural Insulated Panels (SIPs) With and Without Phase Change Materials (PCMs) Using a Dynamic Wall Simulator, In: Civil, Environmental and Architectural Engineering. 2005, University of Kansas: Lawrence.

[14] Zhang M, Medina MA, King JB. Development of a Thermally Enhanced Frame Wall with Phase-Change Materials for On-Peak Air Conditioning Demand Reduction and Energy Savings in Residential Buildings. International Journal of Energy Research 2005; 29: 795-809.

[15] Ismail KA, Castro JN. PCM thermal insulation in buildings. International Journal of Energy Research 1997; 21: 1281–96.

[16] Zafer URE. Passive Cooling Ceiling System Using Eutectic (PCM) Solutions. In: Anaheim Winter Meeting, ASHRAE 2004, Anaheim, CA 2004.

[17] Hawes D, Feldman D, Banu D. Latent Heat Storage in Building Materials. Energy and Buildings 1993; 20: 77–86.

[18] International Institute of Refrigeration. Guide to refrigerated transport; 1995.

[19] Spence SWT, Doran WJ, Artt DW. Design, Construction and Testing of an Air-cycle Refrigeration System for Road Transport. International Journal of Refrigeration 2004; 27: 503-10.

[20] Spence SWT, Doran WJ, Artt DW, McCullough G. Performance Analysis of Feasible Air-Cycle Refrigeration System for Road Transport. International Journal of Refrigeration 2005; 28: 381-8.

[21] James SJ, James C, Evans JA. Modeling of food transportation systems – a review. International Journal of Refrigeration 2006; 29(6): 11.

[22] Tso CP, Yu SCM, Poh HJ, Jolly PG. Experimental Study on the Heat and Mass Transfer Characteristics in a Refrigerated Truck. International Journal of Refrigeration 2001; 25: 340-50.

[23] Chatzidakis SK, Chatzidakis KS. A Heat Transfer Simulation of a Multi-Compartment Isothermal Liquid Foodstuff Tank Tested According to the International ATP Agreement. Energy Conversion and Management 2005; 46: 197-221.

[24] Chatzidakis SK, Athienitis A, Chatzidakis KS. Computational energy analysis of an innovative isothermal chamber for testing of the special equipment used in the transport of perishable products. International Journal of Energy Research 2004; 28: 899-916.

[25] Agreement Transport Perishable. Agreement on the International Carriage of Perishable Foodstuffs and on the Special Equipment to be Used for such Carriage. 2007 [cited; Available from: http://www.unece.org/trans/main/wp11/atp.html.

[26] Chatzidakis SK, Chatzidakis KS. Refrigerated Transport and environment. International Journal of Energy Research 2004; 28: 887-97.

[27] RUBITHERM GmbH. Paraffins - RT-5. 2008 [cited; Available from: http://www.rubitherm.com/english/index.htm.

[28] ASHRAE. ASHRAE Handbook. I-P ed. Fundamentals; 1997.

[29] ASHRAE. ASHRAE Handbook. I-P ed. Refrigeration; 1998.

Appendix A

DSC curve for the coolant sample of 50-50 water glycol mixture. DSC calorimeter test was performed by Yuan Fang.

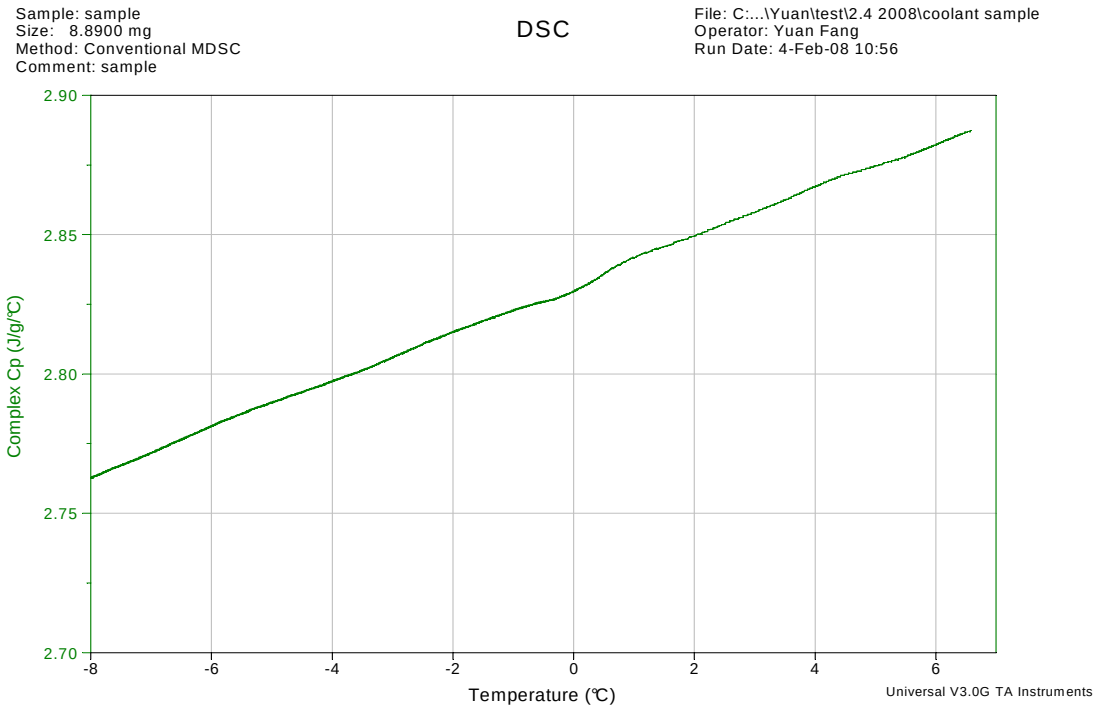

Appendix B

Two inline rotary flow meters were installed with the simulators. These were connected to data logger and used to send electric current pulse. The range for the flow meters was from 4 to 20 mA which represented 0.5 to 15 gpm flow. Figure 69 and 70 is flow rate measured by the flow meters.

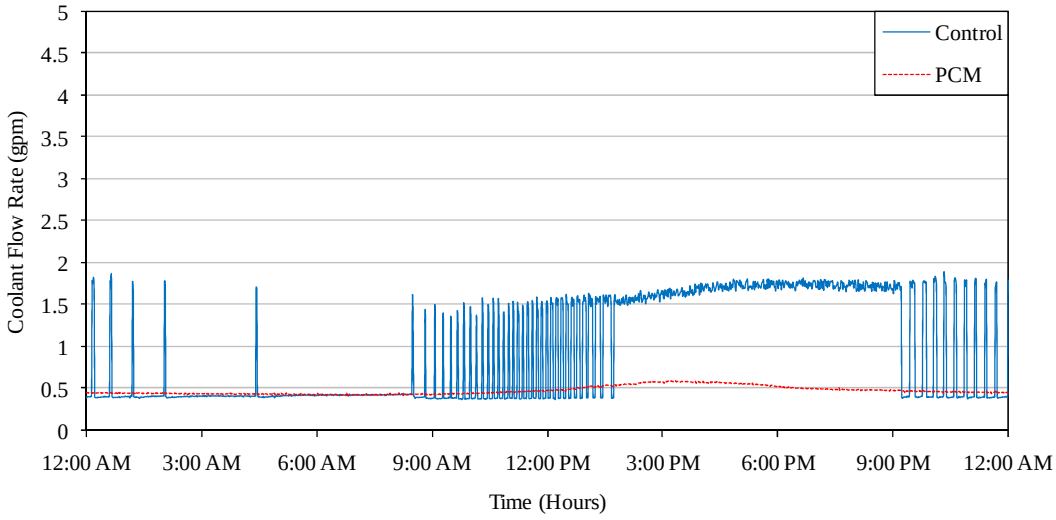

Figure 84. Flow meter reading of the control simulator experiment day

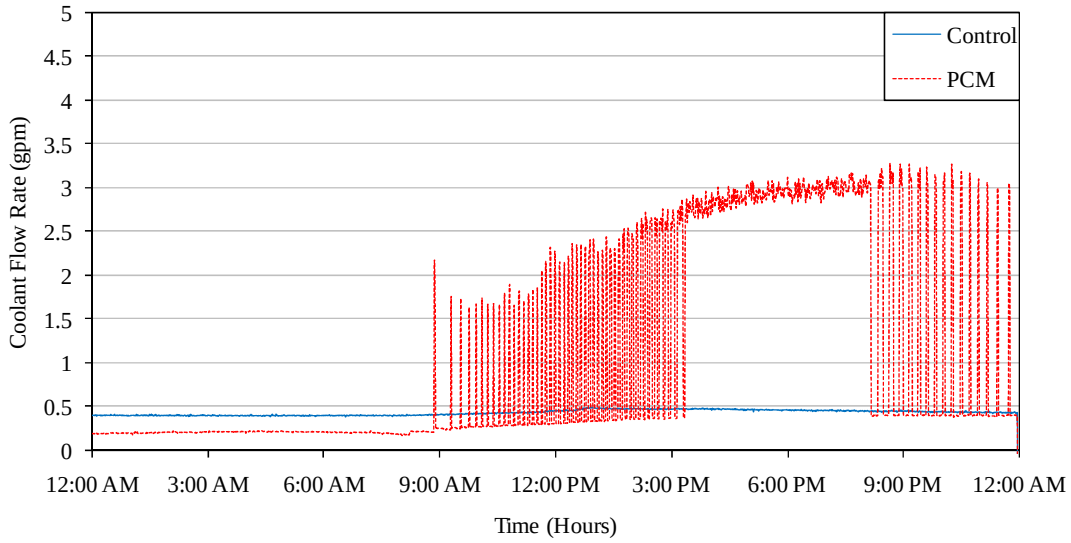

Figure 85. Flow meter reading of the PCM-enhanced simulator experiment day